STUDIES ON DEVELOPMENT OF NOVEL RARE EARTH DOPED (Bi,Pb)-2212 SUPERCONDUCTORS WITH ENHANCED PROPERTIES

Thesis submitted to the

Cochin University of Science & Technology

for the degree of

DOCTOR OF PHILOSOPHY

in

PHYSICS

by

P. M. SARUN

Under the supervision of

Dr. U. Syamaprasad

National Institute for Interdisciplinary Science and Technology
COUNCIL OF SCIENTIFIC & INDUSTRIAL RESEARCH
TRIVANDRUM – 695019
INDIA

JUNE 2010

Declaration

*Certified that the work presented in this dissertation entitled "**Studies on development of novel rare earth doped (Bi,Pb)-2212 superconductors with enhanced properties**" is based on the original research work done by me under the guidance and supervision of **Dr. U. Syamaprasad**, Scientist 'G' and Head, Superconducting & Magnetic Materials group, National Institute for Interdisciplinary Science and Technology (CSIR), Trivandrum - 695019, India and no part of this dissertation has been submitted previously for the award of any degree in any other University.*

Place : Trivandrum.
Date : June 23, 2010.

P.M. SARUN

NATIONAL INSTITUTE FOR INTERDISCIPLINARY SCIENCE & TECHNOLOGY

An ISO 9001 Certified Laboratory
(Formerly - Regional Research Laboratory)
Council of Scientific & Industrial Research
Industrial Estate P.O., Trivandrum -695 019, INDIA
Tel :91-471-2515 373/2515 233; Fax : +91-471-2491 712
Email : syam@csrrltrd.ren.nic.in; syamcsir@gmail.com.
Website: www.niist.res.in

Dr. U. SYAMAPRASAD
SCIENTIST G, SENIOR DEPUTY DIRECTOR AND HEAD
APPLIED SUPERCONDUCTIVITY & CERAMICS SECTION

Certificate

*Certified that the work presented in this dissertation entitled "**Studies on development of novel rare earth doped (Bi,Pb)-2212 superconductors with enhanced properties**" is an authentic record of the research work carried out by **Mr. P. M. Sarun** under my supervision in partial fulfilment of the requirement for the degree of **Doctor of Philosophy** of the Cochin University of Science and Technology (CUSAT) and further that no part of this dissertation has been presented previously for the award of any other degree.*

Place : Trivandrum.
Date : June 23, 2010.

U. Syamaprasad
(Research Guide)

Acknowledgements

At the outset, I express my sincere and heartfelt gratitude to my supervising guide, Dr. U. Syamaprasad, National Institute for Interdisciplinary Science and Technology, Trivandrum, India for his guidance, timely motivations and continuous support throughout the period of my Ph.D. work.

Next, I would like to thank Dr. Suresh Das, Director, National Institute for Interdisciplinary Science and Technology (CSIR), Trivandrum, India; Dr. B. C. Pai and Dr. T. K. Chandrashekar, former Directors for providing all the necessary facilities to carry out this work and for their encouragement during this work.

I owe my sincere gratitude to my colleagues S. Vinu and R. Shabna for their inspirations, sincere help, creative suggestions and the warmth of deep friendship during the entire course of this work.

I express my deep gratitude and love to my junior colleagues P. M. Aswathy, J. B. Anooja and G. R. Anuraghi for their timely and prompt effort, valuable suggestions and sincere help to strictly scrutinize my dissertation to make conceptual, grammatic and typographic errors as minimum as possible. Without their help, it would have been very difficult for me to complete the dissertation on the given time frame.

I owe my sincere gratitude to my senior colleagues Dr. A. Biju, Principal, M. E. S. Asmabi College, Kodungallur, Thrissur, Kerala, India, and Dr. R. P. Aloysius, Scientist, National Physical Laboratory, New Delhi, India, whose

encouragements and invaluable advises were equally important for the timely completion of this work.

I take this chance to express my deep gratitude to Mr. P. Guruwsamy, Technical Officer, National Institute for Interdisciplinary Science and Technology (CSIR), Trivandrum, India, for his encouragement, technical suggestions and sincere support during the entire course of this work.

I express my sincere thanks to Dr. K. G. K. Warrier, Dr. Peter Koshy, Dr. P. Prabhakar Rao, Dr. Ananthakumar and Dr. V. M. Sreekumar, National Institute for Interdisciplinary Science and Technology (CSIR), Trivandrum, India for their help during this work.

Words are insufficient to express my gratitude to my colleagues K. Vinod, Neson Varghese, R. G. Abhilash Kumar, A. Nazeer, B. Premlal, A. Vasudevan, S. Rahul, P. Anees, Syju Thomas, K. M. Devadas, Sivaprakash, Santhosh, K. T. Jakson, S. Surya, Rossamma Sebastian, V. G. Prabitha and Navya Robert, for their moral support, help and co-operation extended by them at various stages of this work.

I express my heartfelt thanks to Mr. S. G. K. Pillai, Mr. M. Chandran and Mr. Robert Philip, for extending different instrumental facilities.

I express my sincere gratitude to Dr. K. P. Vijayakumar, Head, Department of Physics, Cochin University of Science and Technology, Cochin for his kind co-operation and support at various stages of this work.

I would like to acknowledge and express my deep sense of gratitude to the Council of Scientific and Industrial Research, New Delhi, for the award of Diamond Jubilee Research Intern and Senior Research Fellowship without which I might not have completed this work.

Finally, I thank my parents, Ex. W. O., Indian Air Force, T. P. Chandramohan and M. Shylaja, for their parental advises and motivations in the hour of need. I also owe a heartfelt thanks to my wife, C. P. Nijina, for being al-

ways a source of inspiration and love, in fact, we are blessed with a cute baby girl recently born on 07-03-2010 at 5.35 a.m. I appreciate their patience and understanding. They have been the chief driving force behind the successful completion of this work.

P. M. SARUN

Preface

Superconductivity, the phenomenon of vanishing of electrical resistance of a material at low temperatures, was discovered by Heike Kamerlingh Onnes at the University of Leiden (Holland) in 1911, in mercury down below 4.2 K which was characterized by a sharp drop in the resistance. In the following years, many metals, elements and inter-metallics were found to be superconducting, but their practical applications were limited due to low values of T_c and H_c (critical magnetic field) and/or complicated fabrication method into wires/coils. The most widely used superconducting materials are the two low temperature superconductors (LTS), NbTi (T_c = 9 K) and Nb_3Sn (T_c = 18 K) discovered in the mid 1950's. NbTi is much easier to fabricate compared to Nb_3Sn and both these conductors are now commercially available. These are required to be cooled by liquid helium, which is very expensive and hence their applications are mainly limited to high field magnets. In the mid-80's the discovery of high temperature superconductors (HTS) with T_c above 77 K stimulated the development of power applications of superconductors. However, they have undergone significant research and have been used for power transmission cables in some major electrical grids. HTS materials have some intrinsic limitations such as high anisotropy, weak-link granular nature and hence the fabrication of HTS materials into wires and coils is not very easy.

Even though there are a large number of high T_c superconducting materials known today, Bi-based superconductors have attracted researchers due to their widespread applications. The material has not only high transition temperature (T_c), but also has extremely high critical magnetic field (H_{c2}). It is less

susceptible to degradation as a result of oxygen loss and less sensitive to attack by water and carbon dioxide compared to any other HTS and its melting point is lower, being in the range 800–900 °C. The main advantage of Bi-based system is its layered structure which can be progressively deformed to induce a high degree of texturing, thereby enhancing the superconducting properties. Among the Bi-based systems, Bi-2212 ($Bi_2Sr_2Ca_1Cu_2O_{8+\delta}$) is considered to be the best candidate for fabrication of long length wires and tapes with moderate current carrying capacities. Moreover, the superconducting transition temperature of Bi-2212 is strongly related to the carrier concentration in the CuO_2 planes. The hole carrier density of the CuO_2 plane in Bi-2212 can be altered by changing the oxygen stoichiometry or by cationic substitution of divalent Ca/Sr in the active layers of Bi-2212 by suitable cations. Hence, the properties of Bi-2212 superconductor can be tailored for specific applications.

The objective of the present work is to study the effect of rare-earth (RE) doping on the superconducting properties of (Bi,Pb)-2212 system and to develop novel superconductors in the system with improved properties, especially, the self- and in-field critical current densities so as to use them for practical applications. This dissertation describes a range of findings in Bi-based superconductor using the cationic substitution of rare earth (RE) elements. Most of the experiments reported here take advantage of the difference in the valency and ionic radii of dopant and doping site.

The dissertation is organized into 7 chapters. The introductory chapter begins with a brief overview on high temperature superconductivity, superconducting materials, structural arrangement, underlying theories, applications and the specialties of Bi-based superconductors. Details of the experimental and analytical techniques in general are outlined in chapter 2 while the specific methods used are described in the respective chapters.

Chapter 3 describes the influence of Bi:Pb ratio on the structural and superconducting properties of pure and a RE (Y) doped (Bi,Pb)-2212 supercon-

ductor. The objective is to investigate the effect of Pb doping at Bi-site in the Y-free and Y added Bi-2212 as a typical case. Pb-substitution at the Bi-site enhances the self-field critical current density (J_c) while slightly brings down the T_c of Bi-2212 superconductor with the best results obtained for Pb content in the range $x = 0.4 - 0.5$.

Chapter 4 presents the preparation and characterization of (Bi,Pb)-2212, stoichiometrically substituted with different REs (Lanthanides) at Sr site with different concentrations and the results are compared with RE-free (Bi,Pb)-2212 superconductor. The rare earth dopants are chosen with different ionic size ranging from La to Lu in the periodic table which include magnetic and nonmagnetic rare-earths. The RE content is varied on a general stoichiometry of $Bi_{1.6}Pb_{0.5}Sr_{(2-x)}RE_xCa_{1.1}Cu_{2.1}O_{8+\delta}$ where $x = 0.0$ to 0.5. The structural and superconducting properties of the RE substituted (Bi,Pb)-2212 superconductors are investigated in detail. Significant changes in structural, microstructural and superconducting properties are observed in the RE substituted system. The superconducting properties such as T_c and J_c are highly enhanced and these are due to the dual effect of the decrease in the hole concentration in CuO_2 planes towards an optimum level and the improvement of coupling between the CuO_2 layers across the charge reservoir layers. Beyond the optimum levels of RE substitution, the T_c and J_c come down which subsequently initiate a Metal to Insulator transition (MIT) in (Bi,Pb)-2212 system.

In chapter 5, an attempt is made to restore the grain morphology and texture of RE substituted (Bi,Pb)-2212 superconductors as in RE-free samples by precisely tuning the sintering temperature. It has been possible to control the grain growth and tailor the microstructure of RE substituted (Bi,Pb)-2212 superconductors as desired and thereby produce superconductors with either highly enhanced self-field J_c or high in-field J_c. The results indicate that the microstructure variations are highly temperature sensitive. The results open up an avenue to prepare RE substituted (Bi,Pb)-2212 incorporating hybrid self-

and in-field superconducting properties by selecting a suitable sintering temperature.

Chapter 6 is a compendium on the analysis of the E–J characteristics and the associated n-indices of RE-free and RE substituted (Bi,Pb)-2212 superconductors at different magnetic fields and an assessment of the suitability of the material for application in persistent mode magnets. The RE substituted (Bi,Pb)-2212 superconductors exhibit a glass-state for flux-lines, showing their improved flux pinning ability due to the creation of point defects as a result of RE substitution. The improved flux pinning ability makes them promising candidates for magnetic applications. Finally, chapter 7 summarizes the work with main conclusions and future directions.

Thus, the findings reported in this dissertation are quite promising and contribute significantly towards the understanding of rare earth doped (Bi,Pb)-2212 superconductors. The novel rare earth modified formulations with high T_cs and J_cs reported here are promising candidates for applications in superconducting current leads/cables and insert-magnets or booster-magnets of high-field nuclear magnetic resonator.

Details of patents and publications.

List of patents granted/filed.

Title	:–	A process for continuous production of Magnesium Diboride based superconductors
Inventors	:–	U. Syamaprasad, R. G. Abhilash Kumar, K. Vinod, R. P. Aloysius, **P. M. Sarun**, S. Thennavarajan, and P. Guruswamy
US patent	:–	Patent no.: US 7,456,134 B2. Date of patent: Nov. 25, 2008.
UK patent	:–	Application no: 0807427.0, NFNO: 0185NF2005/GB, filing date: 23-04-2008.
German patent	:–	NFNO: 0185NF2005/DE, filing date: 21-05-2008.
Japan patent	:–	NFNO: 0185NF2005/JP, filing date: 26-05-2008.
Indian patent	:–	NFNO. 0185NF2005/IN, filing Date: 25/11/2005, APN No. 3156DEL2005.

List of Publications in SCI journals.

1. P. M. SARUN, S. VINU, R. SHABNA, and U. SYAMAPRASAD, Structural and transport critical current density of $Bi_{1.6}Pb_{0.5}Sr_{2-x}Lu_xCa_{1.1}Cu_{2.1}O_{8+\delta}$ superconductor, *IEEE Trans. Appl. Phys.* **20**, 61 (2010).
2. P. M. SARUN, S. VINU, R. SHABNA, and U. SYAMAPRASAD, Suppression of dissipative flux-motion in a high-Tc (Bi,Pb)-2212 superconductor by Dy-doping, *J. Alloy. and Compd.* **497**, 6 (2010).
3. P. M. SARUN, S. VINU, R. SHABNA, A. BIJU, and U. SYAMAPRASAD, Influence of Ho-doping on the electro-magnetic field dependent E-J characteristics of (Bi,Pb)-2212 superconductor, *IEEE Trans. Appl. Supercond.* **19**, 35 (2009).
4. P. M. SARUN, S. VINU, R. SHABNA, A. BIJU, and U. SYAMAPRASAD, Investigation of self-and in-field dependent n-value of Tb-doped (Bi,Pb)-2212 superconductor, *J. Appl. Phys.* **106**, 043910 (2009).

5. P. M. SARUN, S. VINU, R. SHABNA, A. BIJU, P. GURUSWAMY, and U. SYAMAPRASAD, Effect of sintering temperature on the microstructural and flux pinning characteristics of $Bi_{1.6}Pb_{0.5}Sr_{1.8}La_{0.2}$ $Ca_{1.1}Cu_{2.1}O_{8+\delta}$ superconductor, *J. Am. Ceram. Soc.* **92**, 411 (2009).
6. P. M. SARUN, S. VINU, R. SHABNA, A. BIJU, and U. SYAMAPRASAD, Properties of superconducting, polycrystalline dysprosium-doped $Bi_{1.6}Pb_{0.5}Sr_{2-x}Dy_xCa_{1.1}$ $Cu_{2.1}O_{8+\delta}$ ($0 \leq x \leq 0.5$), *Mater. Res. Bull.* **44**, 1017 (2009).
7. P. M. SARUN, S. VINU, R. SHABNA, A. BIJU, and U. SYAMAPRASAD, Microstructural and superconducting properties of Yb-substituted (Bi,Pb)-2212 superconductor sintered at different temperatures, *J. Alloys Compd.* **472**, 13 (2009).
8. P. M. SARUN, A. BIJU, R. SHABNA, S. VINU, and U. SYAMAPRASAD, Highly enhanced superconducting properties of Bi-2212 by Y and Pb co-doping, *Physica B* **404**, 1602 (2009).
9. P. M. SARUN, S. VINU, R. SHABNA, A. BIJU, and U. SYAMAPRASAD, Highly enhanced superconducting properties of Eu-doped (Bi,Pb)-2212, *Mater. Lett.* **62**, 2725 (2008).
10. P. M. SARUN, A. BIJU, P. GURUSWAMY, and U. SYAMAPRASAD, Enhanced flux pinning of an Nd-added (Bi,Pb)-2212 superconductor, *J. Am. Ceram. Soc.* **90**, 3138 (2007).
11. P. M. SARUN, R. P. ALOYSIUS, and U. SYAMAPRASAD, Preparation of high performance (Bi,Pb)-2223 superconductor using a sol-gel synthesized amorphous precursor through controlled gelation, *Mater. Lett.* **60**, 3797 (2006).
12. S. VINU, P. M. SARUN, R. SHABNA, A. BIJU, and U. SYAMAPRASAD, Microstructure and electrical properties of $Bi_{1.6}Pb_{0.5}$ $Sr_{2-x}Lu_xCa_{1.1}Cu_{2.1}O_{8+\delta}$ superconductor, *Mater. Chem. Phys.* **119**, 135 (2010).
13. S. VINU, P. M. SARUN, R. SHABNA, A. BIJU, and U. SYAMAPRASAD, Enhancement of flux pinning and Anderson-Dew-Hughes pinning analysis in $Bi_{1.6}Pb_{0.5}$ $Sr_{2-x}Tb_xCa_{1.1}Cu_{2.1}O_{8+\delta}$ superconductor, *J. Alloys Compd.* **477**, L13 (2009).
14. S. VINU, P. M. SARUN, R. SHABNA, A. BIJU, and U. SYAMAPRASAD, Analysis of thermo-magnetic fluctuations in $Bi_{1.6}Pb_{0.5}$ $Sr_{2-x}Lu_xCa_{1.1}Cu_{2.1}O_{8+\delta}$ ($0.000 \leq x \leq 0.125$) superconductor, *J. Alloys Compd.* **487**, 1 (2009).
15. S. VINU, P. M. SARUN, R. SHABNA, A. BIJU, P. GURUSWAMY, and U. SYAMAPRASAD, Influence of sintering temperature on microstructure, critical current density and pinning potential of superconducting $Bi_{1.6}Pb_{0.5}Sr_{1.8}Dy_{0.2}Ca_{1.1}Cu_{2.1}O_{8+\delta}$ ceramics, *Solid Stat. Sci.* **11**, 1150 (2009).
16. S. VINU, P. M. SARUN, R. SHABNA, and U. SYAMAPRASAD, Analysis of thermo-magnetic fluctuations above the glass-transition temperature in $Bi_{1.6}Pb_{0.5}Sr_{2-x}$ $Eu_xCa_{1.1}Cu_{2.1}O_{8+\delta}$ ($0.000 \leq x \leq 0.180$) system, *Solid Stat. Sci.* **11**, 1530 (2009).
17. S. VINU, P. M. SARUN, R. SHABNA, and U. SYAMAPRASAD, Refinement of microstructure and highly improved electrical properties of $Bi_{1.6}Pb_{0.5}Sr_{1.925}Ho_{0.075}$ $Ca_{1.1}Cu_{2.1}O_{8+\delta}$ superconductor, *J. Appl. Phys.* **106**, 063920 (2009).
18. S. VINU, P. M. SARUN, R. SHABNA, A. BIJU, and U. SYAMAPRASAD, Scaling of the vortex-liquid resistivity and temperature and magnetic field dependent

activation energy in Ho-doped (Bi, Pb)-2212 superconductor, *J. Appl. Phys.* **105**, 123901 (2009).

19. S. VINU, P. M. SARUN, R. SHABNA, and U. SYAMAPRASAD, Erratum: Enhancement of critical current density and flux pinning properties of Gd-doped (Bi,Pb)-2212 superconductor (J. Appl. Phys. (2008) 104 (043905)), *J. Appl. Phys.* **105**, 129901 (2009).
20. S. VINU, P. M. SARUN, R. SHABNA, A. BIJU, and U. SYAMAPRASAD, Enhancement of critical current density and flux pinning properties of Gd-doped (Bi,Pb)-2212 superconductor, *J. Appl. Phys.* **104**, 043905 (2008).
21. S. VINU, P. M. SARUN, A. BIJU, R. SHABNA, P. GURUSWAMY, and U. SYAMAPRASAD, The effect of substitution of Eu on the critical current density and flux pinning properties of (Bi,Pb)-2212 superconductor, *Supercond. Sci. Technol.* **21**, 045001 (2008).
22. S. VINU, P. M. SARUN, R. SHABNA, A. BIJU, and U. SYAMAPRASAD, The influence of sintering temperature on the microstructure and superconducting properties of $Bi_{1.7}Pb_{0.4}Sr_{1.8}Nd_{0.2}Ca_{1.1}Cu_{2.1}$ $O_{8+\delta}$ superconductor, *Supercond. Sci. Technol.* **21**, 085010 (2008).
23. S. VINU, P. M. SARUN, R. SHABNA, A. BIJU, and U. SYAMAPRASAD, Improved microstructure and flux pinning properties of Gd-substituted (Bi,Pb)-2212 superconductor sintered between 846 and 860 °C, *Mater. Lett.* **62**, 4421 (2008).
24. S. VINU, P. M. SARUN, R. SHABNA, A. BIJU, P. GURUSWAMY, and U. SYAMAPRASAD, Effect of Dy substitution at the sr site on the critical current density and flux-pinning properties of (Bi,Pb)-2212 superconductor, *J. Am. Ceram. Soc.* **91**, 3585 (2008).
25. R. SHABNA, P. M. SARUN, S. VINU, A. BIJU, and U. SYAMAPRASAD, Charge carrier localization and metal to insulator transition in cerium substituted (Bi,Pb)-2212 superconductor, *J. Alloys Compd.* **493**, 11 (2010).
26. R. SHABNA, P. M. SARUN, S. VINU, and U. SYAMAPRASAD, Superconductor-Metal-Insulator crossover in $Bi_{1.7}Pb_{0.4}Sr_{2-x}Ce_xCa_{1.1}Cu_{2.1}O_{8+}$ ($0.2 \leq x \leq 0.6$) sintered between 845 °C $\leq$ Ts $\leq$ 865 °C, *J. Alloys Compd.* **(Accepted)**, (2010).
27. R. SHABNA, P. M. SARUN, S. VINU, and U. SYAMAPRASAD, Structural and electrical properties of $Bi_{1.7}Pb_{0.4}Sr_{2-x}Ho_xCa_{1.1}$ $Cu_{2.1}O_{8+\delta}$ system across the metal to insulator transition, *J. Alloys. Compd.* **481**, 797 (2009).
28. R. SHABNA, P. M. SARUN, S. VINU, A. BIJU, and U. SYAMAPRASAD, Doping controlled metal to insulator transition in (Bi,Pb)-2212 system, *Supercond. Sci. Technol* **22**, 045016 (2009).
29. R. SHABNA, P. M. SARUN, S. VINU, and U. SYAMAPRASAD, Doping dependent metal to insulator transition in the (Bi,Pb)-2212 system: The evolution of structural and electronic properties with europium substitution, *Chinese Phys. B* **18**, 4000 (2009).
30. R. SHABNA, P. M. SARUN, S. VINU, and U. SYAMAPRASAD, Transport Properties near the Metal to Insulator transition in Sm substituted (Bi,Pb)-2212 system, *J. Appl. Phys.* **105**, 113925 (2009).

31. R. SHABNA, P. M. SARUN, S. VINU, A. BIJU, P. GURUSWAMY, and U. SYAMAPRASAD, Metal-insulator transition and conduction mechanism in dysprosium doped $Bi_{1.7}Pb_{0.4}Sr_2Ca_{1.1}Cu_{2.1}O_{8+\delta}$ system, *J. Appl. Phys.* **104**, 013919 (2008).
32. A. BIJU, P. M. SARUN, R. P. ALOYSIUS, and U. SYAMAPRASAD, Flux pinning properties of Yb substituted (Bi,Pb)-2212 superconductor, *J. Alloys Compd.* **454**, 46 (2008).
33. A. BIJU, P. M. SARUN, R. P. ALOYSIUS, and U. SYAMAPRASAD, Comparison of superconducting properties of Ce added (Bi,Pb)-2212 with other rare earth additions, *J. Alloys Compd.* **433**, 68 (2007).
34. A. BIJU, P. M. SARUN, R. P. ALOYSIUS, and U. SYAMAPRASAD, Structural and superconducting properties of neodymium added $(Bi,Pb)_2Sr_2CaCu_2O_y$, *Mater. Res. Bull.* **42**, 2057 (2007).
35. A. BIJU, K. VINOD, P. M. SARUN, and U. SYAMAPRASAD, Highly enhanced flux pinning in Pb and rare earth co-doped Bi-2212, *Appl. Phys. Lett.* **90**, 072505 (2007).
36. A. BIJU, P. M. SARUN, S. VINU, P. GURUSWAMY, and U. SYAMAPRASAD, Critical current density and flux pinning in a $Bi_{1.7}Pb_{0.4}Sr_{2-x}La_xCa_{1.1}Cu_{2.1}O_y$ system, *Supercond. Sci. Technol.* **20**, 781 (2007).
37. A. BIJU, P. M. SARUN, R. P. ALOYSIUS, and U. SYAMAPRASAD, Superconductivity and flux pinning in Dy added (Bi,Pb)-2212 superconductor, *Supercond. Sci. Technol.* **19**, 1023 (2006).
38. A. BIJU, R. SHABNA, P. M. SARUN, S. VINU, and U. SYAMAPRASAD, Effect of Yb, Gd, and Nd substitution at the Sr site on the Metal-Insulator transition of the (Bi,Pb)-2212 system, *Inter. J. Appl. Ceram. Technol.* **7 [S1]**, E16 (2010).
39. K. VINOD, R. G. ABHILASHKUMAR, A. BIJU, P. M. SARUN, and U. SYAMAPRASAD, Flux pinning properties of magnesium diboride added (Bi,Pb)-2212 superconductors, *J. Alloys Compd.* **439**, L1 (2007).
40. V. G. PRABITHA, A. BIJU, R. G. ABHILASHKUMAR, P. M. SARUN, R. P. ALOYSIUS, and U. SYAMAPRASAD, Effect of Sm addition on (Bi,Pb)-2212 superconductor, *Physica C* **433**, 28 (2005).

Conference Presentations

1. Critical current density and flux pinning properties of $Bi_{1.7}Pb_{0.4}Sr_{2-x}Gd_xCa_{1.1}Cu_{2.1}O_{8+\delta}$ superconductor, Presented at International Conference on Advanced Functional Materials, Thiruvananthapuram, December 9-10, 2009.
2. Transport property near the metal to insulator transition in samarium substituted (Bi,Pb)-2212 system, Presented at International Conference on Advanced Functional Materials, Thiruvananthapuram, December 9-10, 2009.
   ("BEST POSTER AWARD" winning article)

3. Thermo-magnetic fluctuations above the glass-transition temperature in Eu-doped (Bi,Pb)-2212 superconductor, Presented at International Conference on Advanced Functional Materials, Thiruvananthapuram, December 9-10, 2009.
4. Structural and Superconducting properties of Gd-substituted $(Bi,Pb)_2Sr_2Ca_1Cu_2O_{8+\delta}$ superconductor, Presented at 21^{th} Kerala Science Congress, Kollam, January 29-31, 2009.
   ("BEST POSTER AWARD" winning article)
5. Highly enhanced superconducting properties of Pb and rare-earth doped Bi-2212 system, Presented at 21^{th} Kerala Science Congress, Kollam, January 29-31, 2009.
6. Impact of Europium substituted on the metal to insulator transition phenomenon in (Bi,Pb)-2212 superconductor, Presented at 21^{th} Kerala Science Congress, Kollam, January 29-31, 2009.
7. Enhanced flux pinning in $Bi_{1.7}Pb_{0.4}Sr_{2-x}La_xCa_{1.1}Cu_{2.1}O_y$ superconductor, Presented at 21^{th} Kerala Science Congress, Kollam, January 29-31, 2009.
8. Metallic, Superconducting and Semiconducting properties of Praseodymium substituted (Bi,Pb)-2212 system, Presented at Special Purpose, Strategic and Futuristic Materials for High Technology Sectors,Thiruvananthapuram, October 16-17, 2008.
9. Critical current density and flux pinning properties of $Bi_{1.6}Pb_{0.5}Sr_{2-x}Eu_xCa_{1.1}Cu_{2.1}O_y$ superconductor, Presented at Special Purpose, Strategic and Futuristic Materials for High Technology Sectors, Thiruvananthapuram October 16-17, 2008.
10. Critical current density and flux pinning properties of $Bi_{1.7}Pb_{0.4}Sr_{2-x}Gd_xCa_{1.1}Cu_{2.1}O_{8+\delta}$ superconductor, Presented at 53^{rd} DAE Solid State Physics Symposium, BARC, Mumbai, December 16-20, 2008.
11. Superconductivity to Semiconductivity - An insight into the dependence of structural and electrical properties of (Bi,Pb)-2212 on a rare-earth modification, Presented at 20^{th} Kerala Science Congress, Trivandrum, January 28-31, 2008.
12. Metal-Insulator transition in $Bi_{1.7}Pb_{0.4}Sr_2Ca_{1.1}Cu_{2.1}Dy_xO_{8+\delta}$ system, Presented at 52^{nd} DAE-Solid State Physics Symposium 2007, Mysore, December 27-31, 2007.
13. Enhanced Flux pinning in La substituted (Bi,Pb)-2212 superconductor, Presented at 52^{nd} DAE-Solid State Physics Symposium 2007, Mysore, December 27-31, 2007.

14. Fabrication of high J_e (Bi,Pb)-2223/Ag multifilamentary tapes using a powder and wire-in-tube method, Presented at International Conference on Advanced Materials and Composites (ICAMC-2007), Trivandrum, October 24-26, 2007.
15. Pinning force density of Y-added (Bi,Pb)-2212 superconductor, Presented at International Conference on Advanced Materials and Composites (ICAMC-2007), Trivandrum, October 24-26, 2007.
16. Investigation on Metal-Insulator transition in $Bi_{1.7}Pb_{0.4}Sr_2Ca_{1.1}Cu_{2.1}Y_xO_{8+\delta}$ superconductor, Presented in International Conference on Advanced Materials and Composites (ICAMC-2007), Trivandrum, October 24-26, 2007.

Dedicated to My Family

"Your right is to work only, but never to the fruit of that,
Let not the fruit of action be your object,
nor let your attachment be to inaction"

— *(Bhagavath Geeta 2/47)*

Contents

Chapter 1

Overview on high T_c superconductivity

Once you eliminate the impossible, whatever remains,
no matter how improbable, must be the truth.
— Sherlock Holmes (by Sir A. Conan Doyle), 1859–1930

1.1 Introduction to superconductivity

Superconducting materials have long held the promise of many wonderful technological benefits. Most applications of superconductivity make use of the special ability of a superconductor to carry electric current without dissipation. While applications such as cross-country, levitating bullet trains are still somewhat out of reach, they grow closer each day. Indeed, superconductors have progressed out of the laboratory into near-commodity, "real world" products such as magnetic resonance imaging systems. However, most of the present successful applications of superconductors utilise so-called "low temperature" materials such as alloys of niobium and titanium. The inconvenience, expense,

and perhaps impracticality associated with the cooling of such materials below their critical temperature (T_c), which is $\sim$ 10 K, has restricted their use to applications where performance outweighs the cost of expensive refrigeration.

In the year 1911, Professor Heike Kamerlingh Onnes et al. at the university of Leiden (Holland), cooled a small tube filled with mercury down below 4.2 K and measured the resistance in the mercury. At 4.25 K, they observed a sharp drop in the resistance which is in disagreement with theories postulating that the resistance of a metal should remain finite to 0 K (Figure 1.1). Later the same year, he reported that *mercury had passed into a new state, which on account of its extraordinary electrical properties may be called the* ***superconducting state*** [1]. The necessary technical basis and opportunity for the discovery had been solidly established in the same group by the liquefaction of the inert gas helium in 1908. He also discovered that not only a high enough temperature, T_c (critical temperature), can destroy superconductivity, but also a high enough magnetic field, H_c (critical magnetic field), and a high enough current density, J_c (critical current density).

After twenty years of the discovery of Onnes, a major breakthrough came in 1933 when Walter Meissner and Robert Ochsenfeld [2] showed that if a superconductor is placed in an external magnetic field, currents are established on its surface which create an equal and opposite magnetic field to the one that is being applied and results in a net zero magnetic field inside the superconductor. As a result, the flux inside the superconductor expelled in magnetic fields below a certain threshold value. This defined a new thermodynamic state and was not a consequence of infinite conductivity. The phenomenon came to be known as the ***Meissner effect***, and laid the foundation for a thermodynamic treatment of superconductivity. The complete expulsion of magnetic flux shows that superconductor is perfectly diamagnetic in the superconducting state. Soon, London brothers proved that the field inside a superconductor in the ***Meissner state*** decays exponentially with distance from the surface. This defines the London penetration depth [3, 4], λ_L , being defined as $H(\lambda_L)$

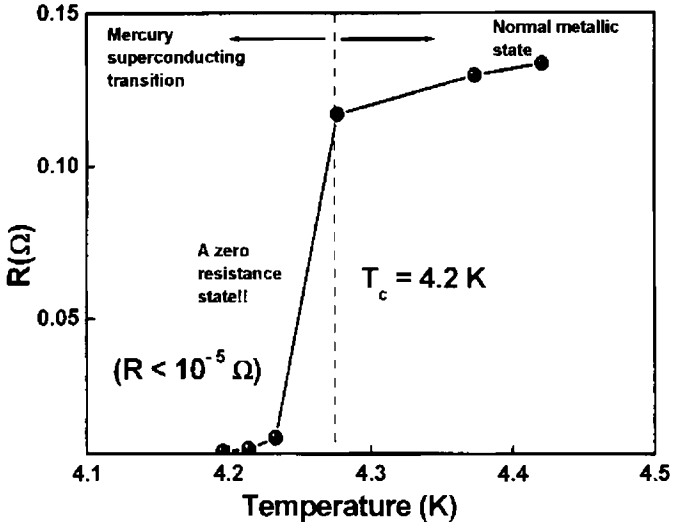

Figure 1.1: Resistance versus temperature for mercury obtained by Kamerlingh Onnes in 1911.

= (1/e)H(0), where H(0) is the field at the surface of the superconductor. This explanation only holds for Type I superconductors.

Further research found that the current, applied magnetic field, and temperature are coupled together to define the superconducting limits of a material as shown in figure 1.2 which reveals that for the occurrence of superconductivity in a material, the temperature must be below the critical temperature (T_c), the external magnetic field must be below the critical field (H_c) and the current density flowing through the material must be below the critical current density (J_c). It is these upper limits of T_c, H_c, and J_c that the material scientists and engineers have attempted to improve, in the hopes of realizing practical applications. Prior to 1986, the superconductors that were used in wide applications were alloys and compounds like NbTi, Nb_3Sn, V_3Sn, and NbN. These materials were used to construct the first series of superconducting high field magnets. Eventhough, the field and current carrying properties were satisfactory, T_c limited their application because of the use of liquid helium as coolent.

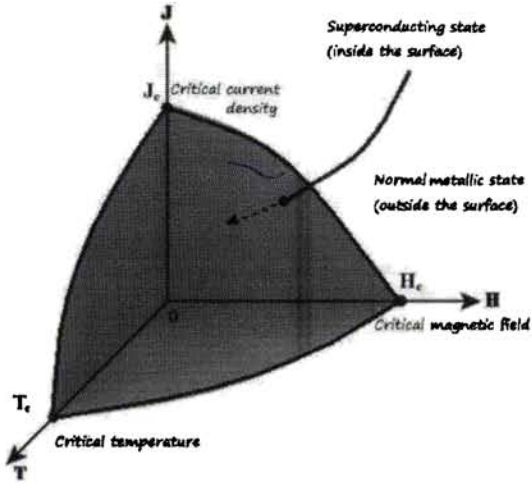

Figure 1.2: Illustration of the functional dependence of the superconducting state with respect to magnetic field, temperature and current density.

It provided a low enough temperature to maintain the operational requirements of the superconductor but the cost of liquid helium made any of its application costlier to maintain or operate.

In 1934, Gorter and Gasimir proposed the first model called two-fluid model [5] to describe superconductivity. Forty years after the discovery of superconductivity, H. Frohlich theoretically predicted the isotope effect [6], which proposed that the T_c decreases when the average isotopic mass increases. In the same year, Ginzburg and Landau developed the phenomenological theory [7,8] which could at least partly explain superconductivity. It takes electrodynamic, quantum mechanic and thermodynamic properties into account and expresses the ***degree of superconductivity*** in a material as a complex order parameter described by the density of superelectrons n_s^* and a phase θ at position $\mathbf{r}$, as $\psi(\mathbf{r}) = n_s^*(\mathbf{r})e^{i\theta(\mathbf{r})}$. Using this expression in an expansion of Gibbs free energy near T_c where the order parameter is small, gives the two ***GL-equations*** which defines two fundamental length scales characterising the superconducting state. They are the penetration depth (λ_L), which has already been mentioned, and

the coherence length, ξ, which characterises the spatial variation of $\psi(\mathbf{r})$ and in an ordinary superconductor, it can be up to a few micrometers in length.

In 1957, Abrikosov [9, 10] successfully predicted the vortex structure in superconductors by applying GL-theory, which provides an immense understanding of the magnetic properties of superconductors. Thus, all the superconductors was divided into two classes, Type I and Type II, based on the ratio of fundamental superconductivity parameters λ_L to ξ. This ratio, $\kappa = \lambda_L/\xi$, is called the ***Ginzburg-Landau parameter***. If κ<0.707, the superconductor is Type I. If κ>0.707, the superconductor is Type II. The more fundamental characteristic distinction for Type I and Type II superconductors is the sign of the interface energy between the normal and superconducting domains. Type I has a positive interface energy, and Type II has a negative interface energy. Type I superconductors do not let the magnetic flux penetrate into its interior (complete Meissner effect) until the magnetic field reaches a critical field H_c above which the magnetic field penetrates the entire material and becomes a normal state conductor. Pure element superconductors mainly belong to the Type I.

The negative normal/superconducting interface energy allows the Type II superconductor to occupy as much interfacial area as possible and hence, Type II superconductors have two critical fields H_{c1} and H_{c2} (Figure 1.3). At H_{c1} the Meissner effect is partly lost and the diamagnetic magnetisation of a sample decreases with increasing field and reaches zero at H_{c2} where superconductivity is destroyed. A type-II superconductor allows the magnetic field to enter the interior of the superconductor in the form of quantised flux lines or vortices. The penetrated magnetic flux consists of discrete quanta called ***fluxons***. Each fluxon has a value of 2.1 x 10^{-15} Wb [11] and is composed of normal state core with a radius of ξ and a vortex of supercurrent with a radius of λ_L. The flux vortices start to enter the sample at H_{c1} where the magnetisation starts to decrease and at H_{c2} the sample is saturated with vortices and the superconductor turns into a normal conductor. This property allows the Type

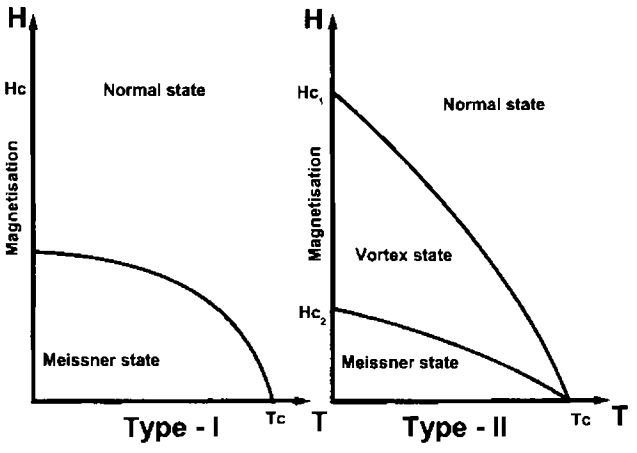

Figure 1.3: The H - T phase diagram for type I and type II superconductors.

II superconductors to remain superconducting in high fields, which is advantageous in many applications such as levitation and transformers. Thus, the GL-theory is a very efficient tool to analyse the physical properties of a superconductor, but it does not give a microscopic explanation to what happens inside the material as it becomes superconducting.

A microscopic quantum theory of superconductivity was first published in 1957 by Bardeen, Cooper and Schreiffer, known as the BCS theory [8, 12, 13], finally explaining the fascinating properties of superconductors from first principles. In a simplified picture of this theory, superconductivity is created by two electrons having wave vectors of opposite sign, $\mathbf{k}+$ and $\mathbf{k}-$ but being equal in magnitude $|\mathbf{k}+| = |\mathbf{k}-|$. Their total wavevector will then be ~ 0, which corresponds to an infinite wavelength. The wavelength is much larger than the distance between the atoms in a crystal, which means that the Cooper pair will not be scattered by the lattice and thus it does not experience any ***resistance*** as it flows through the material. The formation of a Cooper pair requires an attractive electron-electron interaction, being mediated through the

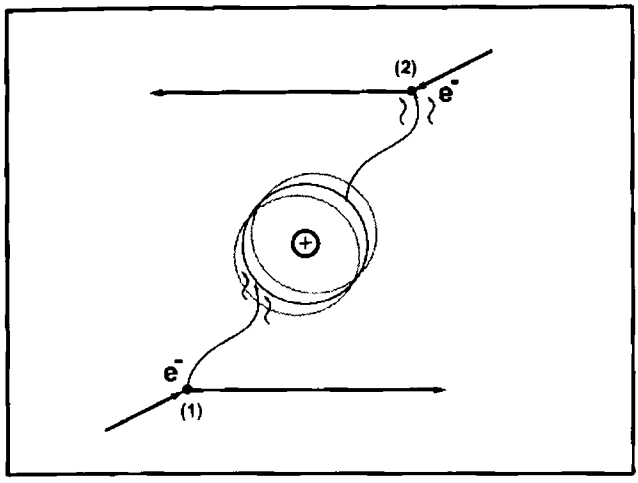

Figure 1.4: Schematic view of the phonon mediated electron pairing. Electron (1) modifies the vibration of the ion, which in turn interacts with electron (2). The net result is an attractive interaction between the two electrons.

lattice (Figure 1.4). The first electron passes through the lattice and causes a small polarisation of the crystal structure and thereby lowers the potential energy between the electron and the atoms. The second electron sees the track of the first electron and takes advantage of the decrease in potential energy caused by the small distortion of the lattice to form a Cooper pair. The coherent superposition of these Cooper pairs into a condensate creates an energy gap in the excitation spectrum which prevents the scattering of electrons and infinite conductivity is maintained in superconducting state. The binding energy of Cooper pairs was estimated to be $\Delta(0) = \frac{3.5}{2} k_B T_c$ at zero kelvin [8, 12, 13], where $\Delta(0)$ is the ***superconducting energy gap***. BCS theory successfully explained superconductivity in low T_c superconductors (LTS), but it failed to satisfactorily explain the high T_c superconductivity in cuprates [14, 15].

No major breakthrough in increasing the T_c was made until the mid 80's (1986), when Bednorz and Muller at the IBM laboratory in Ruschlikon near

Zurich reported superconductivity at 30 K in the La-Ba-Cu-O system [30]. While the critical temperature of 30 K may not seem like much an improvement, it introduced a new material structure, perovskite. Variations of this structure caused the T_c of these materials to quickly increase above the boiling point of nitrogen. These findings blossomed a new era in the superconductivity research, known as ***high-Tc cuprates***. Today, many different cuprate compounds have been found that display superconducting properties at rela-

Table 1.1: Superconducting materials under various classifications [16–29]

Type/class	Example	T_c(K)
Elements	Hg	4.2
	Nb	9.2
	Pd (irradiated)	3.2
	W (thin film)	5.5
	B (under pressure)	11
	Li (under pressure)	20
Amorphous materials	$U_{85.7}Fe_{14.3}$	1.0
	$Th_{80}Co_{20}$	3.8
Organic materials	$(TMTSF)PF_6$[a]	0.9
	κ_H-$(ET)_2Au(CF_3)_4$.TCE[b]	10.5
	κ-$(ET)_2Cu[N(CN)_2]Br$	11.8
Magnetic material	$ErRh_4B_4$	10
Alloys	VTi	7.0
	NbTi	9.0
	MoTc	16.0
A15 type (A_3B)	V_3Ga	14.0
	V_3Si	17.0
	Nb_3Sn	18.0
	Nb_3Ge	23.2

[a] TMTSF = tetra-methyl-tetra-selenium-fulvalene
[b] TCE = 1,1,2-trichloroethane

Table 1.2: Superconducting materials under various classifications (continued)

Type/class	Example	T_c(K)
Laves phase (AB_2)	ZrV_2	9.6
	$LaOs_2$	8.9
Chevrel phase ($AB_xMo_6S_8$)	$SnMo_6S_8$	12.0
	$PbMo_6S_8$	15.0
Heavy electron systems	UPd_2Al_3	2.0
	$CeCu_2Si_3$	0.6
Oxides	$Ba(PbBi)O_3$	13
	$LiTi_2O_4$	13.7
Cuprates	$YBa_2Cu_3O_7$	92
	$Bi_2Sr_2Ca_1Cu_2O_8$	80
	$Bi_2Sr_2Ca_2Cu_3O_{10}$	110
	$Hg_2Sr_2Ca_2Cu_3O_{10}$	135
Doped Fullerenes	$Rb_{2.7}Tl_{2.2}C_{60}$	45
	Cs_3C_{60}	47.4
Borides	ZrB_{12}	5.82
	YRh_4B_4	11.3
	MgB_2	39
Borocarbides	YPd_2B_2C	23
Oxypnictides	$LaFeAsO_{0.9}F_{0.1}$	26
	$SmFeAsO_{0.85}$	55

tively high temperatures. The highest reliable T_c ever measured up to now was in the $HgBa_2Ca_2Cu_3O_8$ system (T_c = 164 K) under 30 GPa pressure [31].

In march 2001, a new type of superconductor, MgB_2 was discovered having a T_c of 39 K [32]. Its peculiarity is that it has a layered structure but not as anisotropic as the cuprates and has two bandgaps open up below T_c [33, 34], implying that there are two types of superelectrons in the material. It has been speculated that this can cause the creation of vortices carrying an arbitrary

fraction of a magnetic flux quantum [35]. Recently, during last year Iron-based superconductor, $LaFeAsF_xO_{1-x}$ (x=0.11) was discovered having a T_c of 26 K [22], which was raised to about 50 – 55 K by doping different rare earths [36, 37], having H_{c2} values of the order of 300 T [27–29]. However, Arsenic toxicity and the necessity of inert atmosphere, high pressure and temperature are the key factors to be addressed before the fabrication of these materials into wires/tapes with better properties [23–25]. Table 1.1 and 1.2 gives some of the superconducting materials of various classes/families.

1.2 High T_c superconductor materials

Bednorz and Muller's discovery that superconductivity at 30 K existed in the layered cuprate $LaBa_2CuO_{4-x}$ opened a whole new area - ***high temperature superconductors*** (HTS) [30]. This new class of compounds gained a great interest and of course the challenge was, how to increase T_c further. Cava et al. [38] substituted Ba by Sr and T_c increased from 30 to 36 K and the width of the transition became narrower. When La was substituted by Y in the above mentioned compounds, a new class of high T_c superconductors $YBa_2Cu_3O_{7-\delta}$ (YBCO or Y-123) was formed by Wu et al. [39, 40]. These compounds are interesting, because they exhibit a $T_c \sim 90$ K, which is higher than the boiling point of liquid nitrogen (77 K). Therefore, scientists and technologists thought that many applications can be achieved by using liquid N_2 which is cheaper and easier to handle than liquid helium. Further, interest on YBCO arose when it was realized that T_c remains unaffected if Y is substituted by different rare earth elements, except for Ce, Pr and Tb [6]. The structure of $YBa_2Cu_3O_{7-\delta}$ was determined by Le Page et al. [40] and Hazen et al [41]. They found an orthorhombic perovskite related layered structure with lattice parameters a = 3.823Å, b = 3.887Å and c = 11.680Å. It was observed that the effect of the oxygen content on the electrical behaviour and

crystal structure of YBCO is very important, because T_c decreases with increasing δ. The system becomes non-superconducting at $\delta > 0.6$ and also the structure changes from orthorhombic to tetragonal [42, 43]. There is a common feature between YBCO and $(LaSr/Ba)_2CuO_4$ because both systems have quasi-2D CuO_2 planes carrying the superconductivity. In addition to the CuO_2 planes, the YBCO system is characterized by additional Cu-O chains along the b-axis which serve as a charge reservoir.

Superconductivity in the Bi-Sr-Ca-Cu-O system was first reported by Bernard Raveau by the substitution of Bi for La in La-Sr-Cu-O ($Bi_2Sr_2CuO_6$ or Bi-2201) which has a crystal structure different from 123 system and has a T_c of $\sim$ 10 K [58]. Later on, Maeda et al. increased the T_c in Bi-Sr-Ca-Cu-O (Bi-2201) system by adding Ca to obtain $T_c > 80$ K and 110 K for $Bi_2Sr_2CaCu_2O_8$ (Bi-2212) and $Bi_2Sr_2Ca_2Cu_3O_{10}$ (Bi-2223), respectively [59]. Hazen et al. [60] and Subramanian et al. [61] studied the crystal structure of $Bi_2Sr_2Ca_1Cu_2O_8$ (Bi-2212) which revealed an orthorhombic layered structure with lattice parameters a = 5.40 Å, b = 5.41 Å and c = 30.9 Å. It was also found that the structure of $Bi_2Sr_2Ca_2Cu_3O_{10}$ (Bi-2223) is similar to Bi-2212 phase because it can be derived from the Bi-2212 phase by inserting an additional (CuO_2+Ca) layer.

Sheng and Hermann [62] discovered the Tl-based high T_c superconductors. The chemical formula of these compounds is similar to that of the Bi-based system. The critical superconducting transition temperature increases by introducing Ca in the Tl-Ba-Cu-O system. Two classes of Tl-based systems were reported [63, 64]. One is $Tl_2Ba_2CaCuO_8$ (Tl-2212) of T_c = 110 K and the other is $Tl_2Ba_2Ca_2Cu_3O_{10}$ (Tl-2223) where T_c = 125 K [65]. The crystal structure of both phases is body-centred tetragonal with a = 3.8 Å and c = 29.2 Å for Tl-2212, while for Tl-2223 the lattice parameter c is larger (35.6 Å) due to an additional (CuO_2+Ca) layer. The most interesting aspect of the crystal structure of Tl-based superconductors is that they can be synthesized with a

High temperature superconductors

Material	T_c (K)	J_c (Acm^{-2})	B_{irr} (T)	Comments	Reference
$YBa_2Cu_3O_7$	92	$2\text{-}5x10^6$	5-9	thin film	Daniels, 2000
	–	$4.5\ x10^6$	9	thin film	Verebelyi, 2000 [44]
$Bi_2Sr_2CaCu_2O_8$	85	$40\ x10^3$	–	thin film	Villard, 2000 [45]
	92	$25\ x10^3$	–	PAIR processed tape	Miao, 1998 [46]
	89	0.2	–	bulk single crystal	Pradhan, 1994 [47]
$Bi_2Sr_2Ca_2Cu_3O_{10}$	110	$12\text{-}63\ x10^3$	0.34	compilation of various tapes from different sources	Schwartzkopf, 1999 [48]
	–	$180\ x10^3$	–	local value from current reconstruction	Feldmann, 2001
$HgBa_2Ca_2Cu_3O_{10}$	130	$3.5\ x10^6$	–	thin film	Yun, 1996 [49]
	132	$< 10^4$	<5	polycrystalline bulk sample	Fujinami, 1998 [50]
$HgBa_2CaCu_2O_8$	124	$3.2\ x10^6$	~ 0.6	thin film	Yan, 1998 [51]
	102		1.2	polycrystalline bulk sample - Ca doped	Akao, 2000 [52]
	110	$< 10^6$	–	thin film	Yu, 1997 [53]
	124	$2.2x10^6$	~ 2.4	thin film on RABiTS^{TM}	Xie, 2000 [54]
$Tl_2Ba_2CaCu_2O_{10}$	99-102	$4\text{-}15x10^5$	–	laser ablation and annealing	Cardona, 1993 [55]
$Tl_2Ba_2Ca_2Cu_3O_{10}$	> 110	$> 10^6$	–	thin film	Juang, 1995 [56]
$TlBa_2CaCu_2O_7$	90-93	$2x10^4$	< 0.8	thin film	Gapud, 1999 [57]

Table 1.3: Properties of selected HTS materials compiled from various sources. All B_{irr} and J_c values are at 77 K and 0 T. B_{irr}, the irreversibility field is the field above which the flux pinning is ineffective and hence the transport critical current density is zero. For comparison, conventional copper cables are operated at 100-400 Acm^{-2}.

variable number of CuO_2 layers and with a variable number of TlO layers, which are the basis for different Tl-compounds. Almost all of these materials contain one or more crystal planes per unit cell consisting of only Cu and O atoms in a square lattice and superconductivity is supposed to originate from the strongly interacting electrons in these CuO_2 planes.

1.3 General crystal structure of HTS

The key structural element of all high T_c superconductors is the set of **n** CuO_2 planes separated by the charge reservoirs. Materials such as $La_{2-x}Sr_xCuO_4$ (La-214) and $Nd_{2-x}Sr_xCuO_4$ (Nd-214) contain one plane per unit cell and are referred to as single layered compounds. The most commonly studied Bi-2212 and Y-123 systems are double-layered systems with n=2 planes per unit cell. The electron transport and processes responsible for superconductivity at high T_c are believed to be intimately connected to CuO_2 planes. Several families of cuprates can be synthesized with n=1,2,3 (Table 1.3). Within each family, the transition temperature increases with number of CuO_2 layers. Also, the cuprates are characterised by superconducting CuO_2 planes separated by non-

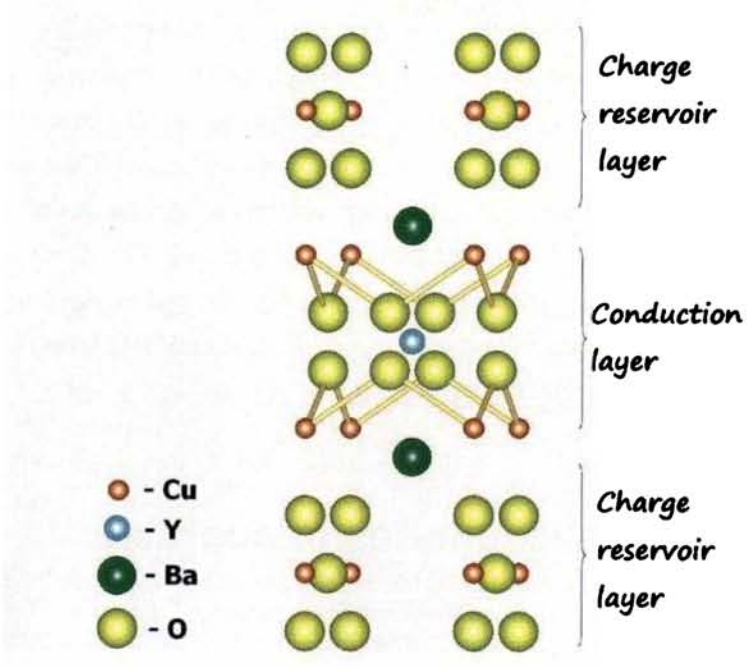

Figure 1.5: An illustration of the general crystal structure of high T_c superconductor : Structure of $YBa_2Cu_3O_{7-\delta}$.

metallic interlayers acting as charge reservoirs for the CuO_2 planes. It has an orthorombic or tetragonal lattice structure, with an elongated c-axis while the a and b axes are of comparable or same length.

The general chemical formula of high T_c superconductors can be empirically represented $A_mE_2Ca_{n-1}Cu_nO_{2n+m+2+y}$, where **A** = Bi/Pb/Tl/Hg/Au/Cu/Ca/B/Al/Ga, **E** = Ba or Sr, **m** and **n** are integers. The choice of E depends on the active layers (AO_x) involved, since it has to provide necessary spatial adjustment of CuO_2 to the AO_x layers. These active layers and ($CuO_2/Ca_{n-1}/CuO_2$) stacks are separated by charge reservoir stack, $EO/(AO_x)_m/EO$. Superconductivity in high T_c superconductor is believed to have its origin from different superconductive interactions existing in the CuO_2 layers. Strongest of all these interactions is the ***intralayer coupling*** within each CuO_2 layer. ***Interlayer coupling***, the superconductive interactions between CuO_2 layers within a given ($CuO_2/Ca_{n-1}/CuO_2$) stack, is weaker than intralayer coupling. The weakest of all is the Josephson's coupling, which exists between different ($CuO_2/Ca_{n-1}/CuO_2$) stacks across the insulating interlayers. For example, in figure 1.5 showing the Y-123 structure, one can clearly see stacks of the simple cubic perovskite. On inspecting the structure, one plane at a time, one finds that the orthorhombic Y-123 structure consists of layers such as, CuO, BaO, CuO_2, Y, CuO_2, BaO and CuO, beginning at the bottom and proceeding upwards. Thus, in Y-123 superconductor, (CuO_2/Y/CuO_2) and BaO layers act as CuO_2 stack and active layer, respectively.

1.4 Characteristic features of cuprates

Referring to the previous section, it is evident that all of high T_c superconductors contain one or more crystal planes per unit cell consisting of only Cu and O atoms in a square lattice. Superconductivity originates from the strongly interacting electrons in these CuO_2 planes. The Cu atoms are believed to be in

the Cu^{2+} or $3d^9$ configuration with spin (1/2). As shown schematically in the left panel of figure 1.6, the overall electronic state is then an antiferromagnetic Mott insulator, because Coulomb repulsion prevents electron hopping from Cu to Cu, and the exchange correlation is antiferromagnetic in nature. A theoretical justification for using this simplified single-band picture was given by Zhang and Rice [66].

Doping these insulating CuO_2 layers with holes (or electrons) causes the appearance of new electronic ordered states [67], including high-temperature superconductivity. This is because with doping, hopping of electrons from Cu to Cu becomes possible-as shown in the right panel of the figure 1.6. A schematic phase diagram of hole-doped cuprates (which are the most widely studied examples of the cuprate high-temperature superconductors) is presented in fig-

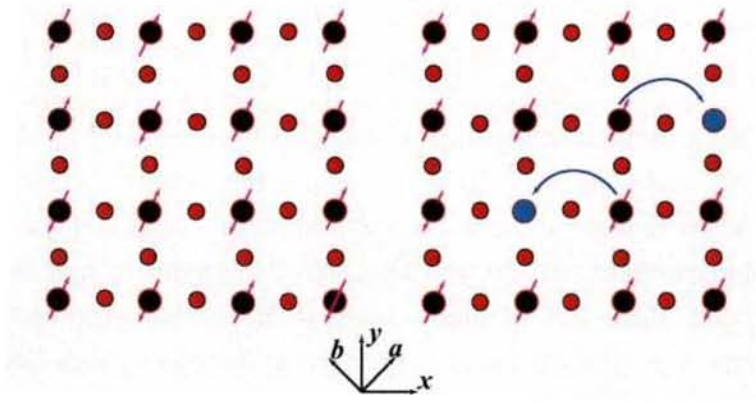

Figure 1.6: Simple model for the relevant electronic degrees of freedom in the CuO_2 plane of cuprate high temperature superconductors. Bond axes (x/y) and BSCCO crystallographic axes (a/b) are shown. Left panel: Square lattice with one spin (1/2) state at every vertex. Coulomb repulsion prevents electron hopping, and antiferromagnetic correlations impose an overall antiferromagnetic ground state. Right panel: With hole doping, electron hopping becomes possible. (Black = Cu, Red = O).

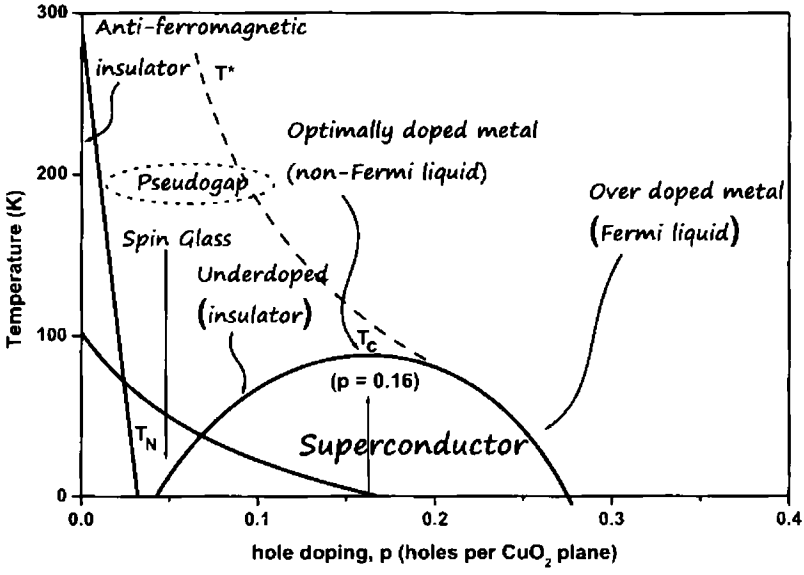

Figure 1.7: Generalized phase diagram of the hole doped cuprate superconductors. T_N = Neel temperature; T* = pseudogap energy. (Hole doping is expressed as holes per CuO_2 plane).

ure 1.7. They exhibit superconducting critical temperatures up to 150 K at ***optimum*** hole doping near $p \sim 0.16$, where p is the number of doped holes per Cu atom. At zero temperature, the undoped parent compound is a charge transfer (Mott) insulator, with an antiferromagnetic ordering of spin states on the copper sites of the CuO_2 lattice. Unlike in regular band-gap insulators, charge transport in Mott insulators is inhibited at the cost of high Coulomb energy associated with ***doubly occupied*** copper sites. Removing electrons (in other words, creating holes) allows charge to flow by leaving some proportion of vacant sites for electrons to hop into, a process which also destroys the antiferromagnetism. Introducing small numbers of mobile charge carriers in this way, with low levels ($p < \sim 0.06$) of hole doping, first produces a poorly conducting (and poorly understood) spin glass state. At slightly higher doping, when a sufficient concentration of charge carriers is present, the superconduct-

ing state mysteriously emerges. The exact reason for this is one of the most important unsolved problems in physics. Superconductivity is most resilient against increases in temperature and magnetic field at an optimal doping level of around $p \sim 0.16$, but persists until above $p \sim 0.25$, at which point the crystal behaves like a metal, and any of the remaining antiferromagnetic order disappears [68].

1.4.1 Symmetry of superconducting energy gap

In conventional superconductors, an attractive electron-electron interaction exists and is mediated by phonons, which represents small distortions in the atomic lattice that couple to the electrons (Cooper pairs). At sufficiently low temperatures, Cooper pair formation can occur without being frustrated by

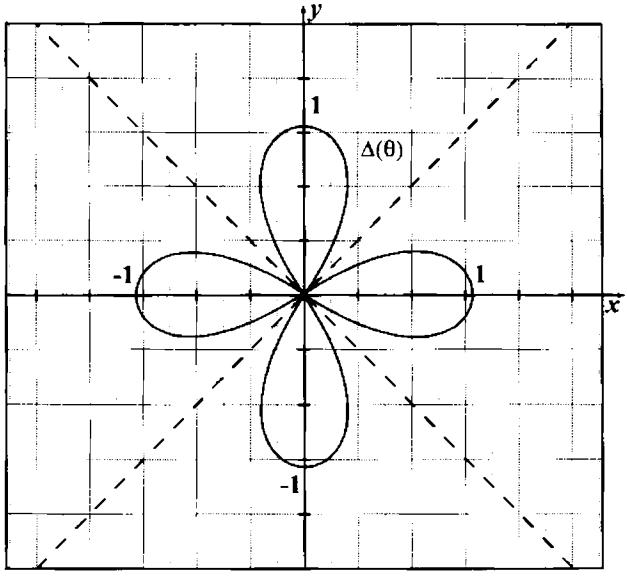

Figure 1.8: Gap magnitude as a function of the direction of the momentum for a d-wave superconductor, showing $d_{x^2-y^2}$ symmetry (units of Δ_0).

thermal excitations. Each pair can be considered as a bound state of two electrons with opposite spin and momentum. The formation of Cooper pairs opens an energy gap, whose width is denoted by Δ, in the density of electronic states at the Fermi level. This gap in the density of states, is a hallmark property of superconductivity and corresponds to the pairing energy of the Cooper pairs. Within the gap, no quantum states exist for the unpaired electron. At energies $E > \Delta$ (outside the gap), new excited states appear which is known as Bogoliubov quasiparticles. Near the Fermi energy, these quasiparticles have a density of states (DOS) and dispersion relation, given by equation (1.1).

$$N_s(E,\theta) \sim \frac{E}{\sqrt{E^2-\Delta^2}} \tag{1.1}$$

Microscopically, the cuprate high-temperature superconductors exhibit many important differences from conventional superconductors. For example, the superconducting wave function of high-temperature superconductors is believed to have $d_{x^2-y^2}$ symmetry [30, 69]. The most critical difference between cuprate and conventional superconductors is that all characteristic length scales are near 1 nm: the Cu interatomic distance $a_0 \sim 0.3$ nm, the interdopant atom distance L $\sim$ 1.5 nm, the Fermi wavelength $\lambda_F \sim 1$ nm, and the superconducting coherence length $\xi \sim 1.5$ nm. This means that different electronic phenomena can interact strongly with each other at the nanoscale in cuprates. No widely accepted pairing mechanism has been identified to explain superconductivity in the cuprates.

$$N_s(E,\theta) \sim \int d\theta \frac{E}{\sqrt{E^2-(\Delta_0 cos 2\theta)^2}} \tag{1.2}$$

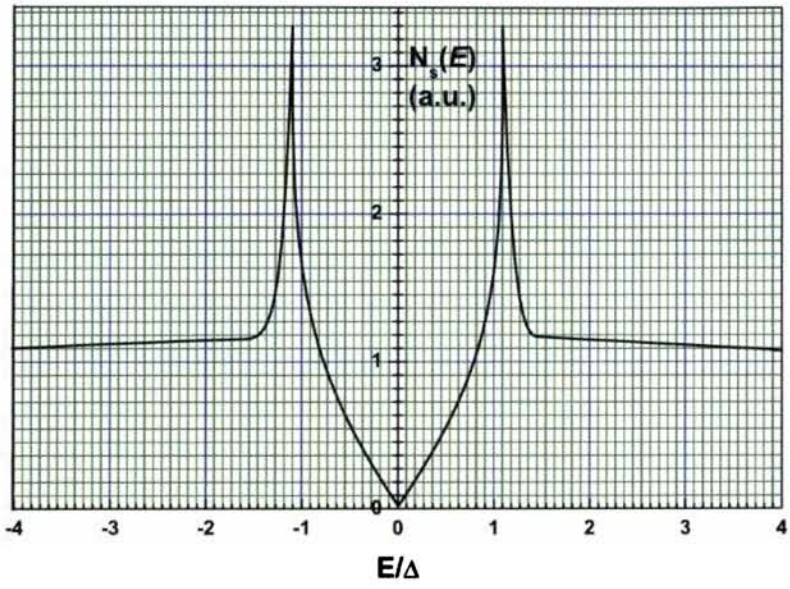

Figure 1.9: The predicted density of states of a BCS superconductor with d-wave gap symmetry.

Figure 1.8 illustrates the momentum dependence of the energy gap. Its $d_{x^2-y^2}$ symmetry means that it has nodes (i.e. takes zero values) in the four directions given by the dashed lines, at 45^o to the main axes. As a result, these directions are often referred to as the nodal directions. In the bismuth-strontium-calcium cuprate family of superconductors, these directions align with the a/b-axes of the crystal. The antinodes, directions in which the gap reaches its maximum value Δ_0, coincide with the x and y directions defined by the square lattice formed by the copper atoms. If the BCS density of states equation (1.1) is modified to take into account this direction-dependent gap function, then the density of states function $N_S(E,\theta)$ will also be direction-dependent. Integrating over all directions gives the expected total density of states which is represented in equation (1.2) [70]: This function is plotted in figure 1.9, which represents the predicted density of states at Fermi level of a BCS superconductor with d-wave gap symmetry. For energy Δ, slightly

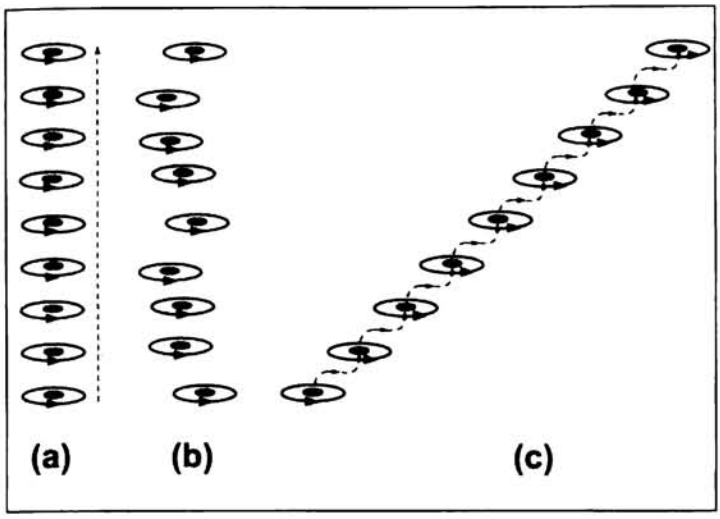

Figure 1.11: Stacks of 2D pancake vortices: (a) straight stack, the configuration of lowest energy at zero temperature, and (b) disordered stack, which occurs at higher temperatures. (c) Sketch of a tilted stack of pancake vortices in successive superconducting layers, connected by interlayer Josephson strings.

diameter of the cylinder is of the order 2ξ and the density of Cooper pairs $|\psi|^2$ decreases to zero at the vortex centers (see Figure 1.10). The direction of the circulating supercurrent around the core is such that the direction of the magnetic field generated by the current coincides with that of the external field and is parallel to the normal core. The magnetic field and the circulating currents decay radially out from the core as $B(r) \propto \ln(\lambda_L/r)$ at short distances and as $B(r) \propto r \exp(-r/\lambda_L)$ at long distances from the vortex centers. The circulating supercurrents surrounding the vortex core, predominantly located in the CuO_2 planes, cause an interaction between the vortices, which is repulsive (attractive) for parallel (antiparallel) vortices. The interaction extends to a distance of the order λ_L. If a thin enough sample is used with thickness $d \ll \lambda_L$, the magnetic screening is less effective and the penetration depth is replaced by an effective two dimensional (2D) penetration depth, which is defined as [71, 72] $\lim_{\lambda_L \gg d} \Lambda = 2\lambda_L^2/d$. This also means that vortex interactions in 2D systems extend over larger length scales compared to bulk materials.

Within a single grain, the J_c is controlled by the flux pinning properties of the materials. Flux pinning is the mechanism where by the dissipative movement of vortex under the Lorentz force is prevented by flux pinning centers. The flux pinning centers can be various defects such as point (cation disorder, oxygen vacancies), line (dislocations), planar (antiphase boundaries, stacking faults, twin boundaries), and volume (precipitates, macroscopic non-uniformity) defects. Good flux pinning is essential for significant transport current density to be sustained in the superconducting state, and to maximize the irreversible field (H_{irr}). The size of the defects is set by the coherence length ξ, and the optimal density of defects is determined by the vortex spacing, given approximately by $(\phi_0/B)^{1/2}$, where B is the applied field. The pining defects are largely unknown for high T_c superconductors, because the coherence length is so small that even atomic-size defects can pin vortex. This extreme sensitivity of high T_c superconductors to nanoscale defect structure is vitally important in determining the current-carrying capability of conductors. An illustration of the definitions of the length parameters λ and ξ in anisotropic high T_c superconductors is given in figure 1.10. Figure 1.11, illustrates how the vortices created in a layered superconductor are broken up into a stack of *pancakes*. When the field is tilted, the pancakes are connected by horizontal Josephson vortices, shown in the figure only as horizontal lines. An important distinction is the fact that pancakes have a normal core, while the Josephson vortices have no such core.

1.4.3 Weak superconducting coupling across grain boundaries

The grain boundaries (GBs) in cuprates are structurally and compositionally heterogeneous on a scale of $\sim$ 5 nm, comparable to the coherence length ξ. (The coherence length ξ is a measure of the distance within which the superconducting electron concentration cannot change drastically in a spatially-

varying magnetic field, simply being interpreted as the pairing length of the superconducting electron pairs.). Low angle GBs consists of grain boundary dislocation cores and conductive, grain-like channels [73]. The atomic disruptions at the dislocation cores and the strain fields surrounding the cores depress the superconducting order parameter [73,74] and disrupt the supercurrent over a region of 1-2 nm near the grain boundary cores. Wider depleted regions have been seen for higher misorientations, resulting weaker coupling across the GBs [75]. The GBs reduce critical current density J_c. It has been established that the J_c across grain boundaries is strongly dependent on the misorientation angle [76] and the J_c across the GBs decreases exponentially with increasing misorientation angle beyond a given critical angle θ_c [77,78]. It is therefore very important to reduce GBs in order to maximize current carrying capability of the grains.

1.4.4 Summary

- The cuprates are extreme type II superconductors [79], with $\lambda_{a,b,c} \gg \xi_{a,b,c}$
- The penetration depth is highly anisotropic [79], with $\lambda_c \gg \lambda_{ab}$.
- Superconductivity arises in the CuO_2 planes, which are antiferromagnetic in the undoped state.
- The charge carriers in the superconducting state are 2e Cooper pairs [80, 81], and are spin singlets [82,83].
- The superconducting wavefunction has $d_{x^2-y^2}$ symmetry (where x and y are the Cu-O bond axes), as does the gap energy [84,85].
- The energy gap is similar to that predicted by d-wave BCS. However, it persists in parts of the phase diagram that are non-superconducting [86,87] and is systematically asymmetric [88].

- The pairing is likely to be local, on the scale of ~ 2 nm. Granular patches of near-constant gap are observed at this length scale, with gap energies varying widely between patches [70].
- Density of states spectra evolve from small gaps and sharp coherence peaks, to wide gaps and low coherence peaks. The same evolution is seen with decreasing bulk doping [89], nearby dopant sites [90], and at the top of the supermodulation.
- At low doping, the lifetimes of nodal quasiparticles are greater, while at high doping, those of the antinodal (x/y-direction) quasiparticles are greater [91].

1.5 Physics behind the high T_c superconductors

High temperature superconductivity cannot be explained by BCS theory because it regards the electrons initially to be non-interacting Fermi gas, as in a metal. By contrast, high temperature superconductors are Mott insulators in their normal state. They have very strong interactions resulting from Coulomb forces and available energy levels on the CuO_2 grid. Understanding the pairing mechanism requires identifying the nature of the quasiparticles being paired, which are likely to be more complicated than the simple electron-like quasiparticles of a metal, and identifying the attractive force that pairs them. Any complete theory of high temperature superconductivity must begin with the structure of the crystal, and explain three main processes:

1. Formation of the relevant fermion state.
2. Propagation of fermion state.
3. Pairing mechanism.

There is no consensus yet on how any of these three processes operate in the cuprates. One of the contending explanations was proposed by Anderson [92] shortly after the discovery of high temperature superconductivity. He addressed processes 2 and 3, arguing that a nearly half-filled Hubbard model could describe the propagation of holes through the CuO_2 plane, and that resonating valence bonds would similarly reduce the energy of the system and result in paired bosonic objects, free to move charge through the crystal without resistance. Process 1 was later filled in by Zhang and Rice [66], whose results are described below in section 1.5.2.

1.5.1 The Hubbard model

The single-band Hubbard model and its variations have become the most common framework used for making theoretical analyses and predictions about the cuprates [93]. They are tight-binding models, which says that each electron is modeled as being bound to a specific discrete site, as opposed existing in a state with more continuous degrees of freedom. In its original formulation, the Hubbard model only allows electrons to move directly to immediately adjacent sites (called nearest neighbour hopping, controlled by the transfer parameter t), but extensions to the model can also include next-nearest neighbour hopping (parameterized as t'), or even greater hops (t'', etc.). Among the biggest successes of this model is its ability to produce a normal state Fermi surface consistent with experimental measurement. As a result, such measurements are routinely parameterized in terms of the hopping parameters of the model.

The Hubbard model consists of a simple two-part Hamiltonian intended to describe a system of strongly interacting particles, such as the electrons in a Mott insulator. The particles are assumed to be on a lattice with up to two present at each site. The Hubbard Hamiltonian is:

$$H = H_{hop} + H_{int} \tag{1.3}$$

and

$$H_{hop} = \sum_{k,\sigma} \varepsilon(k) n_{k,\sigma} \tag{1.4}$$

and

$$H_{int} = \sum_{x \in \Lambda} U_x n_{x,\uparrow} n_{x,\downarrow} \tag{1.5}$$

where, H_{hop}, the energy required by the particles to hop from one site to another, Λ is the set of lattice points and n is the number operator. This form is originally written by Gutzwiller [94] in which, the kinetic energy term H_{hop} is given in momentum space terms. The second term (H_{int}) represents the energy required for two particles to occupy the same lattice site, and is referred to as the interaction term. Shortly after Gutzwiller wrote it in this form, the first term of the Hamiltonian was rewritten in real space terms by Hubbard [93]:

$$H_{real\ space} = \sum_{x,y,\sigma} t_{x,y} c^{\dagger}_{x,\sigma} c_{y,\sigma} + \sum_{x} U_x n_{x,\uparrow} n_{x,\downarrow} \tag{1.6}$$

where, c and $c^{\dagger}$ are creation and annihilation operators respectively, t is the kinetic energy (or ***transfer***) term, and $\sigma \in \{\uparrow, \downarrow\}$. While x and y can refer to any sites in the lattice, the matrix element $t_{x,y}$ is non-zero only when they are nearest neighbours. Despite its simple form, with suitable choices of t and U, the Hubbard model can be shown to exhibit a range of properties including magnetic order such as antiferromagnetism [95]. As $U \rightarrow 0$ for nonzero t in equation (1.6), the system approaches a non-interacting state, with plane wave solutions and a dispersion relation given by $\varepsilon(\vec{k})$ in equation (1.4). At the other extreme, as U becomes large with respect to t, the energy required for two particles to occupy the same site becomes large and the system is referred to as *strongly correlated*. In the half filled Hubbard model, the number of electrons become same as lattice sites. By increasing $U \rightarrow t$, the model

describes a transition from metal to Mott insulator (a *Mott transition*), since the increasing Coulomb repulsion at a particular site, prevents electron transport from site to site. This brings us closer to a plausible model of the normal state CuO_2 plane in the cuprates.

1.5.2 The t-J model

Although the Hubbard model can display many properties of Mott insulators, it does not, at least in its original form, offer any direct insights into the cuprates. For that, a model was needed that represented the behaviour of electrons and holes in the CuO_2 plane. Emery proposed [96] a three-band Hamiltonian that accounted for the various energy contributions of electrons and holes in the copper and oxygen orbitals, and of those hopping between them. Zhang

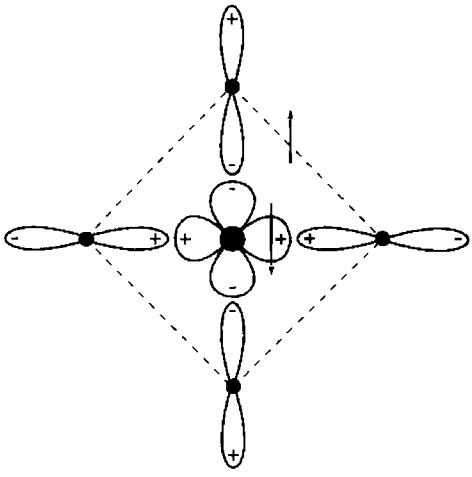

Figure 1.12: The Zhang-Rice singlet. Four oxygen atoms (black) surround a central copper atom (blue). A down-arrow represents the spin of the hole present on any copper site, and an up-arrow represents the spin of a dopant-induced hole on the oxygen sites.

and Rice were able to simplify this construction significantly by introducing the object now known as the Zhang-Rice singlet state [66]. It was known experimentally that holes in the CuO_2 plane actually lie on oxygen sites. In the half-filled (U - t) Hubbard model, each copper atom can be regarded as having a $d_{x^2-y^2}$ hole, since it has a $d_{x^2-y^2}$ state with only one electron in it. This hole is depicted in as having spin-$\downarrow$ in figure 1.12. Zhang and Rice argued that once the material is hole doped, any hole on the surrounding oxygen atoms can form a lower energy state by hybridizing with the central copper hole to form a singlet state, as depicted in the figure 1.12. These singlets would then be free to travel around the crystal, hopping from site to site, always centred around one copper atom. Because the motion is centred on the copper atoms, the system can be described with a one-band model that disregards the oxygen sites. The result is a theoretical justification for the validity of using the ***t-J model***, as originally proposed by Anderson [97], to represent the in-plane electronic structure of the cuprates. This model is constructed by taking the $U \rightarrow t$ limit of the Hubbard model, and introducing an antiferromagnetic interaction term:

$$H_{int(t-J)} = J \sum_{\langle i,j \rangle} \left(\mathbf{S}_i . \mathbf{S}_j - \frac{1}{4} n_i n_j \right) \tag{1.7}$$

where $\langle i, j \rangle$ are nearest-neighbour pairs, $\mathbf{S}_i$ are spin 1/2 operators. The full *t-J* Hamiltonian thus is:

$$H_{real\ space} = \sum_{x,y,\sigma} t_{x,y} c^{\dagger}_{x,\sigma} c_{y,\sigma} + J \sum_{\langle i,j \rangle} \left(\mathbf{S}_i . \mathbf{S}_j - \frac{1}{4} n_i n_j \right) + \sum_x U_x n_{x,\uparrow} n_{x,\downarrow} \tag{1.8}$$

The antiferromagnetic interaction energy J is equal to $4t^2/U$ because of the possibility of a virtual spin-flipping process involving a hop to an adjacent occupied site and back. This model produces an antiferromagnetic ground state (in the U$\rightarrow \infty$, or undoped limit) since the energy of the system can be lowered by ensuring that neighboring electrons have oppositely aligned spins.

Numerical studies of the two-dimensional *t-J* model suggest that at optimal values of the parameter *J/t* ($\sim$ 0.3 - 0.4), the holes form bound pairs with an effective attractive force acting between them. These pairs can then be expected to condense at low temperatures, leading to superconductivity [98]. In this picture, the formation of the pairs does not immediately require that they condense into a single ground state, which potentially explains the pseudogap state - the region of the phase diagram exhibiting a precursor energy gap but no superconductivity (Figure 1.7). It should be noted that, despite being the most frequently cited, the Zhang-Rice singlet is not the only plausible state to be proposed as the charge carrying unit in the cuprates. It is necessarily centred on the copper atoms of the CuO_2 plane, but experimental evidence of oxygen-centred, static charge ordered states has recently begun to emerge.

1.5.3 Gutzwiller projection

The method of Gutzwiller projection was proposed [94] as a variational approach to solving the Hubbard model in magnetic metals by taking into account strong local Coulomb repulsions. In the Hubbard model, as mentioned, these strong repulsions correspond to a situation where $U \rightarrow t$. In its complete form, the Gutzwiller projection operator takes a wave function and projects out the components that represent doubly occupied lattice sites. This is a projection in the mathematical sense since it lowers the dimensionality of the space of wave functions (a Hilbert space), which has the benefit of reducing the computational complexity of the problem. The form of the operator originally written down by Gutzwiller, referred to here as the ***partial Gutzwiller projector*** $\hat{P}_{partial}$, included the variational parameter α (written in a different but equivalent form by Gutzwiller), which was to be determined so as to minimize the ground state energy:

$$\hat{P}_{partial} = \prod_i [1 - \alpha n_{i\uparrow} n_{i\downarrow}] \tag{1.9}$$

Setting $\alpha = 0$ in equation (1.9) corresponds to the uncorrelated state and gives us the identity operator. Setting $\alpha = 1$ gives us a complete projection, which we refer to as the (complete) Gutzwiller projection:

$$\hat{P} = \prod_i [1 - n_{i\uparrow} n_{i\downarrow}] \tag{1.10}$$

This form is used in most recent applications, such as Anderson's proposal concerning the origin of the asymmetry in the cuprate tunnelling spectrum [88]. Gutzwiller projection has a range of applications, not all confined to the electronic structure of crystals. For example, Liquid Helium consists of densely packed fermionic atoms. As a result of the proximity of the atoms to each other, it can be considered a strongly interacting system: no two Helium atoms can be in the same location, just as no two electrons in a strongly correlated electron system can be on the same site. As helium atoms are not arranged in a lattice, the Hubbard model is not directly applicable. Still, by starting with a more general form of the Hamiltonian that does not require a lattice structure, the Gutzwiller projection operator can enforce the prohibition on double occupancy. By this method of analysis, it is possible to model Helium sufficiently accurate to predict a range of real physical properties [99].

1.5.4 Resonating valence bond state

Very soon after the discovery of cuprate superconductors, Anderson suggested [97] a pairing mechanism termed the ***resonating valence bond*** **(RVB)** . In contrast to the BCS theory of conventional superconductors, the pairing mechanism proposed by Anderson for high-temperature superconductivity does not rely on phonons. Instead, the pairing is electronic and magnetic in origin. Singlet pairs of opposite-spin electrons are formed, reducing magnetic energy. By analogy with resonating states like Pauling's Benzene ring and Bethe's linear antiferromagnetic chain, the configuration of these pairs is

allowed to resonate among all possible arrangements, further increasing stability. Anderson forms the RVB state by Gutzwiller projection of a BCS wave function. So, rather than trying to create superconductivity out of the parent Mott insulator state, he begins with a superconducting state and adds in the effect of strong electron-electron correlations. Gutzwiller projection is carried out in order to ensure single occupancy of each of the lattice sites. At half filling, when the number of electrons and lattice points is the same, the RVB pairs cannot move and the material is insulating: this is consistent with the parent Mott state. Below half filling, when the material is hole doped, these pairs become mobile (since the electrons can hop into neighboring holes) and can carry the supercurrent. As mentioned, this pre-formed pair model has the advantage of offering an intuitive explanation for the pseudogap, as the binding energy for the immobile, uncondensed pairs.

1.6 Present status and the need for further development of HTS applications

More than a couple of decades have passed since high T_c superconductors were discovered amid a rash of over-enthusiastic claims that these materials would immediately revolutionize the power, transport and communications industries. The public perception may be that after years of research and unprecedented industrial investment, there still seems to be no theory of high T_c superconductivity and no practical applications either. However, the reality is very different. Many aspects of physics and chemistry in cuprate superconductors are now well understood, while the remaining problem is providing a rich source of new physics. More importantly, a wide range of major industrial applications are set to appear within next few years. The key factor that has limited the widespread use of conventional low T_c superconductors (LTS), such as Nb_3Sn and NbTi, is the cost of cooling them at around 4 K with liquid

Helium technology. In fact, the cost of the LTS wire itself is low. With the discovery of HTS materials, expectations of an immediate technology revolution based on HTS were heightened. This development was not at all sudden. As with any new technology, it typically took 15 – 20 years to solve the technical challenges and to reduce costs. In the case of high T_c superconductors, particularly, some demanding issues are presented by the microstructure of these materials.

High T_c superconductors are brittle ceramic materials, have layered atomic structure which causes the materials to have highly anisotropic physical and superconducting properties. It is possible to form single crystals, thin films or polycrystalline ceramics from these materials. Generally two types of wire architecture are considered for the manufacturing of long flexible wires : either, thin epitaxial films of HTS material grown on long flexible substrates, or polycrystalline filaments of HTS supported in a metallic wire matrix. Several issues emerged from early investigations using granular ceramics. HTS materials have very short coherence length (less than 2 nm). This means that the grain boundaries should be smooth and free from disorder over a length scale significantly less than 2 nm. In addition, HTS are quasi two-dimensional structures comprising weakly coupled CuO_2 layers, making it highly anisotropic. The two factors - the coherence length and the anisotropy suggest that the performance of polycrystalline HTS wires can be enhanced by improving the microstructure, namely making it dense, increasing the degree of grain alignment and having high quality grain boundaries. Otherwise, J_c would seriously degrade in a weak magnetic field. Even in the absence of the external magnetic field, J_c in a weak-linked superconductor may suffer from the ***self-field*** generated when current passes through the wire.

Although there are different kind of HTS materials, only $Bi_2Sr_2Ca_1Cu_2O_{8+\delta}$ (Bi-2212) and $Bi_2Sr_2Ca_2Cu_3O_{10+\delta}$ (Bi-2223) have been used successfully to form long-length HTS wires. No other HTS system has yet been textured in any practical sense to form long-length wires.

1.6.1 Wire manufacture

Wires of high T_c superconductors comprising many filaments of Bi-2212/Bi-2223 are typically processed by first packing a precursor powder into Ag tubes, which are extruded and drawn until they reach about 1 mm in diameter. These wires may then be re-bundled and drawn several times until the desired number of filaments and wire dimensions are reached. The resulting product is then rolled to form a flat tape and heat-treated until the precursor reacts to form sintered Bi-2212/Bi-2223. During these processes, various grain deformation takes place in the precursor and the resultant product becomes progressively aligned. The tape may be rolled and heat-treated several times until the grain alignment, density and concentration of Bi-2212/Bi-2223 are optimised.

A unique advantage of Bi-based systems is that texturing can be induced by progressively deforming Bi-2212 or Bi-2223. The flexible behaviour of these materials derives from the weak bonding across the double layer of bismuth oxide (BiO), which provides a ***slip system*** which allows deformation induced texturing. However, this double layer also seriously degrades the intrinsic performance of the Bi-based superconductors.

Among the HTS cuprates, Bi-based systems have relatively low J_c in magnetic field, which limits their use in practical applications. The weakly linked CuO_2 layers readily decouple in an applied magnetic field, causing resistive conduction even though the HTS material remains strictly superconducting. This decoupling is governed by the spacing between the CuO_2 layers. The spacing is large in Bi-2212 and Bi2223 because the CuO_2 layer is separated by a double layer of BiO. As a result, the sustainable magnetic field for these two materials is about two orders of magnitude lower than $YBa_2Cu_3O_{7-\delta}$ (Y-123). Although this does not preclude the use of Bi-based superconductors in applications, it does mean that this material must be used at intermediate temperatures when large magnetic fields are required. For example, the operating

temperature of HTS motors using Bi-2223 wires in 1 – 3 T magnetic fields is currently confined below 35 K.

The motivation for finding a practical wire technology for Y-123, therefore obviously leads to epitaxial thin films deposited on deformation-textured substrates using coated conductor technology. Short length of these so-called **second generation** HTS wire have demonstrated J_c values as high as 10 $MAcm^{-2}$ at 77 K. Currently, the manufacturing process is prohibitively slow as it uses vacuum deposition techniques. However, very promising results have recently been obtained using rapid technique by depositing HTS material from solution.

A further practical issue lied in the cost of producing HTS wire. Silver remains an indispensable, yet expensive, component of Bi-based wire technology. Moreover, the processing of the wires is very slow, requiring up to a week for extrusion, drawing, rolling and heat treatment. According to a number of manufacturers, several years ago the cost of HTS wire was around $1500 per kiloamp per metre, divided almost equally between raw materials, mechanical treatment and heat treatment. Recently, however, American Superconductor Corporation expects to reduce the price to around $50 per kiloamp per metre. In part, such gains are based on the continual increase in the J_c of production wires.

In spite of these challenges, enormous progress has been made in developing wire technology and in prototyping a broad range of HTS based products, to the extent that several companies have now reached commercial levels. Virtually, defect-free wires exceeding 100 A per strand at 77 K for Bi-2223 are now available in lengths of several hundred meters. Wires up to 1 km in length have also been demonstrated. Currently several companies are rapidly scaling up their manufacturing capacity to several hundred kilometres of wire per year.

Many applications of HTS have come forth in recent years. These applications were based on wire and film development technology. In both cases,

wider issues involving cryogenics, the interface between the HTS and the ambient environment and nonlinear scaling up issues have been addressed.

1.6.2 HTS power cables

In most countries, the loss in distributing electrical power from power stations to consumers is at the 7-9% level which is worth about 1.7 billion pounds per year in U.K. alone. This is a compelling motivation for superconducting cables, which at least in a DC environment could virtually eliminate such electrical losses. Although cooling losses would remain, these can be engineered to be small.

A broad range of prototype HTS cables have already been implemented. All have a similar design comprising concentric sheaths of insulation, cooling ducts, shielding , dielectric and conductor and are cooled to 70-77 K using liquid nitrogen which is pumped through the central core. Several commercial scale HTS cables were tested in fully operational environments starting from 2005. The major project includes a Pirelli led project at Detroit Edison in Michigan. Pirelli manufactures cables from HTS wires made by American Superconductor Corporation. In addition, HTS cables were demonstrated by Southwire in Georgia, US, but these were not connected to the electricity grid. Meanwhile, the Tokyo Electric Power company, the largest private electric utility in the world has funded demonstration of HTS cables at Sumitomo Electric and Furukawa Electric. Other active HTS-cable programmes are maintained by BICC in the UK, Nordic Superconductors in Denmark, Australian Superconductors Ltd and Fujikura and Chubu Electric Power company in Japan.

Detroit Edison's 100 MVA cable is 120 m long and comprises three single phase HTS cables rated at 24 kV. It replaces nine copper cables at a substation in Detroit and supplies sufficient power for 30,000 residential customers

with a substantial reduction in the total weight of the cables (about 70 times less than the weight of copper cables). Once the operational demonstrations are proved to be successful, complete commercial implementations can be expected within next few years. Also, a recent study predicts that HTS cables will account for 56 % of the underground transmission market within 10 years of the first commercial sale [100].

1.6.3 Motors and Magnets

According to industry reports, the total worldwide market for electric motors rated above 1000 horsepower (HP) is 1.3 billion USD per year. Moreover, such motors are estimated to use about 30 % of all the electricity generated in the US. The conversion of HTS technology is beneficial in this area, which include reducing the size and losses by 50 %, as well as improving the stability during operation. A size reduction of this magnitude is a major benefit for certain applications, such as ship propulsion.

Currently, the major programme in HTS motors is being undertaken by a long-standing partnership between American Superconductor and Reliance Electric. Following the success of a 286 HP prototype motor, the partners had completed the first commercial - scale HTS motor - a 1000 HP AC synchronous $air-core$ motor. The cryo-cooled rotor contains four HTS coils, which allow higher magnetic fields than their conventional counterparts while eliminating the need for heavy iron cores. They also completed a 5000 HP commercial HTS motor. Based on the success of these demonstrations, American Superconductor received a contract from the US Navy to design a 25000 HP HTS ship-propulsion motor.

A range of demonstration HTS magnets have been developed since HTS wire development in the early 1990s. An HTS magnet was installed in the beamline of a carbon-dating van der Graff accelerator at the Institute for Geo-

logical and Nuclear Sciences in Wellington, New Zealand, and has been operating ever since. The magnet was built by the consortium of American superconductor, Alphatech International based in Auckland and Industrial Research Ltd, a New Zealand government research institute. The Bi-2223 magnet is designed to operate at 50 K, and is cooled using a single stage refrigerator. Although, it is only needed to develop a field of 0.74 T, it demonstrates the long-term reliability, in a moderately demanding application, which is an important achievement of wider commercialisation of HTS technology in general.

A number of other companies have similar ambitions and 21 T insert coils made by Oxford Superconducting Technology had been demonstrated at the National High Magnetic Field Laboratory in Florida. In another development, Oxford Magnet Technology and Seimanns Corporate Technology built a prototype magnetic resonance imaging body scanner with two coils made from Bi-2223 wires which were manufactured separately by Nordic Superconductor Technology and by Vacuum Schmelze. The more impressive results from demonstration magnets reported by Navel Research Laboratory, US, tested an HTS electromagnet producing a highest HTS magnetic field of 7.25 T using coils made by American Superconductor. Another successful demonstration was performed by Hitachi together with the National Research Institute for Metals and Tsukuba Magnet Laboratory, Japan. They have demonstrated a 23.4 T superconducting magnet with a 13 mm bore. This consisted of an 18 T low T_c superconducting magnet with two Bi-2212 booster coils operating at 4.2 K and was almost at the 23.5 T threshold needed for nuclear magnetic resonance application at 1 GHz.

1.6.4 Further developments in HTS technology

Other HTS technologies are also making their mark, most notably fault current limiter and low thermal conductivity current leads to reduce heat leaks into the cryo environment of low temperature superconducting high field mag-

nets. Some 1600 of these current leads, each carrying 13,000 A is deployed on the low temperature superconducting magnets in the Large Hadron Collider particle accelerator at CERN in Geneva. In parallel with these wire and bulk applications, a spectrum of thin film applications for microwave antennas, filters and superconducting quantum interference devices has also emerged.

It is clear from the broad base of applications and their proximity to commercial side demonstrations that HTS technologies are on the threshold of the promised superconductor revolution. As manufacturers scale up production, prices will inevitably be driven down and the commercial viability will be further enhanced. Besides this, information technology industry is also exploring for faster communication, larger memory capacity and faster processing power and it is clear that the market pull for electronic HTS technologies will grow dramatically in the next few decades. Based on these considerations, a consortium of European companies has estimated that the total world market in superconducting products will reach 20 billion Euro by 2020. Finally, the recent appearance of MgB_2 and new Iron based HTS material which exhibits novel properties remind us that novel materials with strange and unexpected properties will continue to appear and our technology horizons will continue to expand.

1.7 The homologue $Bi_2Sr_2Ca_{n-1}Cu_nO_{2n+4+\delta}$ system of superconductors

Bi-based high T_c cuprate superconducting materials can be represented by the homologue series having general formula $Bi_2Sr_2Ca_{n-1}Cu_nO_{2n+4+\delta}$ that contain either, n = 1, 2, or 3 CuO_2 layers per unit cell. Primitive unit cells of single-layer, bilayer, and trilayer Bi-based differ only in the number (n-1) of CuO_2-Ca-CuO_2 slabs packed along the c-axis; upon insertion of one or two slabs, the c-axis parameter of the crystallographic cells increases from 24.6 to

30.6 and 37.1 Å [101]. All the members in the series are superconductors with different T_c values. The $Bi_2Sr_2Cu_1O_{6+\delta}$ superconductor (n = 1) has shown a T_c around $\sim$ 10 K [58]. $Bi_2Sr_2CaCu_2O_{8+\delta}$ (n=2) and $Bi_2Sr_2Ca_2Cu_3O_{10+\delta}$ (n = 3) has a T_c of $\sim$ 80 K and 110 K, respectively [59]. The compounds with higher value (n = 4 and 5) also exist in multiphase mixture of bulk or thin films having a T_c of 90 K [102] and 50 K [103], respectively.

1.7.1 Bi-2201

$Bi_2Sr_2Cu_1O_{6+\delta}$ is usually referred to as Bi-2201 has a T_c of $\sim$ 10 K. Its structure contains a CuO_2 layer at its centre surrounded by a Sr-O layer and then a Bi-O layer on each side. The equilibrium phase is over doped with holes and is a semiconductor. This phase is orthorhombic (Amaa) with cell parameters; a = 5.36 Å, b = 5.37 Å and c = 24.37 Å. The number of formula units per cell is z = 4. The superconducting Raveau phase is reported to have a wide range of solid solubility and pseudo tetragonal crystal symmetry. Bi-2201 has the simplest prototype structure due to the presence of single octahedrally coordinated Cu-O planes with no intervening Ca layer like other Bi-based superconductors.

1.7.2 Bi-2212

$Bi_2Sr_2CaCu_2O_{8+\delta}$ (Bi-2212) is the most important and extensively studied high T_c phase. The crystal structure of Bi-2212 is composed of three building blocks other than two CuO_2 planes: (1) Bi_2O_2 block, (2) SrO block, and (3) Ca block. These three blocks are charge reservoirs and, at the same time, sources of disorder which result in the structural supermodulation of the BiO layers. The excess oxygen atoms are located in or near the Bi_2O_2 block which acts as the hole dopant. Bi^{+3} ions tend to replace the Sr^{+2} ions in the SrO

Table 1.4: Structural parameters of $Bi_2Sr_2CaCu_2O_{8+\delta}$ obtain by Rietveld Refinement [104].

Cell parameter	a=5.415Å	b=5.419Å	c=30.90Å		V = 906.7Å^3
Atom	Position	x	y	z	Occupancy
Bi(1)	8i	0	0	0.1989	1
Sr	8i	0	0.5	0.1091	1
Ca	4b	0	0.5	0	0.8
Bi(2)	4b	0	0.5	0	0.2
Cu	8i	0	0	0.0543	1
O(1)	16j	0.25	0.25	0.0510	1
O(2)	8i	0	0.5	0.1980	1
O(3)	8i	0	0	0.1200	1

block (sometimes called *site mixing*). The Ca^{+2} ions in the plane sandwiched by two CuO_2 planes can easily be replaced by rare-earth ions with relatively smaller ionic radii. Bi^{+3} and RE^{+3} substituted for Sr^{+2} and Ca^{+2} decrease

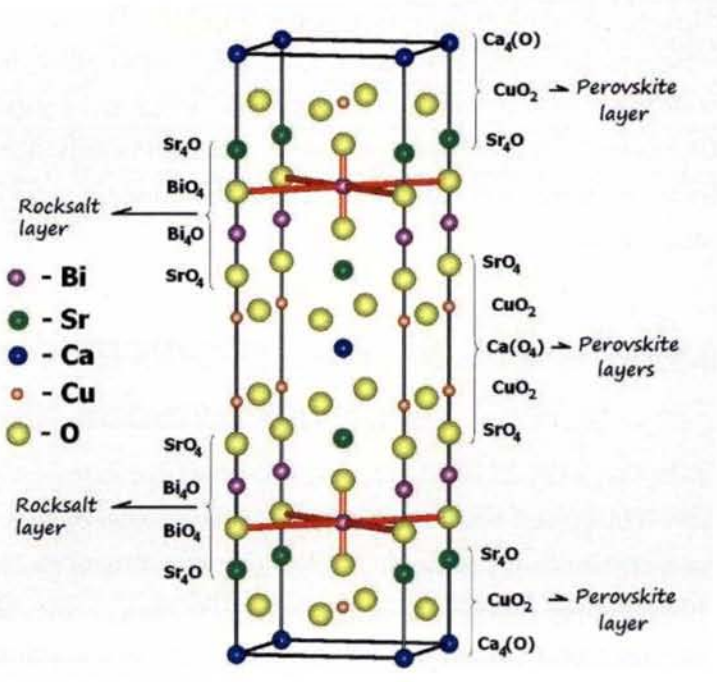

Figure 1.13: Ideal crystal structure of Bi-2212 perovskite superconductor.

the hole density in the CuO_2 layer. Ca adopts eight co-ordinates. There is no oxygen at this level. Therefore, Cu has only five nearest neighbours in square pyramidal co-ordination rather than elongated octahedral co-ordination of Bi-2201. The structure may be described with the orthorhombic *Amaa* group with cell parameters being a = 5.414 Å, b = 5.418 Å and c = 30.89 Å, with z = 4 (Figure 1.13). The detailed structural parameter of $Bi_2Sr_2CaCu_2O_{8+\delta}$ is given in Table 1.4.

1.7.3 Bi-2223

$Bi_2Sr_2Ca_2Cu_3O_{10+\delta}$, referred to as Bi-2223, shows the highest T_c of 110 K among Bi-based superconductors. Its structure consists of additional CuO_2 and Ca layers, inserted with CuO_2/Ca/CuO_2 block of Bi-2212 yielding CuO_2/Ca/CuO_2/Ca/CuO_2 club sandwich. The other Cu atoms are in square pyramid co-ordination while inner Cu atoms are in square plane co-ordination. These layers are separated by insulating layers with a rock salt structure. These rock salt layers lead to a distance of 1.2 nm, the coherence length between the blocks. Hence, anisotropy is large (>30), pinning is weak and transport properties are very sensitive to magnetic fields. The space group assigned to this phase is *Amaa* with a = 5.39 Å, b = 5.41 Å and c = 37.1 Å, with z = 4.

1.8 Motivation

Eventhough there are a large number of high T_c superconducting (HTS) materials known today, Bi-based superconductors (BSCCO) have attracted researchers because of their wide spread applications. As mentioned earlier, there are three superconducting phases in the BSCCO system, $Bi_2Sr_2Cu_1O_x$ (Bi-2201), $Bi_2Sr_2Ca_1Cu_2O_x$ (Bi-2212) and $Bi_2Sr_2Ca_2Cu_3O_x$ (Bi-2223). The three phases differ mainly by the number of Cu-O layers that rest between

the Bi-O layers which cap the unit cell. Presently, the most promising of the BSCCO compounds for long length conductor manufacture is Bi-2223, which is the BSCCO phase with the highest T_c, of $\sim$ 110 K. These materials have micaceous crystal structures, and their grains can be highly aligned by careful thermomechanical processing.

Currently, they are the primary HTS conductors available in lengths suitable for large-scale electrical applications throughout the electric power infrastructure. These include generators, transmission cables, distribution transformers, fault current limiters, motors and energy storage [105–108]. The main advantage of Bi-based system is its layered structure and hence a high degree of texturing can be induced in by progressively deforming it. Although single crystals of compounds such as Y-Ba-Cu-O had very high critical current densities and strong flux pinning, they are not useful in polycrystalline forms because supercurrent effectively cannot cross the boundaries between grains which are misaligned by more than $\sim 10^o$, making most of the grains ***weakly linked*** [109]. This problem in YBCO is not so acute in BSCCO.

Although Bi-2223 can be made into useful conductor forms, its superconducting properties are not as good as Bi-2212 at low temperatures. The principal reason behind this is the comparatively larger anisotropy of Bi-2223 than that of Bi-2212. In the proposed work, Bi-2212 (T_c = 80 K) is selected for the investigation because of the broad mono-phase field of stability as a function of temperature, chemical composition and chemical stability. But, the two-dimensional character of the Bi-2212 is responsible for poor flux pinning within the grains. However, at temperatures below around 30 K, where flux pinning is strong, Bi-2212 conductors can carry significant current densities in very high magnetic fields. While, conventional low Tc materials can carry significantly greater current densities at low magnetic fields, the Bi-2212 can carry higher current densities at fields above 8 T. Thin films or single crystals of a number of other high T_c materials can carry even greater J_c values, but presently they cannot be economically made into long lengths of conduc-

tor. The fact that Bi-2212 can carry high current densities in high fields at low temperatures, and still significant currents at high temperatures, makes it a promising material to study. Improvements in the current carrying capacity at either or both high and low temperatures in the presence of external magnetic field could make Bi-2212 feasible for many practical applications. Therefore, enhancement of flux pinning in Bi-2212 has become one of the challenges, and many research groups attempted to introduce pinning centres into the system by different methods [110–117]. Doping of impurity atoms which create point defects or secondary phase precipitate of nano size in the system can act as flux pinners [111–117]. Even though such doping enhances flux pinning, very often it causes a reduction in T_c.

1.9 Objectives of the present work

Doping in Bi-2212 superconductor generally involves incorporation of impurities or charge carriers into the inert parent material by chemical substitution or addition or removal of oxygen atoms from the charge reservoir planes. Doping an impurity atom in Bi-2212 system strongly perturbs the surrounding electronic environment and can therefore be used as a powerful tool to probe the high temperature superconductors (HTS) at atomic scale and hence can explore its fundamental mechanism and occurrence. Besides these, its thermodynamic and structural stability is relatively invariant against large variations in the processing conditions or on different cationic substitutions. To explain the effect of elemental substitution on superconducting properties, substitution is done at the Cu atom sites within the CuO_2 layer or between unequal valence elements outside the CuO_2 layer. Elemental substitution within CuO_2 layer results in a broken magnetic arrangement, thus leading to the partition of the cooper pair electrons within the Cu-O layer, while the latter results in a variation of hole concentration within CuO_2 layer. Tarascon et al. [118] con-

ducted a detailed study on cationic substitution on Bi-2212 and their effects on chemical and physical properties.

Substitution of magnetic and non-magnetic transition metals namely, Fe, Co, Ni and Zn, respectively at CuO_2 layers reduced the T_c or effectively destroy the superconductivity in Bi-2212 [119–122]. Due to the flux pinning effects of transition elements, scattered reports on improvement in the J_c of Bi-2212 were reported for low level addition of Fe, Co, Ni and Ti [123–127]. Extensive studies on substitution, out of CuO_2 layer in Bi-2212 have been performed, of which majority of them were done on the substitution of Yttrium (Y) at Ca site [128–149] because of the comparable ionic size of Ca^{2+} and a few at Sr and Bi-sites [150, 151]. Tarascon et al. show that the rare earth (RE) substitutions depend on the nature of RE and how nicely it accommodates in the crystal structure of Bi-2212 [118]. Other reports reveal that the larger sized RE substitutes better on Ca site, while smaller sized RE replaces only a lesser amount of Ca [131]. But, the results are scattered due to different processing methods, processing parameters and many other different aspects of study. Hence, comparison of the results is not possible. It is expected that cationic substitution of the divalent Ca^{2+}/Sr^{2+} by a trivalent ion induces variation in hole concentration of the Cu-O_2 planes in the Bi-2212 superconductors [129–133]. This results in the achievement of an optimum carrier concentration which enhances the critical temperature (T_c) of the system [152]. All these studies were done on the general formula of $Bi_2Sr_2Ca_1Cu_2O_{8+\delta}$ which is a Pb-free system. No such RE doping studies were reported earlier in (Bi,Pb)-2212 except the preliminary investigations of rare earth addition in bulk Bi-2212 by Aloysius et al. [153] and Biju et al. [117] which turned out as the main motivation for the present study.

Therefore, the main objective of this work was to investigate the influence of RE doping and processing conditions on the structural, electro-magnetic and superconducting properties of Bi-2212 superconductor and to develop novel superconductors with enhanced properties.

References

[1] H. K. ONNES, *Leiden Commn.* **124**, 1226 (1911).

[2] W. MEISSNER and R. OSCHENFELD, *Naturwissenschaften* **21**, 787 (1933).

[3] F. LONDON and H. LONDON, *Proc. Roy. Soc.* **A149**, 71 (1935).

[4] F. LONDON and H. LONDON, *Physica* **2**, 341 (1935).

[5] C. J. GORTER and H. B. GASIMER, *Physik* **35**, 963 (1934).

[6] H. FROHLICH, *Phy. Rev.* **79**, 845 (1950).

[7] V. L. GINZBURG and L. D. LANDAU, *Sov. Phys. JETP* **20**, 1064 (1950).

[8] V. L. GINZBURG, *Rev. Mod. Phys.* **2004**, 981 and references therein (76).

[9] A. A. ABRIKOSOV, *Sov. Phys. JETP* **5**, 1174 (1957).

[10] A. A. ABRIKOSOV, *Zh. Eksp. Teor. Fiz.* **32**, 1442 (1957).

[11] A. C. ROSE-INNES and E. H. RHODERICK, *Introduction to Superconductivity, 2nd Edition* , Pergamon Press, Oxford (1978).

[12] J. BARDEEN, L. N. COOPER, and J. R. SCHREIFFER, *Phys. Rev.* **108**, 1175 (1957).

[13] J. BARDEEN, L. N. COOPER, and J. R. SHRIEFFER, *Phys. Rev.* **106**, 162 (1957).

[14] P. A. LEE, N. NAGAOSA, and X. G. WEN, *Rev. Mod. Phys.* **78**, 17 (2006).

[15] J. W. CLARK, V. A. KHODEL, M. V. ZVEREV, and V. M. YAKOVENKO, *Physics Reports* **391**, 123 (2004).

[16] D. JROME, A. MAZAUD, M. RIBAULT, and K. BECHGAARD, *J. Phys. Lett. (Paris)* **41**, L95 (1980).

[17] G. SAITO, H. YAMOCHI, T. NAKAMURA, T. KOMATSU, M. NAKASHIMA, H. MORI, and K. OSHIMA, *Physica B* **169**, 372 (1991).

[18] C. P. POOLE, H. A. FARACH, and R. J. CRESWICK, editors, *Superconductivity*, Academic Press, California, 1995.

[19] R. HOTT, R. KLEINER, T. WOLF, and G. ZWICKNAGL, *Frontiers in Superconducting Materials*, (Editor:A. V. Narlikar) Springer-Verlag Berlin Heidelberg, 2005.

[20] C. BUZEA and T. YAMASHITA, *Supercond. Sci. Technol.* **14**, R115 (2001).

[21] C. BUZEA and K. ROBBIE, *Supercond. Sci. Technol.* **18**, R1 (2005).

[22] Y. KAMIHARA, T. WATANABE, M. HIRANO, and H. HOSONO, *J. Am. Chem. Soc.* **130**, 3296 (2008).

[23] R. Z. AN, L. WEI, Y. JIE, Y. WEI, S. X. LI, L. Z. CAI, C. G. CAN, D. X. LI, S. L. LING, Z. FANG, and Z. Z. XIAN, *Chin. Phys. Lett.* **25**, 2215 (2008).

[24] M. V. SADOVSKII, *cond-mat. arXiv:0812. 0302v1* (2008).

[25] X. WANG, S. R. GHORBANI, G. PELECKIS, and S. X. DOU, *Adv. Mater.* **21**, 236 (2009).

[26] T. ISHIGURO, K. YAMAJI, and G. SAITO, *Organic superconductors, Second edition* , Springer Verlag, Berlin, Heidelberg, New York (1998).

[27] Y. JIA, P. CHENG, L. FANG, H. Q. LUO, H. YANG, C. REN, L. SHAN, C. Z. GU, and H. H. WEN, *Appl. Phys. Lett.* **93**, 032503 (2008).

[28] A. YAMAMOTO, A. A. POLYANSKII, J. JIANG, F. KAMETANI, C. TARANTINI, F. HUNTE, J. JOROSZYNSKI, E. E. HELLSTROM, P. J.

LEE, A. GUREVICH, D. C. LARBALESTIER, Z. A. REN, J. YANG, X. L. DONG, W. LU, and Z. X. ZHAO, *Supercond. Sci. Tehcnol.* **21**, 095008 (2008).

[29] W. YI, L. SUN, Z. REN, W. LU, X. DONG, H. ZHANG, X. DAI, Z. FANG, Z. LI, G. CHE, J. YANG, X. SHEN, F. ZHOU, and Z. ZHAO, *Euro. Phys. Lett.* **83**, 57002 (2008).

[30] J. G. BEDNORZ and K. A. MULLER, *Z. Phys. B* **64** (1986).

[31] L. GAO, Y. Y. XUE, F. CHEN, Q. XIONG, R. L. MENG, D. RAMIREZ, C. W. CHU, J. H. EGGERT, and H. K. MAO, *Phys. Rev. B* **50**, 4260 (1994).

[32] J. NAGAMATSU, N. NAKAGAWA, T. MURANAKA, Y. ZENITANI, and J. AKIMITSU, *Nature* **410**, 63 (2001).

[33] A. Y. LIU, I. I. MAZIN, and J. KORTUS, *Phys. Rev. Lett.* **87**, 087005 (2001).

[34] P. SZABO, P. SAMUELY, J. KAMARK, T. KLEIN, J. MARCUS, D. FRUCHART, S. MIRAGLIA, C. MARCENAT, and A. G. M. JANSEN, *Phys. Rev. Lett.* **87**, 137005 (2001).

[35] E. BABAEV, *Phys. Rev. Lett.* **89**, 067001 (2002).

[36] Z. A. REN, W. LU, J. YAND, W. YI, X. L. SHEN, Z. C. LI, G. C. CHE, X. L. DONG, L. L. SUN, F. ZHOU, and Z. X. ZHAO, *Chin. Phys. Lett.* **25**, 2215 (2008).

[37] C. WANG, L. LI, S. CHI, Z. ZHU, Z. REN, Y. LI, Y. WANG, X. LIN, Y. LUO, S. JIANG, X. XU, G. CAO, and Z. A. XU, *Euro. Phys. Lett.* **83**, 67006 (2008).

[38] R. J. CAVA, B. BATLOGG, R. B. V. DOVER, D. W. MURPHY, S. SUNSHINE, T. SIEGRIST, J. P. REMEIKA, E. A. RIETMAN, S. ZAHWRAK, and G. I. ESPINOSA, *Phys. Rev. Lett.* **58**, 1676 (1987).

[39] M. K. WU, J. R. ASHURN, C. J. TORNG, P. H. HOR, R. L. MENG, L. GAC, Z. J. HUANG, Y. Q. WANG, and C. W. CHU, *Phys. Rev. Lett.*

58, 90 (1987).

[40] Y. L. PAGE, W. R. MCKINNON, J. M. TARASCON, L. H. GREENE, G. HULL, and D. M. HWANG, *Phys. Rev. B* **35**, 7245 (1987).

[41] R. M. HAZEN, L. W. FINGER, R. J. ANGEL, C. T. PREWITT, N. L. ROS, H. K. MAO, C. G. HADIDIACOS, P. H. HOR, R. L. MENG, and C. W. CHI, *Phys. Rev. B* **35**, 7238 (1987).

[42] E. A. RIETMAN, S. M. ZAHURAK, and D. WERDER, *Phys. Rev. B* **36**, 571 (1987).

[43] R. J. CAVA, B. BATLOGG, K. M. RABE, E. A. RIETMAN, P. K. GALLGAHE, and L. W. RUPP, *Physica C* **156**, 523 (1988).

[44] D. T. VEREBELYI, D. K. CHRISTEN, R. FEENSTRA, C. CANTONI, A. GOYAL, D. F. LEE, M. PARANTHAMAN, P. N. ARENDT, R. F. DEPAULA, J. R. GROVES, and C. PROUTEAU, *Appl. Phys. Lett.* **76**, 1755 (2000).

[45] G. VILLARD, F. LEGENDRE, S. POISSONNET, P. REGNIER, C. BIFULCO, and G. GIUNCHI, *Physica C* **341–348**, 2007 (2000).

[46] H. MIAO, H. KITAGUCHI, H. KUMAKURA, K. TOGANO, T. HASEGAWA, and T. KOIZUMI, *Physica C* **303**, 81 (1998).

[47] A. K. PRADHAN, S. B. ROY, P. CHADDAH, C. CHEN, and B. M. WANKLYN, *Phys. Rev. B* **49**, 12984 (1994).

[48] L. A. SCHWARTZKOPF, J. JIANG, X. Y. CAI, D. APODACA, and D. C. LARBALESTIER, *Appl. Phys. Lett.* **75**, 3168 (1999).

[49] S. H. YUN and J. Z. WU, *Appl. Phys. Lett.* **1996**, 862 (68).

[50] K. FUJINAMI, H. SUEMATSU, M. KARPPINEN, and H. YAMAUCHI, *Physica C* **307**, 202 (1998).

[51] S. L. YAN, Y. Y. XIE, J. Z. WU, T. AYTUG, A. A. GAPUD, B. W. KANG, L. FANG, M. HE, S. C. TIDROW, K. W. KIRCHNER, S. C. TIDROW, and K. W. KIRCHNER, *Appl. Phys. Lett.* **30**, 2989 (1998).

[52] T. AKAO, S. R. LEE, K. MIZOGAMI, H. SUEMATSU, and H. YAMAUCHI, *Physica C* **338**, 76 (2000).

[53] Y. YU, H. M. SHAO, Z. Y. ZHENG, A. M. SUN, M. J. QIN, X. N. XU, S. Y. DING, X. JIN, X. X. YAO, J. ZHOU, Z. M. JI, S. Z. YANG, and W. L. ZHANG, *Physica C* **289**, 199 (1997).

[54] Y. Y. XIE, T. AYTUG, J. Z. WU, D. T. VEREBELYI, M. PARANTHAMAN, A. GOYAL, and D. K. CHRISTEN, *Appl. Phys. Lett.* **77**, 4193 (2000).

[55] A. H. CARDONA, H. SUZUKI, T. YAMASHITA, K. H. YOUNG, and L. C. BOURNE, *Appl. Phys. Lett.* **62**, 411 (1993).

[56] J. Y. JUANG, J. H. HORNG, S. P. CHEN, C. M. FU, K. H. WU, T. M. UEN, and Y. S. GOU, *Appl. Phys. Lett.* **66**, 885 (1995).

[57] A. A. GAPUD, J. Z. WU, L. FANG, S. L. YAN, Y. Y. XIE, M. P. SIEGEL, and D. L. OVERMYER, *Appl. Phys. Lett.* **74**, 3878 (1999).

[58] C. MICHEL, M. HERRIEN, M. M. BOREL, A. GRANDIN, F. DESLANDES, J. PROVOST, and B. RAVEAU, *Z. Phys. B. Condens. Matter* **68**, 421 (1987).

[59] H. MAEDA, Y. TANAKA, M. FUKUTOMI, and T. ASANO, *Jpn. J. Appl. Phys.* **27**, L209 (1988).

[60] R. M. HAZEN, C. T. PREWITT, R. J. ANGEL, N. L. ROSS, L. W. FINGER, C. G. HADIDIACOS, D. R. VEBLEN, P. H. HOR, R. L. MENG, Y. Y. SUN, Y. Q. WANG, Y. Y. XUE, J. Z. HUANG, L. GAO, J. BERTOLD, and C. W. CHU, *Phys. Rev. Lett.* **60**, 1174 (1988).

[61] M. A. SUBRAMANIAN, C. C. TORARDI, J. C. CALABRESE, J. GOPALAKRISHNAN, K. J. MORRISSEY, T. R. ASKEW, R. B. FLIPPEN, U. CHOWDHRY, and A. W. SLEIGHT, *Science* **239**, 1015 (1988).

[62] Z. Z. SHENG and A. M. HERMANN, *Nature* **332**, 138 (1988).

[63] R. M. HAZEN, L. W. FINGER, R. J. ANGEL, C. T. PREWITT, N. L. ROSS, C. G. HADIDIACOS, P. J. HEANY, D. R. VEBLEN, Z. Z.

SHENG, A. E. ALI, and A. M. HERMANN, *Phys. Rev. B* **60**, 1657 (1988).

[64] M. A. SUBRAMANIAN, J. C. CALABRESE, C. C. TORARDI, J. GOPALAKRISHNAN, T. R. ASKEW, R. B. FLIPPEN, K. J. MORRISSEY, U. CHOWDHRY, and A. W. SLEIGHT, *Nature* **332**, 420 (1988).

[65] S. S. P. PARKIN, V. Y. LEE, E. M. ENGLER, A. I. NAZZAL, T. C. HUANG, G. GORMAN, R. SAVOY, and R. BEYERS, *Phys. Rev. Lett.* **60**, 2539 (1988).

[66] F. C. ZHANG and T. M. RICE, *Phys. Rev. B* **37**, 3759 (1988).

[67] J. A. SLEZAK and J. C. DAVIS, *MRS Bull.* **30**, 437 (2005).

[68] S. WAKIMOTO, H. ZHANG, K. YAMADA, I. SWAINSON, H. KIM, and R. J. BIRGENEAU, *Phys. Rev. Lett.* **92**, 217004 (2004).

[69] W. L. MCMILLAN and J. M. ROWELL, *Phys. Rev. Lett.* **14**, 108 (1965).

[70] K. M. LANG, V. MADHAVAN, J. E. HOFFMAN, E. W. HUDSON, H. EISAKI, S. UCHIDA, and J. C. DAVIS, *Nature* **415**, 412 (2002).

[71] P. MINNHAGEN, *Rev. Mod. Phys.* **59**, 1001 (1987).

[72] J. PEARL, *Appl. Phys. Lett.* **5**, 65 (1964).

[73] T. OHNISHI, R. H. HAMMOND, and W. JO, *J Mater. Res.* **19**, 977 (2004).

[74] W. WONG-NG, I. LEVIN, R. FEENSTRA, L. P. COOK, and M. VAUDIN, *Supercond. Sci. Technol.* **17**, S548 (2004).

[75] W. WONG-NG, L. P. COOK, J. SUH, I. LEVIN, and R. FEENSTRAA, *Supercond. Sci. Technol.* **18**, 442 (2005).

[76] D. M. FELDMANN, D. C. LARBALESTIER, R. FEENSTRA, A. A. GAPUD, J. D. BUDAI, T. G. HOLESINGER, and P. N. ARENDT, *Appl. Phys. Lett.* **83**, 3951 (2003).

[77] T. G. HOLESINGER, P. N. ARENDT, R. FEENSTRA, A. A. GAPUD, E. D. SPECHT, D. M. FELDMANN, and D. C. LARBALESTIER, *J Mater. Res.* **20**, 1216 (2005).

[78] S. R. FOLTYN, H. WANG, L. CIVALE, Q. X. JIA, P. N. ARENDT, B. MAIOROV, Y. LI, M. P. MALEY, and J. L. MACMANUS-DRISCOLL, *Appl. Phys. Lett.* **87**, 162505 (2005).

[79] C. BERNHARD, C. NIEDERMAYER, U. BINNINGER, A. HOFER, C. WENGER, J. L. TALLON, G. V. M. WILLIAMS, E. J. ANSALDO, J. I. BUDNICK, C. E. STRONACH, D. R. NOAKES, , and M. A. BLANKSON-MILLS, *Phys. Rev. B* **52**, 10488 (1995).

[80] D. A. BONN, *Nature Phys.* **2**, 159 (2006).

[81] C. E. GOUGH, M. S. COLCLOUGH, E. M. FORGAN, R. G. JORDAN, M. KEENE, C. M. MUIRHEAD, A. I. M. RAE, N. THOMAS, J. S. ABELL, and S. SUTTON, *Nature* **326**, 855 (1987).

[82] M. TAKIGAWA, P. C. HAMMEL, R. H. HEFFNER, and Z. FISK, *Phys. Rev. B* **39**, 7371 (1989).

[83] W. N. HARDY, D. A. BONN, D. C. MORGAN, R. LIANG, and K. ZHANG, *Phys. Rev. Lett.* **70**, 3999 (1993).

[84] D. J. V. HARLINGEN, *Rev. Mod. Phys.* **67**, 515 (1995).

[85] D. A. WOLLMAN, D. J. V. HARLINGEN, W. C. LEE, D. M. GINSBERG, and A. J. LEGETT, *Phys. Rev. Lett.* **71**, 2134 (1993).

[86] H. DING, T. YOKOYA, J. C. CAMPUZANO, T. TAKAHASHI, M. RANDERIA, M. R. NORMAN, T. MOCHIKU, K. KADOWAKI, and J. GIAPINTZAKIS, *Nature* **382**, 51 (1996).

[87] M. R. NORMAN, H. DING, M. RANDERIA, J. C. CAMPUZANO, T. YOKOYA, T. TAKEUCHI, T. TAKAHASHI, T. MOCHIKU, K. KADOWAKI, and P. GUPTASARMA, *Nature* **392**, 157 (1998).

[88] P. W. ANDERSON and N. P. ONG, *arXiv:cond-mat/0405518* (2004).

[89] K. MCELROY, D. H. LEE, J. E. HOFFMAN, K. M. LANG, E. W. HUDSON, H. EISAKI, S. UCHIDA, J. LEE, and J. C. DAVIS, *arXiv:cond-mat/0404005* (2006).

[90] K. McElroy, J. Lee, J. A. Slezak, D. H. Lee, H. Eisaki, S. Uchida, , and J. C. Davis, *Science* **309**, 1048 (2005).

[91] M. Plate, J. D. F. Mottershead, I. S. Elfimov, D. C. Peets, R. Liang, D. A. Bonn, W. N. Hardy, S. Chiuzbaian, M. Falub, M. Shi, L. Patthey, , and A. Damascelli, *Phys. Rev. Lett.* **95**, 077001 (2005).

[92] P. W. Anderson, *Low Temp. Phys* **32**, 282 (2006).

[93] J. Hubbard, *P. Roy. Soc. Lond. A. Mat.* **276**, 238 (1963).

[94] M. C. Gutzwiller, *Phys. Rev. Lett.* **10**, 159 (1963).

[95] H. Tasaki, *J. Phys. -Condens. Mat.* **10**, 4353 (1998).

[96] V. J. Emery, *Phys. Rev. Lett.* **58**, 2794 (1987).

[97] P. W. Anderson, *Science* **235**, 1196 (1987).

[98] E. Dagotto, *Rev. Mod. Phys.* **66**, 763 (1994).

[99] D. Vollhardt, *Rev. Mod. Phys.* **56**, 99 (1984).

[100] J. Tallon, *Physic World* **March**, 27 (2006).

[101] J. M. Tarascon, Y. Le-Page, P. Barboux, B. G. Bagley, L. H. Greene, W. R. Mckinnon, G. W. Hull, M. Giroud, and D. M. Hwang, *Phys. Rev. B* **38**, 8885 (1988).

[102] T. Kawai, Y. Egami, H. Tabate, and S. Kawai, *Nature* **349**, 200 (1991).

[103] H. Wang, X. Wang, S. Zhang, Z. Lu, and M. Jiang, *Appl. Phy. Lett.* **57**, 710 (1990).

[104] S. A. Sunshine, T. Siegrist, L. F. Schneemeyer, D. W. Murphy, R. J. Cava, B. Batlogg, R. B. van Dover, R. M. Fleming, S. H. Glarum, S. Nakahara, R. Farrow, J. J. Krajewski, S. M. Zahurak, J. V. Waszczak, J. H. Marshall, P. Marsh, L. W. R. Jr., and W. F. Peck, *Phys. Rev. B* **38**, 893 (1988).

[105] A. P. Malozemoff, J. Maguire, B. Gamble, and S. Kalsi, *IEEE Trans. Appl. Supercond.* **12**, 778 (2002).

[106] D. C. LARBALESTIER, A. GUREVICH, D. M. FELDMANN, and A. POLYANSKII, *Nature* **414**, 368 (2001).

[107] P. VASE, R. FLUKIGER, M. LEGHISSA, and B. GLOWACKI, *Supercond. Sci. Technol.* **13**, R71 (2000).

[108] D. C. LARBALESTIER and ET AL., *Power applications of superconductivity in Japan and Germany (World Technology and Engineering Center, Loyola College, MD)* (1997).

[109] D. DIMOS, P. CHAUDHARI, and J. MANNHART, *Phys. Rev. B* **41**, 4038 (1990).

[110] G. VILLARD, D. PELLOQUIN, A. MAIGAN, and A. WAHL, *Appl. Phys. Lett.* **69**, 1480 (1996).

[111] P. E. KAZIN, Y. D. TRETYAKOV, V. V. LENNIKOV, and M. JANSEN, *J. Mater. Chem.* **11**, 168 (2001).

[112] P. M. SARUN, R. P. ALOYSIUS, and U. SYAMAPRASAD, *Mater. Lett.* **60**, 3797 (2006).

[113] X. L. WANG, E. T. MUROMACHI, A. H. LI, Z. X. CHENG, S. KESHAVARZI, M. J. QIN, and S. X. DOU, *J. Appl. Phys.* **95**, 6699 (2004).

[114] M. V. MAKAROVA, P. E. KAZIN, Y. D. TRETYAKOV, M. JANSEN, M. REISSNER, and W. STEINER, *Physica C* **419**, 61 (2005).

[115] A. AMIRA, M. F. MOSBAH, P. MOLINIE, and A. LEBLANC, *Solid. State. Sci.* **7**, 53 (2005).

[116] E. AGRANOVSKI, A. Y. ILYUSHECHKIN, I. S. ALTMAN, T. E. BOSTROM, and M. CHOI, *Physica C* **434**, 115 (2006).

[117] A. BIJU, R. G. A. KUMAR, R. P. ALOYSIUS, and U. SYAMAPRASAD, *Physica C* **449**, 109 (2006).

[118] J. M. TARASCON, P. BARBOUX, G. W. HULL, R. RAMESH, L. H. GREENE, M. GRIOUD, M. S. HEDGE, and W. R. MCKINNON, *Phys. Rev. B* **39**, 4316 (1989).

[119] A. MAEDA, T. YABE, S. TAKEBAYASHI, M. HASE, and K. UCHINOKURA, *Phys. Rev. B* **41**, 4112 (1990).

[120] B. LONNBERG, T. LUNDSTROM, and P. NORLING, *Physica C* **191**, 147 (1992).

[121] M. SHIGEMON, T. OKABE, S. UCHIDA, T. SUGIOKA, J. SHIMOYAMA, S. HORII, and K. KISHO, *Physica C* **408**, 40 (2004).

[122] G. D. GU, G. J. RUSSELL, and N. KOSHIZUKA, *Physica C* **282-287**, 2107 (1997).

[123] D. H. HA, K. W. LEE, K. OKA, Y. YAMAGUCHI, F. IGA, and Y. NISHIHARA, *Physica C* **260**, 242 (1996).

[124] T. W. LI, R. J. DROST, P. H. KES, C. TRACHOLT, H. W. ZANDBERGEN, N. T. HIEN, A. A. MENOVSKY, and J. J. M. FRANSE, *Physica C* **274**, 197 (1997).

[125] R. NOETZEL and K. WESTERHOTT, *Phys. Rev. B* **58**, 15108 (1998).

[126] X. L. WANG, H. K. LIU, S. X. DOU, J. HORVOT, and G. D. GIU, *Spercond. Sci. Technol.* **15**, 356 (2002).

[127] C. TRAHOLT, H. W. ZANDBERGEN, T. W. LI, R. J. DROST, P. H. KES, A. A. MENOVSKY, N. T. HIEN, and J. J. M. FRANSE, *Physica C* **290**, 239 (1997).

[128] T. TAMEGAI, K. KOGA, K. SUZUKI, M. ICHIHARA, F. SAKAI, and Y. IYE, *Jpn. J. Appl. Phys.* **28**, L112 (1989).

[129] P. MANDAL, A. PODDER, B. GHOSH, and P. CHOUDHURY, *Phys. Rev. B* **43**, 13102 (1991).

[130] Y. GAO, P. PERNAMBUCWISE, J. E. CROW, J. OREILLY, N. SPENCER, H. CHEN, and R. E. SALOMON, *Phys. Rev. B* **45**, 7436 (1992).

[131] P. E. KAZIN, D. D. ZAITSEV, Y. D. TRETYAKOV, and M. JANSEN, *Inorg. Mater.* **37**, 812 (2001).

[132] P. MURUGAKOOTHAN, R. JAYAVEL, C. R. V. RAO, C. SUBRAMANIAN, and P. RAMASAMY, *Supercond. Sci. Technol.* **7**, 367 (1994).

[133] D. B. MITZI, L. W. LOMBARDO, A. KAPITULNIK, S. S. LADERMAN, and R. D. JACOWITZ, *Phys. Rev. B* **41**, 6564 (1990).

[134] S. TOCHIHARA, A. GOTO, H. YASINOKA, H. MAZAKI, M. OSADA, and M. KAKIHANA, *IEEE Trans. Appl. Supercond.* **9**, 2320 (1999).

[135] D. MANDRUS, L. FORRO, C. KENDZIORA, and L. MIHALY, *Phys. Rev. B* **45**, 12640 (1992).

[136] C. KENDZIORA, L. FORRO, D. MANDRUS, J. HARTGE, P. STEPHENS, L. MIHALY, R. REEDER, D. MOECHER, M. RIVERS, and S. SUTTON, *Phys. Rev. B* **45**, 13025 (1992).

[137] Q. CAO, K. Q. RUAU, S. Y. LI, X. H. CHEN, G. G. QIAN, and L. Z. CAO, *Physica C* **334**, 237 (2000).

[138] G. C. KIM, M. CHEON, H. KIM, Y. C. KIM, and D. Y. JEONG, *Phys. Rev. B* **72**, 064525 (2005).

[139] J. S. SHIN, H. ENOMOTO, T. KISHIMOTO, and H. OZAKI, *Jpn. J. Appl. Phys.* **31**, L320 (1992).

[140] E. BACA, V. HOLGUIN, W. LOPERA, and P. PRIETO, *Physica C* **341-348**, 655 (2000).

[141] R. J. SANDERSON and K. C. HEWITT, *Physica C* **425**, 52 (2005).

[142] H. MAZAKI, M. KAKIHANA, and H. YASUOKA, *Jpn. J. Appl. Phys.* **30**, 38 (1991).

[143] W. A. GROEN, D. M. DE LEEUW, and L. F. FEINER, *Physica C* **165**, 55 (1990).

[144] N. L. WANG, A. W. MCCONNELL, B. P. CLAYMAN, and G. D. GU, *Phys. Rev. B* **59**, 576 (1999).

[145] S. M. KHALIL, *J. Phys. Chem. Solids* **64**, 855 (2003).

[146] C. JANOWITZ, U. SEIDEL, R. S. UNGER, L. DUDY, A. KRAPF, R. MANZKE, and H. HOCHST, *J. Supercond. Incorp. Novel. Mag.* **17**,

49 (2004).

[147] A. MAEDA, M. HASE, I. TSUKADA, K. NODA, S. TAKEBAYASHI, and K. UCHINOKURA, *Phys. Rev. B* **41**, 6418 (1990).

[148] I. NOWIK, I. FELNER, and E. R. BAUMINGER, *Phys. Rev. B* **45**, 4912 (1992).

[149] M. A. VAN VEENENDAAL, R. SCHLATMANN, G. A. SAWATZKY, and W. A. GROEN, *Phys. Rev. B* **47**, 446 (1993).

[150] N. HUDAKOVA, K. KNIZEK, and J. HEJTMANEK, *Physica C* **406**, 58 (2004).

[151] D. PRABHAKARAN and C. SUBRAHMANIAN, *Mater. Sci. Engg. B* **52**, 169 (1998).

[152] R. J. CAVA, *J. Am. Ceram. Soc.* **83**.

[153] R. P. ALOYSIUS, P. GURUSWAMY, and U. SYAMAPRASAD, *Supercond. Sci. Technol.* **18**, L23 (2005).

Chapter 2

Preparation & characterization methods

The important thing in science is not so much to obtain new facts as to discover new ways of thinking about them.

— William Lawrence Bragg, 1890–1971

2.1 Introduction

For preparation of $Bi_2Sr_2Ca_1Cu_2O_{8+\delta}$ (Bi-2212) high T_c superconducting bulk material, the classical ceramic processing route is the simplest choice of preparation which consists of steps such as precursor synthesis, shaping and firing. As in classical ceramics, the quality of the precursor has a strong influence on the microstructure and the properties of the final product. The preparation of high T_c superconductor precursor can be divided into three steps, namely, selection of starting materials, mixing and calcination. This chapter briefly describes the general preparative aspects and various characterization techniques used in the study.

2.2 Method of synthesis

For Bi-2212 many different starting materials like oxide and carbonate [1–7], hydroxides [7–11], nitrates [12–17] and metals [18] have been reported. Different preparation methods such as the sol-gel route [1,2], solid state route [3–6, 11], melt quenching [7], precipitation routes [12, 15], spray pyrolysis [13, 14], freeze drying [17], and electrostatic deposition route [8–10, 16, 19] have been described in the literature. The diversity of applied starting compounds and the preparation routes have the common goal to get a reactive and homogeneous mixture of the starting elements. This is very important for the preparation of Bi-2212 bulk components with high critical current densities (J_c).

Each production route has its own benefits and drawbacks. The major challenges are the control of the stoichiometry, achievement of homogeneity, prevention of contamination and the purity of processing agents.

The calcination process is usually done in several steps, at different temperatures ranging from 750 °C to 860 °C and heating times from minutes [13, 14] to days [11]. These parameters mainly depend on the characteristics of the starting materials and the processing route [20, 21]. However, independent of the starting material chosen, a heat treatment in air in excess of 800 °C is needed in order to get the Bi-2212 phase.

The solid state approach is the most often route used for Bi-2212 precursor synthesis, because of its simplicity. In methods such as sol-gel, the starting materials react to form intermediates after decomposition of the organic ligands below 350 °C upon heating in air. Therefore, the reaction pathways to Bi-2212 are similar, while the formation rates vary, depending on which starting compounds are chosen.

During calcination of the starting materials, after burnout or decomposition of the carbonates, the Bi-2201 phase starts to form around 600 °C. At 700

°C, the Bi-2212 phase starts to form, however only above 800 °C it rapidly forms at the expense of Bi-2201 due to intercalation [22, 23]. The reaction rates can be accelerated using reactive precursors with high surface area or by tuning the calcination parameters such as temperature, heating rate and oxygen partial pressure in the atmosphere.

2.3 Preparative method used for the present study

The calcined Bi-2212 precursors were prepared by conventional solid-state synthesis using high-purity chemicals such as oxides and carbonates as the ingredients (> 99.9%, Aldrich). The required amount of ingredients was estimated according to the stoichiometry used. The ingredients were accurately weighed using an electronic balance (Mettler AE240) having a least count of 1 μg. Subsequently, these ingredients were mixed and ground using a planetary ball mill (Fritsch pulverrisette 6) in an agate bowl with agate balls.

After the milling process, the ingredients get homogenized with a reduction in particle size and increase in the contact area between different ingredients. Extreme care is taken to avoid contamination of the ingredients during weighing and milling process. The homogenized mixtures were placed in alumina crucibles and subjected to three stages of calcination in air between temperatures 800 °C – 830 °C/20 h in air using a programmable furnace. Intermediate grinding in acetone medium was employed between each calcination stage to avoid agglomerates and compositional variations that may still exist or may arise due to calcination. The temperature and duration of calcination were varied depending on the nature of the samples.

The calcined powders were compacted into pellets having an approximate diameter of 12 mm and thickness of 1mm by filling in a cylindrical die. Uni-

axial stress of 500 MPa was applied using a hydraulic press (Herzog TP 20P). The bulk density of the pellets prior to and after sintering were estimated by measuring the mass, thickness and diameter of the pellets. This is done to monitor the density variation during sintering because unlike other ceramic materials, Bi-based superconductors show ***retrograde densification*** behaviour due to its characteristic layered structure, i.e., upon sintering the density reduces from its value before sintering. The mass was precisely measured using an electronic balance, thickness and diameter of the pellets were measured using a micrometer screw gauge at different points and average values were taken.

The pellets were sintered between 845 °C to 860 °C for 120 h (60 h + 60 h) in two stages with one intermediate pressing under the same stress of 500 MPa. Intermediate pressing between the sintering stages is necessary to minimise the ***retrograde densification*** of the samples [24]. After heat treatment the bulk samples were cut and polished to a typical dimension of 12 mm x 4 mm x 1 mm. The flowsheet of the different stages of processing is shown in figure 2.1.

Terminals for electrical contact were also made during compaction of calcined powder. This was done by embedding silver strips in the pellets during pressing or by coating high quality conducting silver paste on the surface of green pellets. Silver strip remains embedded to the sample through out the sintering process while silver paste forms a strong coating which become a smooth surfaced metallic spot after the intermediate pressing process during sintering. Both these type of contacts can reduce the contact resistance by about an order compared to the usual method of making the electrical contact, i.e., coating silver paste on the final sintered pellets followed by an annealing.

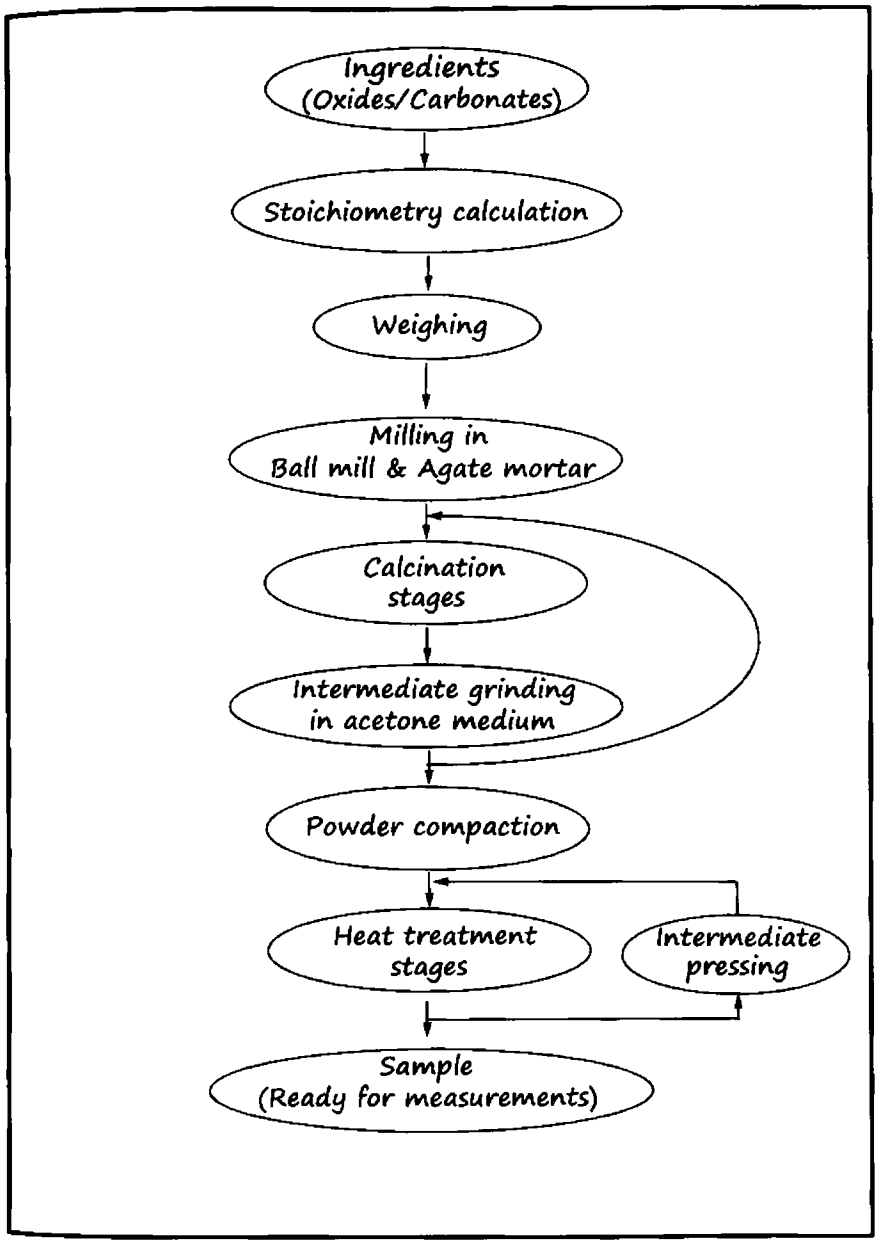

Figure 2.1: Flowsheet showing the preparation method of Bi-2212 polycrystalline samples.

2.4 Methods used for structural characterization

2.4.1 X-ray diffraction (XRD) analysis

Solid matter can be categorized as amorphous and crystalline materials. Those materials in which the atoms are arranged in random directions similar to the disorder present in a liquid are known as ***amorphous materials***. ***Crystalline materials*** are those materials in which the atoms are arranged in a regular pattern, and there is a smallest volume element that by repetition in three dimensions describes the crystal. This smallest volume element is called a ***unit cell***. The dimensions of the unit cell is described by three axes : ***a***, ***b***, ***c*** and the angles between them α, β, γ.

An electron in an alternating electromagnetic field will oscillate with the same frequency as the field. When an X-ray beam hits an atom, the electrons

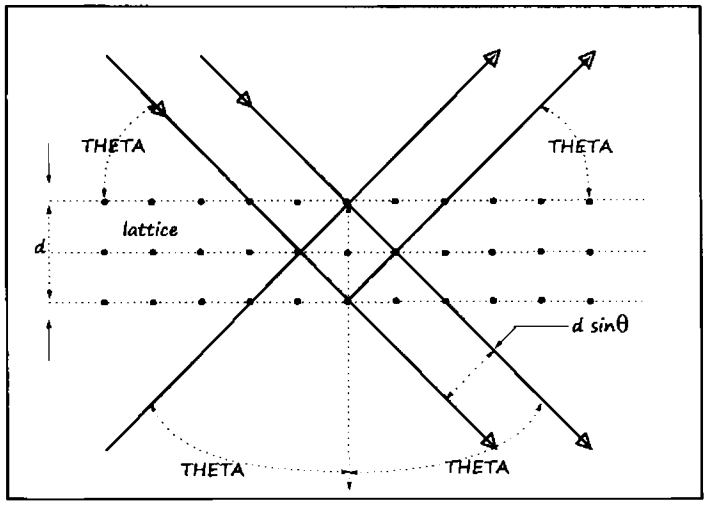

Figure 2.2: An illustration of X-ray diffraction from a crystal lattice.

around the atom starts to oscillating with the same frequency as the incoming beam. In almost all directions interference is destructive, that is, the combining waves are out of phase and there is no resultant energy leaving the solid sample. However, the atoms in a crystal are arranged in a regular pattern, and in a some particular directions interference is constructive, i.e., the waves are in phase and well defined X-ray beams leave the sample at various directions. Hence, a diffracted beam may be described as a beam composed of a large number of scattered rays mutually reinforcing one another. English physicists Sir W.H. Bragg and his son Sir W.L. Bragg developed the relationship, $n\lambda = 2d\ sin\theta$ in 1913 to explain why the cleavage faces of crystals appear to reflect X-ray beams at certain angles of incidence (theta, θ). The variable **d** is the distance between atomic layers in a crystal, and the variable lambda λ is the wavelength of the incident X-ray beam and **n** is an integer giving the order of reflection. This observation is an example of X-ray wave interference (***Roentgenstrahlinterferenzen***), commonly known as X-ray diffraction (XRD), and was the direct evidence for the periodic atomic structure of crystals (Figure 2.2). The Braggs were awarded the Nobel Prize in physics in 1915 for their work in determining crystal structures beginning with NaCl, ZnS and diamond.

About 95% of all solid materials can be described as crystalline. When X-rays interact with a crystalline substance (phase), one gets a diffraction pattern. In 1919 A. W. Hull published a paper titled, ***"A New Method of Chemical Analysis"***. Here he pointed out that ***".....every crystalline substance gives a pattern; the same substance always gives the same pattern; and in a mixture of substances each produces its pattern independently of the others".*** The X-ray diffraction pattern of a pure substance, therefore, acts like a fingerprint of the substance. Thus, the powder diffraction method is a powerful tool suited for characterization and identification of polycrystalline phases.

In powder or polycrystalline diffraction it is important to have a sample with a smooth plane surface. Normally, the samples were ground to particles of

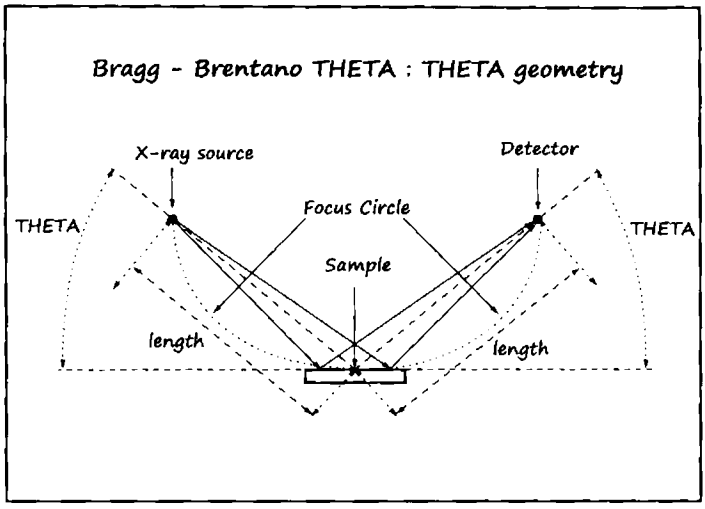

Figure 2.3: Schematic diagram of Bragg-Brentano geometry used in X-ray diffractometer.

about 0.002 mm to 0.005 mm cross section. The ideal sample is homogeneous and the crystallites are randomly distributed. The sample is pressed into a sample holder so as to get a smooth flat surface. Ideally, the sample consists of random distribution of all possible h, k, l planes. Only crystallites having reflecting planes (h, k, l) parallel to the specimen surface will contribute to the reflected intensities and each possible reflection from a given set of h, k, l planes will have an equal number of crystallites contributing to it. In order to produce all possible reflections, X-ray is scanned through the glancing angle θ on the sample.

The mechanical assembly that makes up the sample holder, detector arm and associated gearing is referred to as ***goniometer***. The working principle of a Bragg-Brentano parafocusing reflection goniometer is shown in figure 2.3. The distance from the X-ray focal spot to the sample is the same as from the sample to the detector. For the $\theta - \theta$ goniometer, the sample is stationary in the horizontal position, while the X-ray tube and the detector both move simultaneously over the angular range θ. In powder diffraction, normally the

line focus or line source of the tube is utilized. The line source emits radiation in all directions, but in order to enhance the focusing it is necessary to limit the divergence in the direction along the line focus. This is realized by passing the incident beam through a soller slit, which contains a set of closely spaced thin metal plates. In order to maintain a constant focusing distance it is necessary to keep the sample at an angle θ and the detector at an angle of 2θ with respect to the incident beam. For $\theta - \theta$ goniometer the tube has to be at an angle of θ and the detector at an angle of θ with respect to the sample.

In the present study powder XRD patterns of samples were taken using a ***Philips X'pert Pro (PW 3040/60)*** X-ray diffractometer with Cu Kα radiation employing ***X'Celerator*** and a monochromator at the diffracted beam side. The system has $\theta - \theta$ Bragg-Brentano geometry with fully automated operation and data acquisition. Programmable slits were used to limit the X-ray beam to the specified sample area. Most of the scans were performed under a tube voltage and current of 40 KV (λ = 1.540566 Å) and 30 mA, respectively. The samples were scanned from 15^o to 50^o (2θ values) with a step size of $\sim 0.02^o$. A typical scan takes about 15 minutes.

Powder diffraction is mainly used for ***finger print identification*** of various solid materials using the powder diffraction file (PDF) which contains 2,18,610 (PDF II Release 2009) different diffraction patterns of compounds, namely, alloys, inorganic, minerals, organic and organo-metallic compounds. Currently two database versions are available, the PDF I and the PDF II. The PDF I database contains information on d-spacing, chemical formula, relative intensity, residual intensity ratio (RIR) quality information and routing digit. The PDF II data base contains full information on a particular phase including cell parameters. The most common use of powder diffraction is chemical analysis which includes phase identification and lattice parameter calculation. The phase identification of compounds consists of two steps, namely, identification of phases using search-match utility and estimation of the amount of

crystalline phases formed in the reaction mixture after various stages of heat treatment conditions.

Phase identification of the samples was performed using ***X'Pert Highscore*** software with support of the ***ICDD PDF II*** database. The phase assemblage of different phases (vol. %) formed in the reaction mixture were quantitatively estimated from the integrated X-ray peak intensities obtained from the XRD patterns using the relation, $F_x = \frac{\Sigma I_x}{\Sigma I_{total}}$ where, x is any phase, F_x is the vol. percentage of the phase, I_x is the integrated peak intensities of phase x and I_{total} is the integrated peak intensities of all the phases in the mixture. As mentioned earlier, Bi-2212 has an orthorhombic structure with *Amaa* symmetry. The d-values of selected peaks of Bi-2212 were used for its lattice parameter calculations using the relation,

$$\left(\frac{1}{d^2}\right) = \left(\frac{h^2}{a^2} + \frac{k^2}{b^2} + \frac{l^2}{c^2}\right). \tag{2.1}$$

The determination of the preferred orientation of the crystallites in polycrystalline aggregates is referred to as texture analysis, and the term texture is used as a broad synonym for preferred crystallographic orientation in the polycrystalline material. The intensity of a given reflection (h, k, l) is proportional to the number of h, k, l planes in reflecting condition (Bragg's law). If the crystallites in the sample have a random orientation the recorded intensity will be uniform. The orientation of the unit cell is used to describe crystallite directions. By collecting data from several reflections, the complete orientation distribution of the crystallites can be build for single polycrystalline phase. Lotgering index (F) is a measure of texture in the material which is calculated from the peak intensity of the XRD patterns of sintered pellets and the corresponding randomized powder. It is calculated using the relation, $F = \left[\frac{P_a - P_r}{1 - P_r}\right]$ where, P is the ratio of intensities from the surface of sample, $P = \left[\frac{\Sigma I_{(00l)}}{\Sigma I_{Total}}\right]$ and P_a refers to P measured for the pellets and P_r for the corresponding ran-

domized powder [25]. A fully aligned sample will have a Lotgering index of 1 and a totally random sample has an index of zero. The best-aligned samples with layered structure as in Bi-2212 have a F in the range 0.8-0.95.

2.4.2 Microstructural analysis

Microstructural analysis of complex non-stoichiometric material has a lot of challenges. Scanning Electron Microscope (SEM) and Energy Dispersive X-ray Spectrometer (EDS) are the ultimate tools to perform a straight forward microanalysis on these materials such as materials evaluation, failure analysis and quality control screening. The only constraint is that the sample can be only up to 7 mm x 7 mm x 10 mm in size and it must be compatible with a 10^{-6} torr vacuum, i.e., non-volatile and not susceptible to electron beam induced damage.

2.4.2.1 Scanning electron microscopy

The objectives of scanning electron microscopy (SEM) is to provide a magnified image and to observe features that are beyond the resolution of the human eye ($\sim 100\mu$m). SEM is normally used to analyse different properties of materials, such as phase, grain shape/size, grain boundary, precipitation, texture and defects.

SEM generates high energy source of electrons, which is focused (in vacuum) into a fine probe that is scanned over the specimen surface. Electrons are accelerated in vacuum until their wavelength becomes extremely short, only one hundred-thousandth that of white light. Beams of these fast-moving electrons are focused on a sample. As the electrons penetrate the surface, a number of interactions occur that can result in the emission of electrons (secondary, backscattered and auger electrons) or photons (characteristic X-rays)

from (or through) the surface which carries the information regarding the surface and the elemental morphology of the sample. A reasonable fraction of the electrons emitted can be collected by appropriate detectors to generate a rasterized digital image on screen; every point that the beam strikes on the sample is mapped directly onto a corresponding point on the screen. Thus, SEM can generate, three types of principal images, namely, secondary electron images (SEI), backscattered electron images (BSE), and elemental X-ray maps. The SEM permits the observation of materials in micro and submicron ranges. The instrument is capable of generating three-dimensional images for analysis of topographic features [26]. Schematic description of the operation and the electron optics of SEM is shown in figure 2.4 [27].

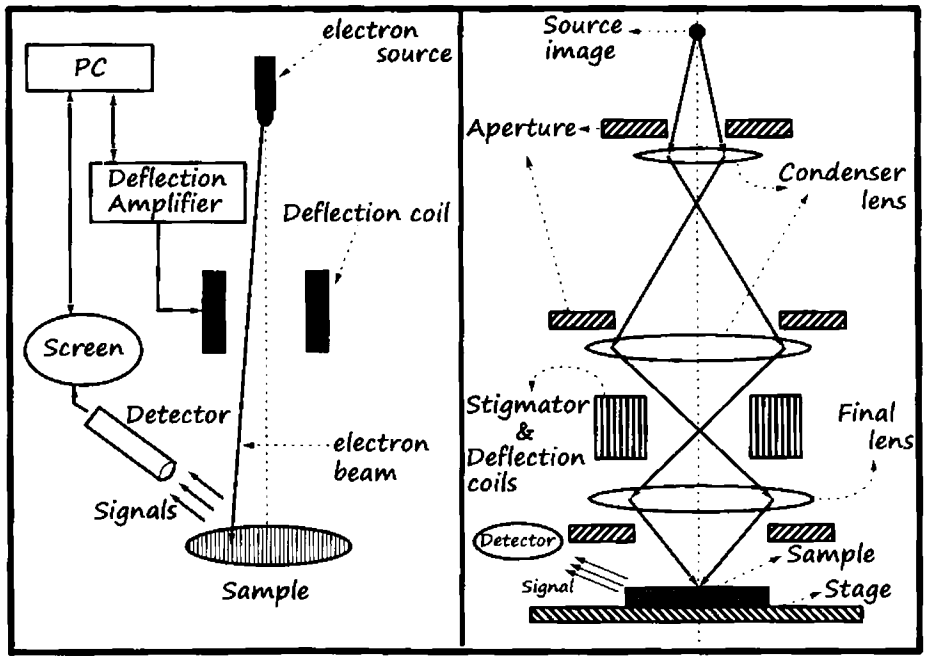

Figure 2.4: Schematic description of the operation and electron optics of an SEM.

In the present study the microstructural analysis was done using a ***JEOL JSM 5600LV*** scanning electron microscope equipped with an energy dispersive X-ray spectrometer (***Phoenix***) used in secondary electron imaging (SEI) mode. The typical images were magnified up to 5000 times. But in some cases, 10,000 times magnified images were also studied. SEM used in this study can magnify images down to about 100 nm (0.1 microns). Freshly fractured surfaces of the samples were mounted on a brass studs using adhesive carbon tapes or conducting silver paste. Since, the superconducting Bi-2212 is electrically conducting, gold coating was not required. Finally, the brass studs with the mounted samples were loaded on the sample holder of the microscope.

2.4.2.2 Energy Dispersive X-ray Spectroscopy

Energy Dispersive X-Ray Spectroscopy (EDS) is an analytical technique that qualitatively and quantitatively identifies the elemental composition of materials analyzed in SEM. EDS analyzes the top two microns of the sample with a spatial resolution of one micron. Beryllium windowed EDS detects all elements with atomic numbers greater than oxygen at concentrations greater than 0.1%. "Windowless" EDS detectors can also detect carbon, nitrogen and oxygen at concentrations greater than 1.0%. EDS displays the distribution of elements as either dot maps or line profiles with a spatial resolution of one micron. It can be used in various applications, such as quality control and test analysis in many industries including: computers, semiconductors, metals, cement, paper, and polymers; in medicine for analysis of blood, tissues, bones, and organs; in pollution control for asbestos identification; in field studies including ore prospecting, archeology, and oceanography; for identification and forgery detection in the fine arts; and for forensic analysis in law enforcement.

When the electron beam of the SEM is scanned across the sample, it generates x-rays from the atoms. X-rays are produced as a result of the ionization of

an atom by high-energy radiation wherein an inner shell electron is removed. To return the ionized atom to its ground state, an electron from a higher energy outer shell fills the vacant inner shell and, in the process, releases an amount of energy equal to the potential energy difference between the two shells. This excess energy, which is unique for every atomic transition, will be emitted by the atom either as an X-ray photon or will be self absorbed and emitted as an Auger electron. The energy of each x-ray is characteristic of the atom from which it escapes. The EDS system collects the x-rays, sorts them by energy and displays the number of x-rays versus their energy. This qualitative EDS spectrum can be either photographed or plotted. This data can then be further analyzed to produce either an area elemental analysis (displayed as a dot map) or a linear elemental analysis (displayed as a line scan) showing the distribution of a particular element on the surface of the sample. The EDS data can be compared to either known standard materials or computer-generated theoretical standards to produce either a full "quantitative" or a "semi-quantitative" analysis. The location of the peaks identifies the elements. The peak heights vary because each transition has a different probability of occurring and the detector's efficiency is a function of energy. The EDS spectrum has a peak width because the energy dispersion is a statistical event, i.e. every photon does not produce the same number of electron - hole pairs and there is thermal noise caused by the amplification process.

The advantages of EDS are the fast data collection, high detector efficiency, ease of use, portability, relative ease of interfacing to existing equipment. While disadvantages include poor energy resolution of peaks, a relatively low peak-to-background ratio in electron-beam instruments due to the high background coming from Bremsstrahlung radiation emitted by electrons suffering deceleration on scattering by atoms and a limit on the input signal rate because of pulse processing requirements.

In the present study, an EDS (***Phoenix***) attached with SEM is used for elemental analysis. Quantitative analysis requires much more effort and care, but

with proper settings, an accuracy of ± 2% of the wt % is obtained (example, for 10 wt% the accuracy is ± 0.2 wt %). The effect of the residual charges are negligible since, the samples are conducting and hence, well grounded. Each spectral data is taken after an exposure time of 60 seconds. Once the spectrum is collected, the background is removed by using a digital filtering algorithm. The obtained profile is compared with the standard materials of known homogeneous compositions at the microscopic level. Using the peak intensities of the standard (I_s) and of the sample (I_i) the weight percent (C_i) were determined by: $\left(\frac{C_i}{C_s}\right) = (ZAF)_i \times \left(\frac{I_i}{I_s}\right) = (ZAF)_i \times k_i$, where "ZAF" is a correction factor which depends on the atomic number of elements (A), absorption coefficient of the material (Z) and the flurosence caused by other atoms, when excited from the emitted X-rays (F) and k_i is $\left(\frac{I_i}{I_s}\right)$.

2.5 Methods used for superconductor characterization

The superconducting properties of the layered Bi-2212 superconductors have been investigated by measuring their resistive transport properties in self- and applied-magnetic fields. All the instruments used in the characterization were communicated to a computer (PC) having a GPIB-PC card through IEEE-488 interface bus. Hence, all the measurements were automated with a PC using appropriate software. Different softwares were developed in Quick Basic to provide complete computer control over each type of measurement. The softwares covered the setup of the various meters including integration times, current ramping, delay time, the reading of the meters, calibration of the temperature data, data conversions such as conversion of the sample voltages to resistance and storing of the data for future analysis. Thus, a dense data set was ensured with the system in good equilibrium throughout. Details of the different experimental techniques used are described in this section.

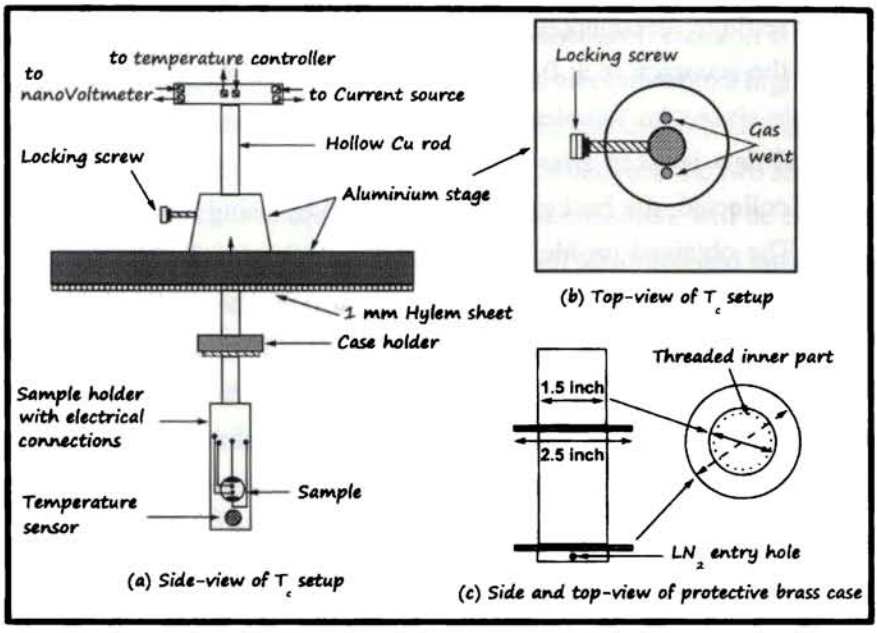

Figure 2.5: Schematic diagram of resistivity – temperature setup used in the present study.

2.5.1 Resistivity – Temperature (ρ–T) measurement

Superconducting state of the sample was characterized by resistivity-temperature measurements for determining the critical temperature (T_c) and width of transition (ΔT_c). In the present work, the temperature at which resistivity starts falling is taken as the T_c and the difference between the temperatures corresponding to the 90% and 10% of normal state resistivity ($T_{90} - T_{10}$) is defined as ΔT_c for the samples.

The resistance (R) in ohms (Ω) versus temperature was measured using the four terminal (probe) method. This method consists of two leads, on the outside, used to supply the current to the unknown specimen and two inside, to measure the voltage drop across the sample. A current of 10 mA was supplied by a ***Keithley 220*** programmable current source (current range : 1 nanoA to 100 mA) while the measured voltage was recorded with ***Keithley 181 and***

2182 digital nanovoltmeters (both have a resolution of 1 nanoVolt). The current flows through the outer leads of the sample but negligible current flows in the voltmeter's leads due its large internal resistance. Therefore, this technique gives an accurate measure of the resistance of the specimen without the influence of contact and lead resistances.

The electrical contacts were soldered onto the silver stripes in the sample surface which were prepared during the processing stage. The measurements were performed from liquid nitrogen temperature (77 K) to room temperature by lifting the probe from the bottom of a dewar at regular intervals of time, keeping a constant lifting step-length. The temperature was monitored by a silicon diode (***DT-470***) temperature sensor placed near to the sample. A ***Lakeshore L340*** temperature controller was used to record the voltage of the sensors and then converted to a temperature value using internal calibration table for the diode sensor provided by manufacturers. The schematic diagram of resistivity – temperature setup used in the present study is given in Figure 2.5.

A set of three different values of current (1, 10 & 100 mA) were used in order to check the ohmic behaviour of the measurements. In addition, the direction of current was reversed periodically for each data point in order to remove the effect of any thermoelectric voltage which is recommended, especially for measurement of very low voltages. The data was recorded in an ASCII file for later analysis. This measurement was performed on circular pellets or bar-shaped samples having straight contact terminals to obtain the resistivity. The resistance values were converted to resistivity using the equation, $\rho = \left(\frac{RA}{l}\right)$, where ρ is the resistivity in Ωcm, R is the resistance in Ω, A is the cross section area in cm^2 of the sample and l is the distance between the two voltage terminals in cm.

2.5.2 Voltage – Current (V-I) characteristics

Voltage versus current (V-I) characteristics are very important for both the evaluation of the superconductor for practical applications and the understanding of its critical current limitation mechanism. For the high T_c materials, the distribution of the flux pinning strength plays a very important role in deciding their V-I characteristics, and the distribution of the local critical current density J_c can be obtained from the V-I properties [28]. Below T_c, the vortices are pinned and a true superconducting state is established for $J < J_c$. J_c is defined as the current density above which vortices become mobile (flux creep and flux flow region) and give rise to an induced electrical field. Above T_c the vortices are not pinned and a low applied current causes a linear resistance in the sample. For larger currents the vortices start to move (flux flow) and give rise to a power law behaviour of the induced electrical field of the form, $V \propto I^n$ where, I is the current flowing, V is the voltage generated across the voltage leads and n is a function of applied magnetic field and temperature. Qualitatively one can conclude that sharper the take off in the V-I characteristics after the J_c value, higher can be the n-value (n-index), which in turn implies the higher flux pinning ability of the superconductor.

In the present work, the transport V-I properties were measured by the four-probe method under self- and applied-fields. In order to reduce the Joule heating at the current contacts due to the large transport currents, a computer controlled pulsed current method was employed using DC power supply system (***Aplab 9711P or Sorrenson DHP-5***) for the V-I measurement. After each current pulse, sufficient time was given to cool the sample before next measurement. The bar-shaped superconducting sample (12 mm x 4 mm x 1 mm) was fixed to the sample holder and mounted in a liquid nitrogen cryostat with a provision for evacuation, using a rotary pump (***Leybold Heraeus TRIVAC***). The measurement temperature can be reduced from 77 K to 64 K by applying vacuum and was monitored by a temperature controller. The direction of

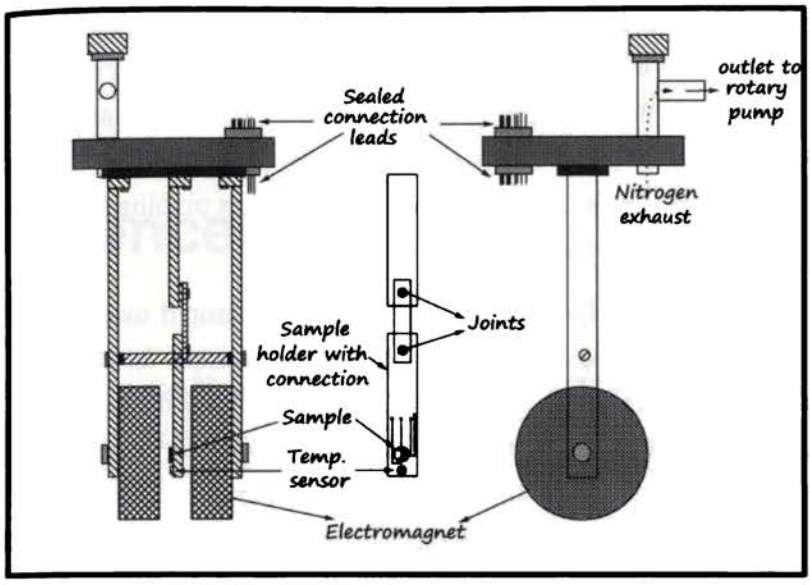

Figure 2.6: Schematic diagram of setup to measure V-I and J_c-B characteristics.

the current is parallel to the direction of the pressed surface and that of the magnetic field is perpendicular to the pressed surface of the pellet. The voltage across the voltage leads was recorded by a digital nanovoltmeter. The schematic diagram of the setup in which V-I measurement was performed is shown in figure 2.6. The critical current I_c was determined from the V-I measurements with a 1 μVcm^{-1} electric field criterion derived from the resistance between voltage terminals. The J_c values of the samples were calculated from I_c and the total cross-sectional area of the samples.

2.5.3 In-field transport critical current (J_c–B) measurement

As mentioned earlier, high T_c superconductors usually have very high H_{c2} values, which in turn imply that their coherence length is too short. Moreover, they are highly anisotropic as far as the electromagnetic properties are con-

cerned. Hence, the dependence of J_c on the applied magnetic field becomes significant. Analysis of the J_c-B characteristics brings out the vital information regarding the flux pinning capability of the superconductor or the ability of the Abrikosov vortices to withstand the melting of the vortex lattice in presence of external magnetic fields. Samples showing higher flux pinning force are the promising candidates for magnetic applications.

In the present study, J_c-B characteristics were measured using the setup shown in figure 2.6. The sample was fixed to the sample holder with the electrical leads soldered onto it and mounted in the liquid nitrogen cryostat. The magnetic field was produced by charging a bipolar electromagnet with required value of current which can generate a maximum field up to 1.5 T. A programmable constant current source (30 A, ***Aplab 9710P***) was used for charging the magnet. The generated magnetic field was calibrated using a Gauss meter (***Lakeshore 410***) with transverse hall probe. The temperature of the sample was kept fixed at 64 K which was precisely monitored by a temperature controller. The voltage values were monitored by digital nanovoltmeters. The measurement was automated using a computer which increases the magnetic field in steps of equal intervals and simultaneously records the value of current through the sample. 100 A rated constant current source was used for this purpose.

2.6 Conclusions

Major experimental facilities and techniques used in the present study for the preparation of bulk polycrystalline Bi-2212 have been reviewed in this chapter. The structural characterization was done using X-ray diffraction, scanning electron microscopy and energy dispersive X-ray spectrometer while the superconductor characterization was done using resistance - temperature curves, V-I and J_c-B characteristics data.

References

[1] P. S. DEVI and H. S. MAITI, *J. Mater. Res.* **9**, 1357 (1996).

[2] G. GUIDI, M. SOLCA, P. L. VILLA, and L. GHERARDI, *J. Mater. Sci.* **32**, 2219 (1997).

[3] M. OCHSENKÜHN-PETROPOULOU, R. ARGYROPOULOU, and K. OCHSENKÜHN, *Mikrochim. Acta* **135**, 139 (2002).

[4] P. G. A. DE-NINNO, M. MARINELLI, G. PAERNO, U. GAMBARDELLA, P. PAROLI, and G. BALESTRINO, *Physica C* **162–164**, 359 (1989).

[5] Y. MOTOI, Y. IKEDA, H. UWE, and T. SAKUDO, *Physica C* **162–164**, 929 (1989).

[6] J. ZHAO and M. S. SEEHRA, *Physica C* **159**, 639 (1989).

[7] H. FUJII, H. KUMAKURA, and K. TOGANO, *Jpn. J. Appl. Phys.* **39**, 2591 (2000).

[8] G. VILLARD, F. LEGENDRE, S. POISSONNET, P. REGNIER, C. BIFULCO, and G. GIUNCHI, *Physica C* **341–348**, 2007 (2000).

[9] G. VILLARD, F. LEGENDRE, S. POISSONNET, P. REGNIER, C. BIFULCO, and G. GIUNCHI, *Physica C* **355**, 312 (2001).

[10] F. L. G. VILLARD, G. POULLAIN, and G. G. P. REGNIER, *IEEE Trans. Appl. Supercond.* **11**, 3038 (2001).

[11] J. F. MITCHELL, J. A. GARCIA, and D. G. HINKS, *Physica C* **245**, 126 (1995).

[12] B. A. SALAH, M. MANSUORI, M. A. FREMY, and ET. AL., *Physica C* **262**, 111 (1996).

[13] L. MANCIC, O. MILOSEVIC, B. MARINKOVIC, M. LOPEZ, and F. RIZZO, *Physica C* **341–348**, 503 (2000).

[14] S. K. SINHA, S. C. GADKARI, S. C. SABHARWAL, L. C. GUPTA, and M. K. GUPTA, *Physica C* **185–189**, 499 (1991).

[15] S. SENGUPTA, E.CAPRINO, K. CARD, and J. R. GAINES, *IEEE Trans. Appl. Supercond.* **9**, 2601 (1999).

[16] R. N. BHATTACHARYA, J. CHEN, and R. D. BLAUGHTER, *IEEE Trans. Appl. Supercond.* **13**, 3343 (2003).

[17] P. KRISHNANRAJ, M. LRLOVIC, N. G. EROR, and U. BALACHANDRAN, *Physica C* **234**, 318 (1994).

[18] T. J. DETRIE and K. H. SANDHAGE, *J. Mater. Res.* **15**, 306 (2000).

[19] P. GENDRE, L. SCHMIRGELD, R. REGNIER, F. LEGENDRE, S. SENOUSSI, and A. MARQUET, *Appl. Supercond.* **3**, 21 (1995).

[20] D. BUHL, T. LANG, and L. J. GAUCKLER, *Supercond. Sci. Technol.* **10** (1997).

[21] D. SAGER, M. KOCH, H. HALLSTEDT, M. CHEN, and L. J. GAUCKLER, *Physica C* **405**, 103 (2004).

[22] D. N. ARGYRIOU, J. A. GARCIA, and D. G. HINKS, *Physica C* **11**, 277 (1996).

[23] F. H. CHEN, H. S. KOO, and T. Y. TSENG, *J. Mater. Sci.* **25**, 3338 (1990).

[24] R. R. KUMAR, R. P. ALOYSIUS, J. BOSE, P. GURUSWAMY, and U. SYAMAPRASAD, *Supercond. Sci. Technol.* **18**, 689 (2005).

[25] F. K. LOTGERING, *J. Inorg, Nucl. Chem.* **9**, 113 (1959).

[26] J. GOLDSTEIN, D. NEWBURY, D. JOY, C. LYMAN, P. ECHLIN, E. LIFSHIN, L. SAWYER, and J. MICHAEL, *Scanning Electron Microscopy and*

X-Ray Microanalysis , Kluwer Academic /Plenum Publishers, New York (2003).

[27] C. R. BRUNDLE, C. A. EVANS-JR., and S. WILSON, *Encyclopedia of materials characterization* , Butterworth (1992).

[28] K. YAMAFUJI and T. KISS, *Physica C* **290**, 9 (1997).

Chapter 3

Influence of Pb on the transport properties of Bi-2212

Everything should be made as simple as possible, but not simpler.
— Albert Einstein, 1879–1955

3.1 Introduction

Superconductivity in the high T_c superconducting cuprates (HTSCs) is two dimensional. This is partly caused by the characteristic crystal structure consisting of alternate stacks of superconducting CuO_2 planes and insulating reservoir blocks along the c-axis. In the superconducting state, carriers move in the c-direction by tunnelling the blocking layers via the Josephson interlayer coupling and hence, the superconducting properties of HTSC are strongly affected by the strength of this coupling. In the case of Bi-based superconductors, most of the H-T vortex phase diagram is dominated by the presence of the vortex liquid phase. This is due to the large anisotropy, which is responsible for weak inter-layer two dimensional pancake vortex coupling [1]. Bi-based

superconductors are the most anisotropic HTSC compounds due to the thick blocking layers consisting of insulating Bi-O double layers.

Among the Bi-based superconductors, $Bi_2Sr_2CaCu_2O_{8+\delta}$ (Bi-2212) system has always been a material of interest for both technologists and theoreticians. This is because the doping studies on these materials were helpful to improve many properties of the system such as critical temperature T_c, critical current density J_c, magnetic behaviour and thereby exploiting the material for practical applications. Besides these, its thermodynamic and structural stability is relatively invariant against large variations in the processing conditions or different cationic substitutions. Doping in Bi-2212 superconductor generally involves adding impurities or charge carriers into the inert parent material by chemical substitution or addition or removal of oxygen atoms from the charge reservoir planes. Doping an impurity atom in Bi-2212 system strongly perturbs the surrounding electronic environment and can therefore be used as a powerful tool to probe the HTSC at atomic scale and hence can explore its fundamental mechanism and occurrence.

This chapter describes the influence of Bi:Pb ratio on the structural and superconducting properties of : 1. (Bi,Pb)-2212 superconductor and 2. (Bi,Pb)-2212 doped with a typical rare earth, Yttrium. Y is used for the investigation because of the comparable ionic radii and the ability to contribute more electrons to the crystal lattice. The solid state route is chosen for the preparation of Bi-2212 superconductor, since it is an easier and scalable method for large scale production.

The detailed analysis of the results on the substitution of Pb at Bi-site of Bi-2212 revealed that the Pb doped Bi-2212 has much superior transport properties than undoped Bi-2212, even though, a slight reduction in the T_c was observed. The range of Pb substitution for achieving the best superconducting properties for Bi-2212 was found to be within $x = 0.4 - 0.5$. Hence, during Y doping in Bi-2212, the Pb content was fixed as $x = 0.4$. The results of this study

show that T_c and J_c are significantly enhanced for optimum Y concentration in Pb doped Bi-2212. These variations in the electrical and superconducting properties of Y doped (Bi,Pb)-2212 were the consequences of the structural and electronic changes due to Pb and Y co-doping.

3.2 Experimental

Pb-doped Bi-2212 superconductor was prepared by conventional solid state diffusion method. The initial stoichiometry of $Bi_{(2.1-x)}Pb_xSr_2Ca_{1.1}Cu_{2.1}O_{8+\delta}$ was chosen such that x = 0.0, 0.1, 0.2, 0.3, 0.4 and 0.5 and the corresponding samples were labelled as Pb0, Pb1, Pb2, Pb3, Pb4 and Pb5, respectively. High purity carbonates and oxides (Aldrich, > 99.9 %) were weighed using an electronic balance (*Mettler AE240*) and thoroughly homogenized using a planetary ball mill (*Fritsch pulverrisette 6*) with agate bowl and balls in acetone medium for 1 hour. The samples were subjected to a three stage calcination process in air at a heating rate of 2 °C/min at 800 °C/15h, 820 °C/25h and 830 °C/40h, respectively, with intermediate grinding in acetone medium. Circular pellets of the samples with dimensions of $\sim$ 12 mm diameter and $\sim$ 1 mm thickness were prepared using a cylindrical die under a pressure of 600 MPa in a hydraulic press (Herzog 12 TP). These pellets underwent a two stage heat treatment (845 °C/60h + 848 °C/60h) with one intermediate uniaxial pressing at the same pressure.

Yttrium added (Bi,Pb)-2212 superconductor with a general stoichiometry of $Bi_{1.7}Pb_{0.4}$ $Sr_{2.0}Ca_{1.1}Cu_{2.1}Y_xO_{8+\delta}$ (where x = 0 to 0.5) was prepared by the same method as described above using high purity carbonates and oxides of the ingredients (Aldrich, > 99.9 %). The Y added (Bi,Pb)-2212 samples are labelled hereafter as Y0, Y1, Y2, Y3, Y4 and Y5, respectively, for x = 0, 0.1, 0.2, 0.3, 0.4 and 0.5.

Phase analysis of the calcined powder and sintered samples were done by a powder X-ray diffractometer (*Philips X'pert Pro*) equipped with an *X'celerator* and a monochromator at the diffraction beam side, using *Cu*Kα radiation to monitor the crystal structure, grain orientation and phase assemblage. *X'Pert Highscore* software was used for the phase identification with the help of *ICDD PDF2* database. Microstructural analysis of the samples were done using scanning electron microscopy (*JEOL JSM 5600LV*) and elemental analyses of the samples were done using energy dispersive X-ray spectrometer (*Phoenix*) equipped with SEM. Density of the samples were determined by measuring their mass and the dimensions. Electrical contacts were made using conducting silver paste, coated prior to the sintering stage and co-fired with the pellets. The transition temperature (T_c) of the samples were determined by R-T measurement using four-probe DC electrical resistance method. The transport critical current density (J_c) measurements were performed using standard four-probe technique adopting the 1μV/cm criterion at 64 K in an indigenously built vacuum bath cryostat.

3.3 Effect of Bi:Pb ratio on the superconductivity of (Bi,Pb)-2212

3.3.1 Introduction

Several investigations have pointed out that Pb substitution in Bi-2212 [2–6] affects the structural modulation and the characteristic incommensurate modulation increases [5, 6]. Studies on single crystals reported that Pb at the Bi-site hinders the insertion of additional oxygen atoms into Bi-O double layers [6]. The substitution of Pb accompanied by removal of oxygen atoms in the Bi-O layers leads to infinite structural modulation (no modulation). As a result, the anisotropy of modulation free crystals is strongly reduced [7]. The

out-of-plane resistivity decreases by four orders of magnitude in Pb-doped crystals [8]. Motohashi et. al have found from the in-plane (ρ_a and ρ_b) and out-of-plane (ρ_c) resistivity measurements that the anisotropy of Bi-2212 single crystals in the normal state is drastically reduced by Pb doping [9, 10].

But most of these results were obtained from single crystals which cannot be used for producing composite polycrystalline conductors for practical applications. Moreover, the maximum current carrying capacity of these materials were estimated by the magnetisation measurements, where the supercurrents induced by magnetic field can only flow through the areas with good conductivity and were less influenced by the extrinsic factors, such as impurity phases, non-uniformity in oxide layer thickness and damage in oxide layers. But in a practical case, these extrinsic factors can not be neglected. Thus, the transport current measurements in polycrystalline samples are necessary for a better understanding of the relationship between the microstructure and current carrying properties of Bi-2212 for practical applications. This section describes the effect of substitution of varying amounts of Pb in Bi-site on the transport properties of polycrystalline Bi-2212.

3.3.2 Result and Discussion

Figure 3.1 shows the XRD patterns of $Bi_{(2.1-x)}Pb_xSr_2Ca_{1.1}Cu_{2.1}O_{8+\delta}$ samples (where x = 0.0 to 0.5) after the second stage calcination at 820 °C for 25 hours (Sample preparation is described under section 3.2). X-ray analysis of the calcined powder indicates that both the Pb-free and the Pb substituted samples consist of multiphases and their diffraction patterns contain peaks of Bi-2212 as the major phase. Minor phases, namely Bi-2201 and Ca_2PbO_4 are present in all the doped samples. In the case of undoped sample, Bi-2201 is the only secondary phase. The volume fraction of different phases such as Bi-2212/(Bi,Pb)-2212, Bi-2201 and Ca_2PbO_4 are estimated by measuring the integrated peak intensities of all the major XRD peaks of the respective phases

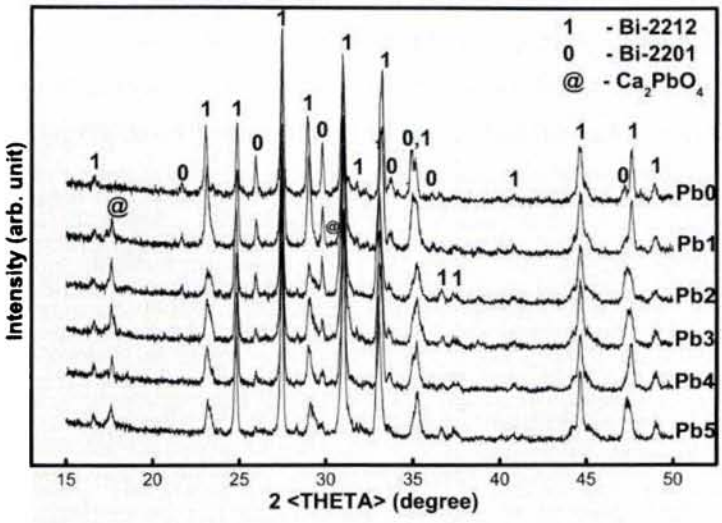

Figure 3.1: XRD patterns of the samples after calcination at 820 °C / 25 h.

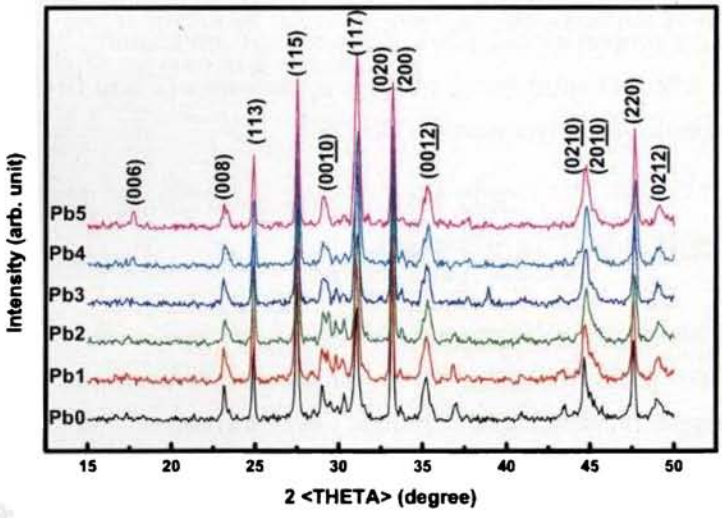

Figure 3.2: XRD patterns of the samples after final stage sintering at 848 °C / 60 h.

using the formula $F_x = \left(\frac{\Sigma I_x}{\Sigma I} \times 100\right)$ where, x is any phase, F_x is the volume percentage of phase x, I_x is the integrated peak intensities of phase x and I

is the integrated peak intensities of all the phases present in the sample. The estimated phase assemblage is given in Table 3.1. It can be seen that the Pb-free sample, Pb0 consists of a considerable amount of Bi-2201 (36.3 %) and the phase remaining is Bi-2212 (63.7 %). No other secondary phases were observed in this sample. In the Pb-doped samples, the volume percentage of (Bi,Pb)-2212 increases with the amount of Pb content up to Pb5 sample (94.8 %). The fraction of Bi-2201 decreases considerably to 3.4 %, while that of Ca_2PbO_4 increases to 1.8 % for Pb5 sample (Table 3.1). This shows that the reaction kinetics become faster for the Pb-doped samples compared to the un-doped sample. The very low fraction of Ca_2PbO_4, the only secondary phase containing Pb in the system, indicates that most of the added Pb gets fixed to Bi-2212 and forms (Bi,Pb)-2212.

Figure 3.2 shows the XRD patterns of the samples after the final stage of sintering at 848 °C. The patterns reveal the presence of Bi-2212/(Bi,Pb)-2212 only and no peaks of any secondary phases containing Pb or any other cations is observed even up to Pb5. This shows that Pb atoms are incorporated into the lattice site of the crystal structure of Bi-2212 up to the solubility limit of Pb at $x \leq 0.5$. Lotgering index (F), a measure of texture [12, 13] of the grains of undoped and Pb substituted samples was calculated from the XRD patterns of the sintered pellets and their ground powders (Table 3.2). It shows that the texture of the samples systematically improves with increasing Pb content in Bi-2212. The Pb5 sample has the highest value of Lotgering index (F_{max} = 0.85), while the sample Pb0 has a F value of 0.76.

Table 3.1: Phase assemblage of undoped and Pb substituted Bi-2212 samples.

Phases	Pb0 (Vol %)	Pb1 (Vol %)	Pb2 (Vol %)	Pb3 (Vol %)	Pb4 (Vol %)	Pb5 (Vol %)
Bi-2212/(Bi,Pb)-2212	63.7	78.1	83.1	86.5	90.5	94.8
Bi-2201	36.3	20.4	15.8	12.2	7.9	3.4
Ca_2PbO_4	–	0.7	1.1	1.3	1.6	1.8

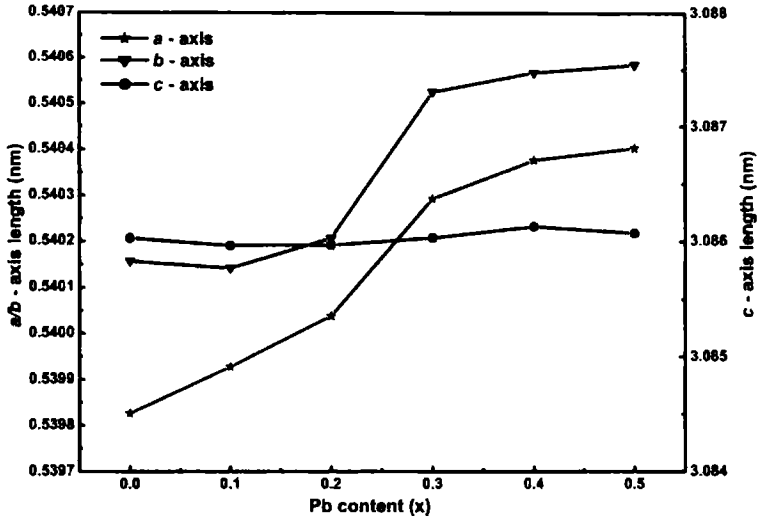

Figure 3.3: Variation of lattice parameters as a function of Pb substitution.

The lattice parameters of the samples calculated from the XRD patterns of the final samples are shown in figure 3.3. The formula, $\left(\frac{1}{d^2}\right) = \left(\frac{h^2}{a^2} + \frac{k^2}{b^2} + \frac{l^2}{c^2}\right)$ is used for the calculation, which is based on an orthorhombic symmetry assumed for (Bi,Pb)-2212. No appreciable change in lattice parameters is observed with Pb-doping. The a and b lattice parameters increase slightly from 5.398 and 5.402 to 5.404 and 5.406, respectively, starting from Pb0 to Pb5. The variation of c lattice parameter is still insignificant. But the formed (Bi,Pb)-2212 system retains its orthorhombic symmetry up to the doping level of $x = 0.5$. These observations show that the replacement of Bi atoms with Pb atoms does not affect the crystal structure of Bi-2212 appreciably because of the comparable ionic radii of Bi^{+3} (1.03 Å) and Pb^{+2} (0.98 Å) ions.

Figure 3.4 shows the SEM micrographs of the fractured surfaces of the samples. The microstructure of the samples seems to improve with the increase in Pb content. Flaky grains with the layered morphology, typical of Bi-2212 are observed in all the samples. Considering the texturing or grain alignment and densification of samples, Pb5 shows the best microstructure among all the

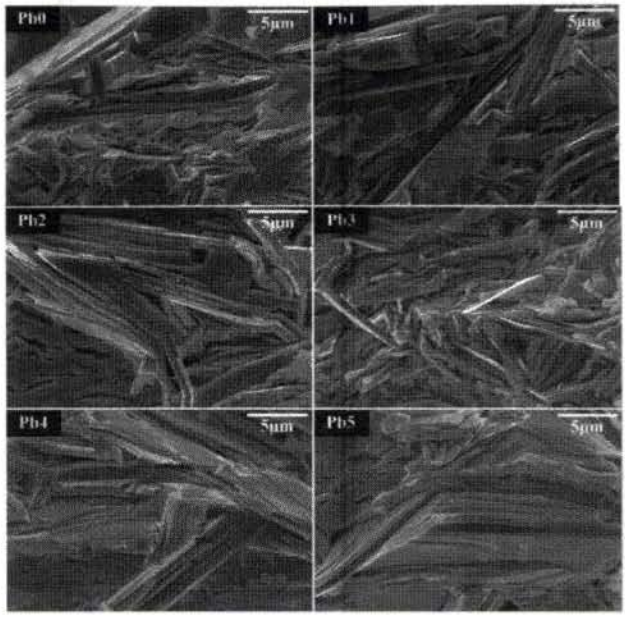

Figure 3.4: SEM micrographs of the fractured surface of undoped and Pb substituted samples taken in secondary electron imaging mode.

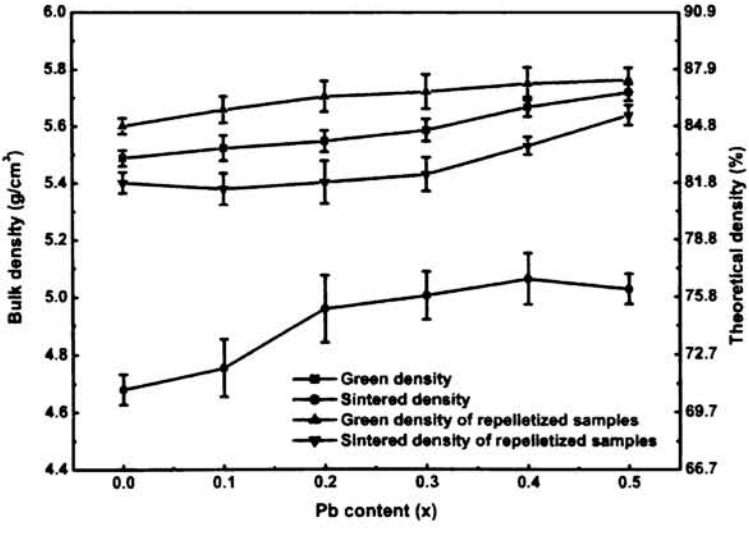

Figure 3.5: Density variation of the samples after different stages of heat treatment.

samples. This is also seen in the density variation of Pb-substituted samples (Figure 3.5). Figure 3.5 shows the variation of the bulk density of the samples at different stages of heat treatment with respect to the Pb content and the obtained density as compared to the theoretical density of Bi-2212 (ρ_{th} = 6.6 g/cm^3). The sintered density of all the samples after the first stage sintering are less by $\sim$ 10 % than that of the corresponding green density (density of pellets prior to the heat treatment). The deterioration of sintered density, usually referred to as the ***retrograde densification***, is a characteristic property of (Bi,Pb)-2212 due to its layered growth mechanism [14–16]. The undoped sample (Pb0) shows a the lower bulk density than the Pb substituted samples at this stage. The density of all the samples is improved significantly by the intermediate pressing. The highest and lowest bulk densities are shown by Pb5 (5.64 g/cm^3) and Pb0 (5.40 g/cm^3) samples, respectively.

Figure 3.6 shows the temperature dependence of resistivity of undoped and Pb substituted samples ($0.0 \leq x \leq 0.5$). All the samples show superconductive transition. A pseudo-transition occurs around $\sim$ 110 K as indicated by a slight drop in resistance for samples with x = 0.1 to 0.4, which is due to the

Table 3.2: Transition width (ΔT_c), Lotgering index (F), Self field J_c at 64 K and temperature coefficient of resistance [α(T)] at normal state of undoped and Pb substituted Bi-2212 samples.

Pb content (x)	ΔT_c (K)	Lotgering index(F)	J_c at 64 K (A/cm^2)	$\alpha(T)$ (10^{-4}/K)
0	3.73	0.61	48	2.46
0.1	4.11	0.64	55	2.51
0.2	4.32	0.68	68	2.58
0.3	4.45	0.71	85	2.63
0.4	4.50	0.78	115	2.65
0.5	4.40	0.85	120	2.72

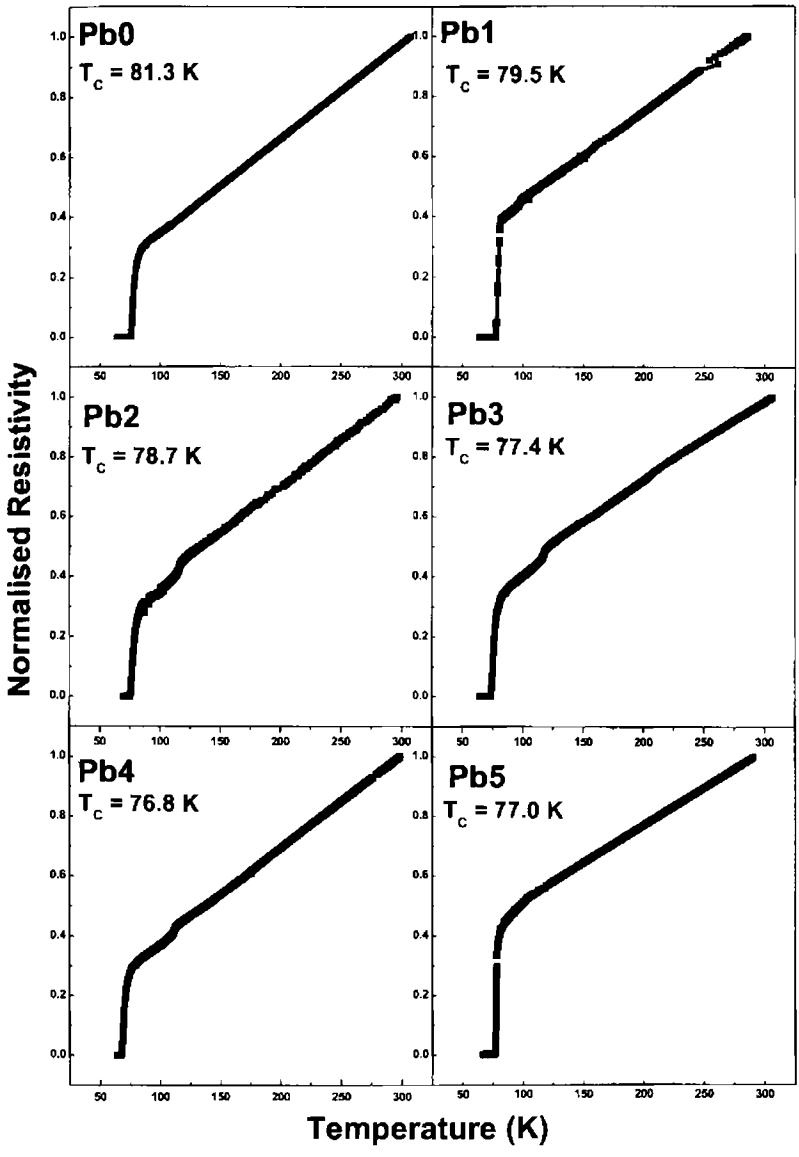

Figure 3.6: Temperature dependent normalized resistivity plots of Pb substituted samples.

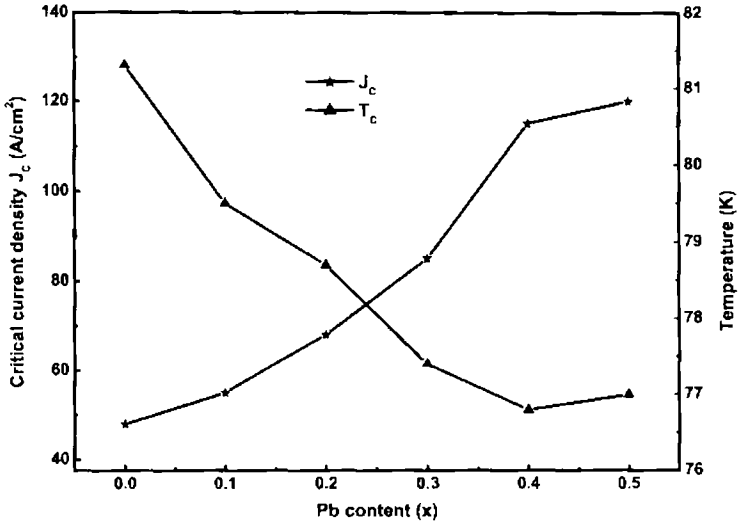

Figure 3.7: Dependence of T_c and J_c on Pb content.

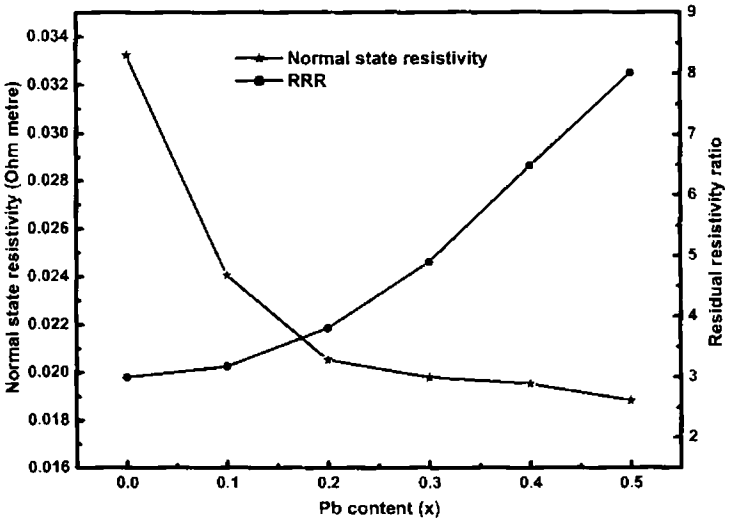

Figure 3.8: Variation of normal state resistivity and RRR with Pb content.

co-existence of the triple layered cuprate $(Bi,Pb)_2Sr_2Ca_2Cu_3O_{10+\delta}$ [(Bi,Pb)-2223] in very low percentages which could not be detected within the detection

limit of the X-ray diffractometer, while Pb0 and Pb5 samples do not show this anomaly. Figure 3.7 shows the variation of critical temperature (T_c) and critical current density (J_c) as a function of Pb content of superconducting samples. The critical temperature as determined from the ρ-T plots shows that the T_c of the Pb substituted samples slightly decreases with Pb content. Lowest T_c is shown by Pb4 sample (76.8 K) while the highest T_c is shown by Pb0 (81.3 K). The values of transition width (ΔT_c) are also found to be almost same for Pb substituted samples but these are slightly higher than that of the undoped Bi-2212 (Table 3.2). The results reveal that the substitution of Pb^{+2} ion for a Bi^{+3} increases the hole concentration of the Bi-2212, which in turn reduces the T_c of Pb substituted Bi-2212 superconductor.

Figure 3.7 also shows that as Pb content increases, J_c value increases, and reaches to a maximum for Pb5 (120 A/cm^2) at 64 K as against 48 A/cm^2 for the pure sample. It is also observed that the rate of increase in J_c at around $x = 0.4 - 0.5$ is significantly reduced. Figure 3.8 shows the variation of normal state resistivity and residual resistivity ratio (RRR) of undoped and Pb-doped Bi-2212 superconductor. It is found that the normal state resistivity of the samples rapidly decreases with Pb content, while the residual resistivity ratio (RRR) increases up to $x = 0.5$. The temperature coefficient of resistance [α(T)], also shows an increasing trend with Pb content (Table 3.2). This implies that the charge carriers in the system increases and the normal state resistivity of the Pb substituted samples get reduced. The improvement in J_c of Pb substituted Bi-2212 is due to the improvement in microstructure and the conductivity along the c-axis which strengthen the Josephson's coupling.

The XRD profile and the lattice parameter results show that the Pb atoms are successfully substituted for Bi-site in Bi-2212 as envisaged in the nominal stoichiometry. Substitution of Pb leads to the replacement of Pb^{+2} by Bi^{+3} ions and this decreases the oxygen content. The introduced divalent Pb ions lead to lesser oxygen content in Bi-O layer which yield a longer periodicity of modulation. The substitution also increases the hole concentration

on the CuO_2 layers. This explains the slight decrease in T_c with Pb substitution. The effect of slight reduction of T_c is not reflected in the observed J_c of Pb substituted samples because of the better microstructural properties and c-axis conductivity of these samples. The Pb-doping reduces the weak-links between the grains which enables a resistance free current distribution in (Bi,Pb)-2212 superconductor. This also contributes to the effective normal state resistivity as compared to undoped Bi-2212, hence further improving the J_c of Pb-substituted (Bi,Pb)-2212 superconductor.

3.4 Effect of Bi:Pb ratio on the superconductivity of RE-doped (Bi,Pb)-2212

3.4.1 Introduction

Cationic substitution of a trivalent Rare Earth (RE) element in the place of a divalent Ca^{+2}/Sr^{+2} ion, induces variation in hole concentration of the CuO_2 planes in the Bi-2212 superconductors [17–21]. Thus, by tuning the level of the substitution, an optimum carrier concentration can be achieved which will enhance the critical temperature (T_c) of the system [22].

Extensive studies on RE substitution in Bi-2212 have been performed of which majority of studies were done on the substitution of Yttrium (Y) at Ca site [17–21, 23–39] because of their comparable ionic size. A few studies were done at the Sr and Bi-sites also [40, 41]. All these studies were done on the general formula of $Bi_2Sr_2Ca_1Cu_2O_{8+\delta}$ which is a Pb-free system. Also, in the previous section, it is experimentally verified that Pb substitution at Bi-site in Bi-2212 significantly improves the c-axis conductivity and thereby improves the coupling between the CuO_2 layers. Thus it is expected that the combined effect of Pb doping at Bi-site associated with RE addition in Bi-2212

can enhance the superconducting properties of the system significantly. In the present section, the enhancement of T_c and self-field J_c of Y added Bi-2212 superconductor co-doped with Pb at Bi-site is discussed.

3.4.2 Results and Discussion

Figure 3.9 shows the XRD patterns of $Bi_{1.7}Pb_{0.4}$ $Sr_{2.0}Ca_{1.1}Cu_{2.1}Y_xO_{8+\delta}$ (where x = 0 to 0.5) samples after the second stage calcination at 820 °C for 25 h (Sample preparation is described under section 3.2). X-ray analysis indicates that all the samples contain peaks of (Bi,Pb)-2212 as the major phase and Bi-2201, Ca_2PbO_4 and Sr_2PbO_4 as minor phases. The volume fraction of different phases such as (Bi,Pb)-2212, Bi-2201, Ca_2PbO_4 and Sr_2PbO_4 were estimated and it can be seen that the volume percentage of (Bi,Pb)-2212 remains almost same up to Y2 sample (94.1 %) and thereafter it decreases to 91.8 % for Y5 (x = 0.5) (Table 3.3). In sample Y5, small amounts of Sr_2PbO_4 is also detected as the secondary phase. This shows that at lower Y stoichiometry replacement of Ca^{+2} by Y^{+3} takes place, but at higher Y stoichiometry replacement of Sr^{+2} by Y^{+3} also takes place resulting in the precipitation of Sr_2PbO_4. Figure 3.10 shows the XRD patterns of the samples after final stage of sintering. The XRD profile indicates that the only phase detected is (Bi,Pb)-2212 and no peaks of any secondary phases are detected up to Y5. This indicates that the solubility limit of Y in the system is $x \leq 0.5$ and the added Y enters into the crystal structure in all the Y doped samples [42]. Lotgering index (F) calculated from the XRD patterns (Table 3.4) shows that the grain orientation gradually comes down as the Y content increases. The pure sample shows the highest value of Lotgering index ($F_{max} = 0.75$), while the sample Y5 shows a F value of 0.41.

Figure 3.11 shows the variation of the bulk density of the samples at different stages of the processing schedule. The measured density as compared to the theoretical density of Bi-2212 (ρ_{th} = 6.6 g/cm^3) in percentage is given in

figure 3.11. The sintered density of all the samples after the first stage sintering are less by $\sim$ 6 % than that of the corresponding green density. The sintered density has been improved by the intermediate press-sintering step. Densities of all the Y added samples are less than the pure sample (5.54 g/cm^3) and the

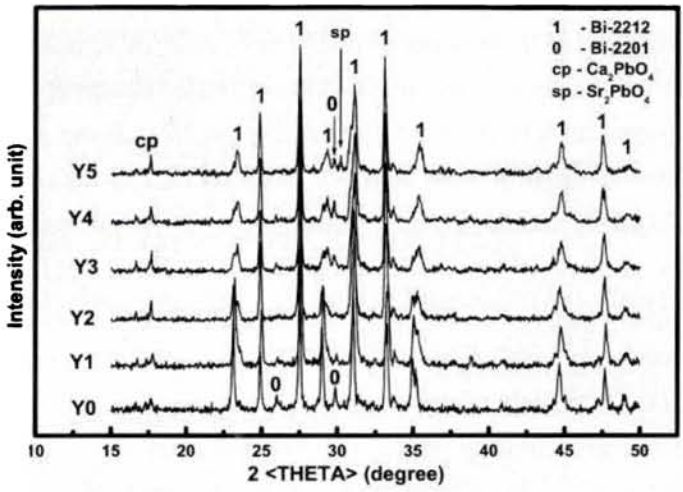

Figure 3.9: XRD patterns of the samples after calcination at 820°C / 25 h.

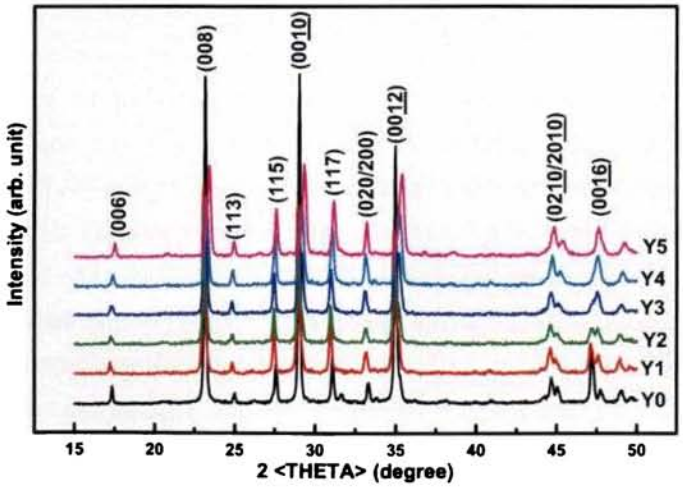

Figure 3.10: XRD patterns of the samples after final stage sintering at 848° C / 60 h.

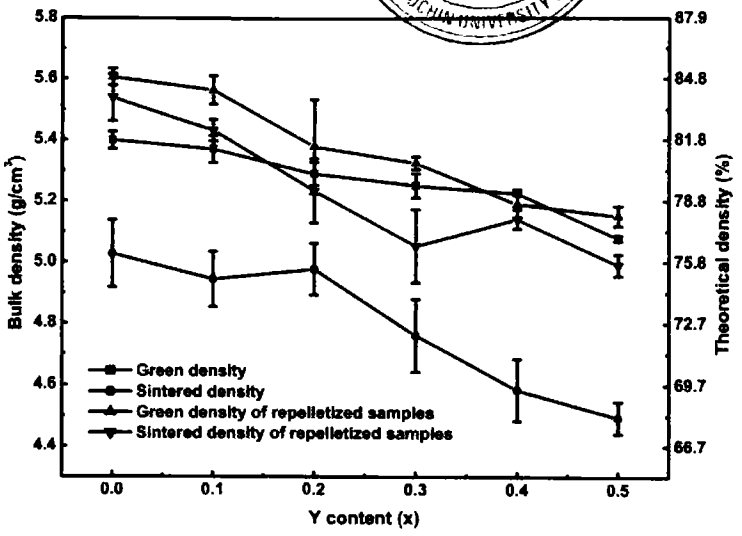

Figure 3.11: Density variation of the samples after different stages of heat treatment.

decrease is found to be a function of Y content. The minimum density was obtained for Y5 (4.99 g/cm^3).

Figure 3.12 shows the SEM microstructure of the samples taken in the SEI mode. The morphology of the grains show a vivid variation with increase in Y content. Characteristic flaky grains of (Bi,Pb)-2212 are seen in all the samples. Clean, large and oriented grains are the identity of Y0 and Y1 samples. As Y level increases, the porosity of the samples increases with deterioration in the

Table 3.3: Phase assemblage of pure and Y added (Bi,Pb)-2212 samples

Phase	Y0 (Vol %)	Y1 (Vol %)	Y2 (Vol %)	Y3 (Vol %)	Y4 (Vol %)	Y5 (Vol %)
(Bi,Pb)-2212	93.9	94.3	94.1	92.2	90.7	91.8
Bi-2201	4.82	2.63	2.44	4.23	6.62	4.25
Ca_2PbO_4	1.28	3.07	3.46	3.57	2.68	2.50
Sr_2PbO_4	0	0	0	0	0	1.45

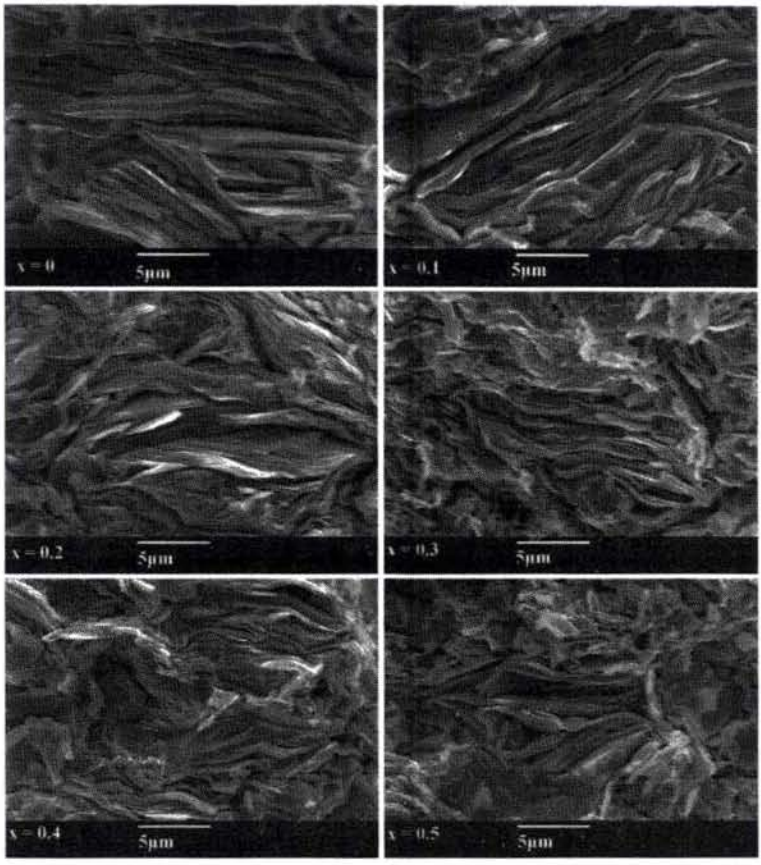

Figure 3.12: SEM micrographs of the fractured surface of the samples taken in the secondary electron imaging mode.

size and orientation of grains for samples ranging from $0.2 \leq x \leq 0.5$. Thus, the decrease in the density of the samples with increase in Y content can be correlated with the higher level of porosity observed in SEM micrographs.

The lattice parameter variation of Y-free and Y-added samples are shown in figure 3.13. With the increase in Y content, a systematic contraction in c-axis length is observed, while there is no appreciable change in the a/b axes length for $0.1 \leq x \leq 0.5$. This reveals that the structure of pure (Bi,Pb)-2212 superconductor having an orthorhombic symmetry transforms to pseudo

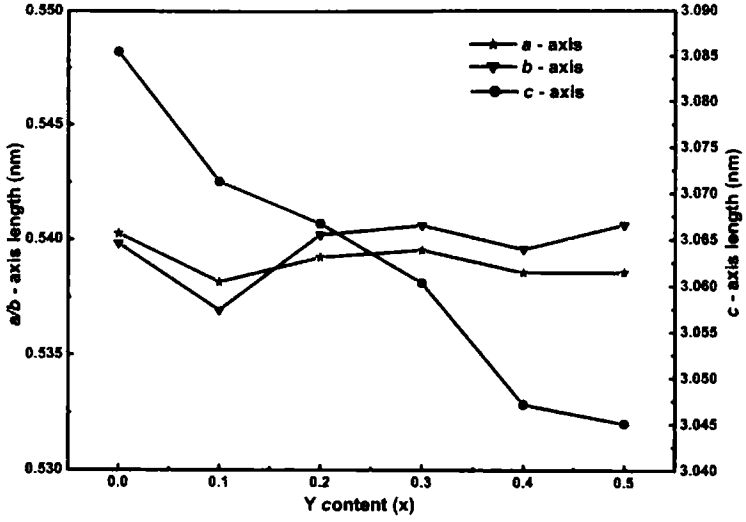

Figure 3.13: Variation of lattice parameters as a function of added Y stoichiometry

tetragonal symmetry for $0.1 \leq x \leq 0.5$. Thus, a slight structural transformation is induced in the Cu-O bond length in the CuO_2 plane as a function of Y content. Also, Y doping imparts additional charge carriers which incorporates excess oxygen into Bi-O layer leading to an increase in oxygen content in the (Bi,Pb)-2212 structure. This induces a contraction in Bi-O layers, which can be attributed to the contraction of c-axis length.

Figure 3.14 shows the temperature dependence of normal state resistivity of Y-free and Y added samples for varying Y content from $x = 0$ to 0.5. All the samples show superconductive transitions. For the Y-free sample a pseudo transition occurs at around $\sim$ 110 K as indicated by a slight drop in resistance. This may be due to the coexistence of the high T_c phase (Bi,Pb)-2223 in very low percentages which could not be detected in the XRD analysis. Also it is found that as the Y content increases, the normal state resistivity of the samples increases while the residual resistivity ratio (RRR) decreases considerably (Figure 3.15). Figure 3.16 shows the variation of T_c and J_c as a function of Y stoichiometry of superconducting samples up to $x = 0.5$. The T_c increases with

increase in Y doping. The maximum T_c obtained is 97.4 K for Y3 sample and thereafter T_c decreases gradually as the Y content increases. The variation ΔT_c is given in table 3.4. It shows that ΔT_c increases initially, reaches a maximum for $x = 0.1$ and thereafter decreases slightly for $0.2 \leq x \leq 0.5$ samples. The large transition width (ΔT_c) observed is due to the change in resistive state of Bi-O layer resulting in the partial isolation of CuO_2 layers across the charge reservoir plane (Bi-O layers) [43,44] as a result of Y addition. The temperature coefficient of resistance α(T) at normal state of pure and Y added (Bi,Pb)-2212 samples is shown in table 3.4. The observed decrease in α(T) and RRR values as a function of Y stoichiometry indicates the decrement in the charge carrier density (holes) in (Bi,Pb)-2212 system, which in turn increases the normal state resistivity of the sample as a whole.

The J_c is found to increase significantly with Y doping (Table 3.4). The maximum J_c obtained is 696 A/cm^2 at 64 K for Y2 sample, while the Y-free sample shows a J_c of 101 A/cm^2 i.e. only $\frac{1}{7}$th of the maximum. It was observed that Y3 measured a maximum T_c, but its J_c (562 A/cm^2) is slightly less than Y2 and this is attributed to the increased porosity, misorientation and shortening of (Bi,Pb)-2212 grains. However, the significant enhancement in J_c observed in general for the Y added samples cannot be attributed to any improvement in microstructure, since pure (Bi,Pb)-2212 sample (Y0) exhibits the best microstructure compared to all the Y added samples.

The enhancement in T_c and J_c of Y added samples are related to the chemical as well as electronic rearrangement introduced due to the dual effect of Y and Pb co-doping in Bi-2212. From the previous section 3.3, it can be seen that there is no appreciable change in T_c of Bi-2212 due to the solo substitution of Pb in Bi-site. The hole carrier density of pure Bi-2212 estimated is 0.37 holes/CuO_2 [45] which is overdoped. The effect of Y addition on T_c is attributed to the change in hole concentration. When Y is added in (Bi,Pb)-2212 system, they are expected to occupy the Ca/Sr site due to their comparable

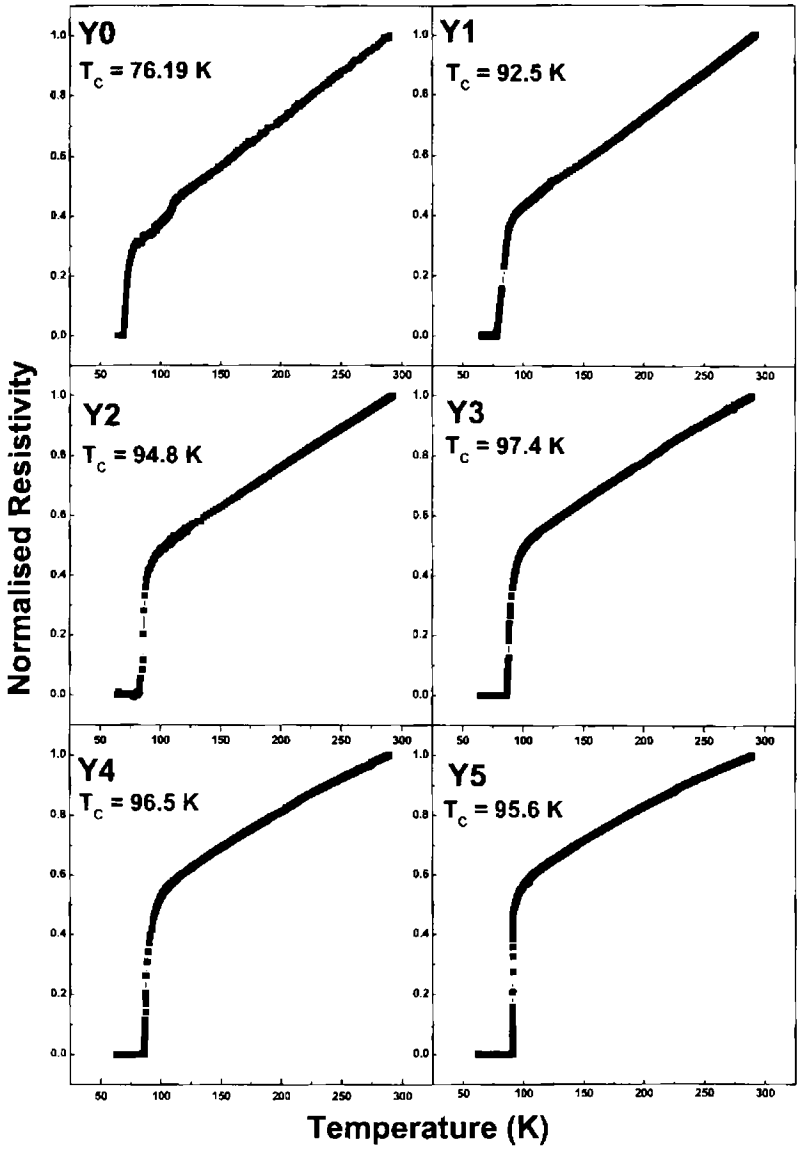

Figure 3.14: Temperature dependent normalized resistivity plots of Y added samples.

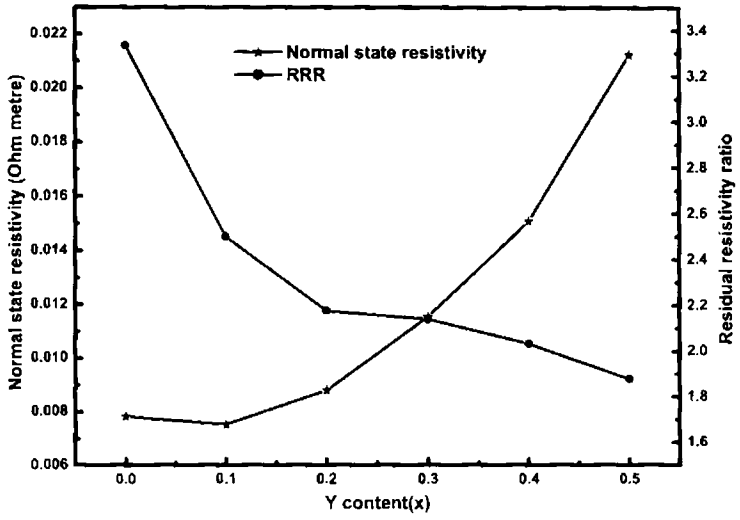

Figure 3.15: Dependence of T_c and J_c on Y stoichiometry.

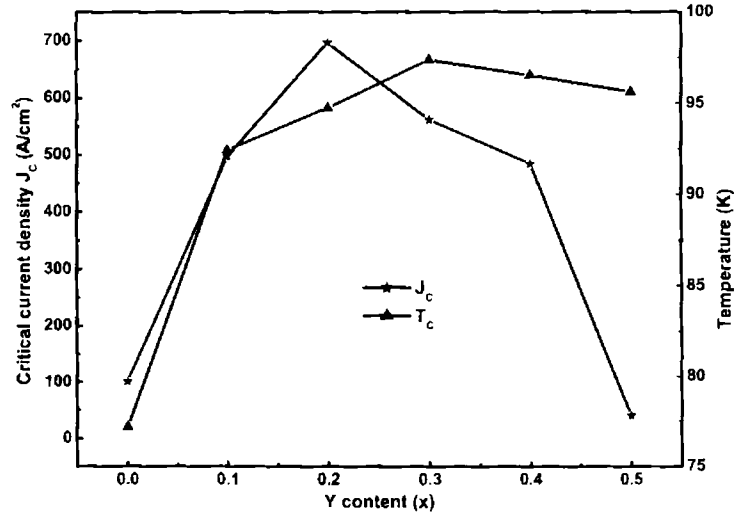

Figure 3.16: Variation of normal state resistivity and RRR with Y content.

ionic size (Ca^{+2} = 0.93 Å, Sr^{+2} = 1.21 Å and Y^{+3} = 0.89 Å). This is evident from the phase assemblage data of the samples particularly at higher doping

concentrations ($x = 0.4$ and $x = 0.5$) and the systematic shrinkage observed in the c-axis parameter with Y addition. The replacement of Ca^{+2}/Sr^{+2} by Y^{+3} ion would result in lowering of the hole concentration from the overdoped pure (Bi,Pb)-2212 to an optimum value at $x = 0.3$ leading to the maximum T_c. As the dopant concentration increases further ($x > 0.3$), the hole carrier concentration decreases and the system goes to underdoped region resulting in lowering of T_c. The electrical conductivity of the blocking layers of Bi-2212 can be systematically enhanced by Pb doping into the blocking layers (Bi-O) [9]. Also, the anisotropy can be substantially reduced by the Pb doping [9, 10]. This increases the Josephson coupling strength between the CuO_2 layers across the insulating Bi-O layers [11] thereby increasing c-axis conductivity and as a result the J_c increases to a maximum. Also, the point defects introduced by the substitution of Y^{+3} at Ca^{+2}/Sr^{+2} sites can act as flux pinning centers, which can enhance the self field J_c. For higher Y contents, excess oxygen ions are incorporated into the oxygen deficient Bi-O layers which make it more insulating. This increases the c-axis resistivity, hence weakening the Josephson coupling strength between the CuO_2 layers across the Bi-O layers resulting in reduction of self field J_c at higher x. Thus it is shown that Y and Pb co-doping

Table 3.4: ΔT_c, Lotgering index (F), Self field J_c (at 64 K) and temperature coefficient of resistance (α) at normal state of pure and Y added (Bi,Pb)-2212 samples

Y Content	ΔT_c (K)	Lotgering Index(F)	J_c at 64 K (A/cm^2)	α(T) (10^{-4}/K)
0	4.45	0.76	101	2.70
0.1	14.6	0.65	497	1.67
0.2	13.0	0.60	696	1.39
0.3	10.7	0.58	562	1.42
0.4	10.6	0.45	484	1.25
0.5	10.1	0.41	40	0.94

in Bi-2212 enhances the superconducting properties of the system to a great extent.

3.5 Summary and Conclusions

Pb-substitution at the Bi-site enhances the self-field J_c while slightly deteriorates the T_c of the Bi-2212 superconductor. The maximum value of the bulk J_c of the Pb-doped (x = 0.5) Bi-2212 sample is $\sim$ 3 times higher than undoped sample. The enhancement of J_c is found to be due to the improved microstructure and the increase in the c-axis conductivity of the system. Considering the fact that the best results are obtained for the Pb content in the range x = 0.4 – 0.5, this composition is chosen for further work presented in the forthcoming chapters.

The studies on the effects of Y addition in Pb doped Bi-2212 show that Y^{+3} ions enter into the crystal structure replacing Ca^{+2} and Sr^{+2}, thereby reducing hole concentration in the electronic structure of the system. Pb co-doping results in the reduction of c-axis resistivity due to the strong Josephson coupling between CuO_2 layers at lower Y contents. The T_c and J_c are significantly enhanced for optimum Y concentration. The maximum T_c is obtained for the sample with x = 0.3 and J_c for the sample with x = 0.2 in the stoichiometry $Bi_{1.7}Pb_{0.4}Sr_{2.0}Ca_{1.1}Cu_{2.1}Y_xO_{8+\delta}$. At higher doping levels secondary phases containing Ca and Sr are observed . The changes in the electrical and superconducting properties are due to the changes in the structural as well as electronic properties induced by Pb and Y co-doping.

References

[1] S. Y. DING, C. REN, X. X. YAO, Y. SUN, and H. ZHANG, *Cryogenics* **38**, 809 (1998).

[2] C. H. CHEN, D. J. WERDER, G. P. ESPINOSA, and A. S. COOPER, *Phys. Rev. B* **39**, 4986 (1989).

[3] J. SCHNEEK, L. PIENE, J. C. TOLEDANO, and C. DAGNEL, *Phys. Rev. B* **39**, 9624 (1989).

[4] O. EIBL, *Physica C* **175**, 419 (1991).

[5] Z. HIROI, I. CHONG, and M. TAKANO, *J. Solid State Chem.* **148**, 98 (1998).

[6] M. MUSOLINO, S. BALS, G. VAN TENDELOO, N. CLAYTON, E. WALKER, and R. FLUKIGER, *Physica C* **399**, 1 (2003).

[7] R. GLADYSHEVSKI, N. MUSOLINO, and F. FLUKIGER, *Phys. Rev. B* **70**, 184522 (2004).

[8] L. WINKELER, S. SADEWASSER, B. BESCHOTEN, H. FRANK, F. NOUVERTNE, and G. GUNTHERODT, *Physica C* **265**, 194 (1996).

[9] T. MOTOHASHI, Y. NAKAYAMA, T. FUJITA, K. KITAZAWA, J. SHIMOYAMA, and K. KISHIO, *Phys. Rev. B* **59**, 14080 (1999).

[10] B. ZHAO, W. H. SONG, J. J. DU, and Y. P. SUN, *Physica C* **386**, 60 (2003).

[11] R. KLEINER and P. MULLER, *Phys. Rev. B* **49**, 1327 (1994).

[12] W. GAO and J. B. V. SANDE, *Supercond. Sci. Technol.* **5**, 318 (1992).

[13] F. K. LOTGERING, *J. Inorg. Nucl. Chem.* **9**, 113 (1959).

[14] D. W. J. JR. and W. W. RHODES, *J. Am. Ceram. Soc.* **72**, 2346 (1989).

[15] R. L. THAYER, S. R. SCHMIDT, S. E. DORRIS, J. W. BULLARD, and M. . T. LANAGAN, *J. Am. Ceram. Soc.* **83**, 2365 (2000).

[16] R. R. KUMAR, J. BOSE, R. P. ALOYSIUS, P. GURUSWAMY, and U. SYAMAPRASAD, *Supercond. Sci. Technol.* **18**, 689 (2005).

[17] P. MANDAL, A. PODDER, B. GHOSH, and P. CHOUDHURY, *Phys. Rev. B* **43**, 13102 (1991).

[18] Y. GAO, P. PERNAMBUC-WISE, J. E. CROW, J. O'REILLY, N. SPENCER, H. CHEN, and R. E. SALOMON, *Phys. Rev. B* **45**, 7436 (1992).

[19] P. E. KAZIN, D. D. ZAITSEV, Y. D. TRET'YAKOV, and M. JANSEN, *Inorg. Mater.* **37**, 812 (2001).

[20] P. MURUGAKOOTHAN, R. JAYAVEL, C. R. V. RAO, C. SUBRAMANIAN, and P. RAMASAMY, *Supercond. Sci. Technol.* **7**, 367 (1994).

[21] D. B. MITZI, L. W. LOMBARDO, A. KAPITULNIK, S. S. LADERMAN, and R. D. JACOWITZ, *Phys. Rev. B* **41**, 6564 (1990).

[22] R. J. CAVA, *J. Am. Ceram. Soc.* **83**, 5 (2000).

[23] T. TAMEGAI, K. KOGA, K. SUZUKI, M. ICHIHARA, F. SAKAI, and Y. IYE, *Jpn. J. Appl. Phys.* **28**, L112 (1989).

[24] S. TOCHIHARA, A. GOTO, H. YASINOKA, H. MAZAKI, M. OSADA, and M. KAKIHANA, *IEEE Trans. Appl. Supercond.* **9**, 2320 (1999).

[25] D. MANDRUS, L. FORRO, C. KENDZIORA, and L. MIHALY, *Phys. Rev. B* **45**, 12640 (1992).

[26] C. KENDZIORA, L. FORRO, D. MANDRUS, J. HARTGE, P. STEPHENS, L. MIHALY, R. REEDER, D. MOECHER, M. RIVERS, and S. SUTTON, *Phys. Rev. B* **45**, 13025 (1992).

[27] Q. CAO, K. Q. RUAU, S. Y. LI, X. H. CHEN, G. G. QIAN, and L. Z. CAO, *Physica C* **334**, 237 (2000).

[28] G. C. KIM, M. CHEON, H. KIM, Y. C. KIM, and D. Y. JEONG, *Phys. Rev. B* **72**, 064525 (2005).

[29] J. S. SHIN, H. ENOMOTO, T. KISHIMOTO, and H. OZAKI, *Jpn. J. Appl. Phys.* **31**, L320 (1992).

[30] E. BACA, V. HOLGUIN, W. LOPERA, and P. PRIETO, *Physica C* **341-348**, 655 (2000).

[31] R. J. SANDERSON and K. C. HEWITT, *Physica C* **425**, 52 (2005).

[32] H. MAZAKI, M. KAKIHANA, and H. YASUOKA, *Jpn. J. Appl. Phys.* **30**, 38 (1991).

[33] W. A. GROEN, D. M. DE LEEUW, and L. F. FEINER, *Physica C* **165**, 55 (1990).

[34] N. L. WANG, A. W. MCCONNELL, B. P. CLAYMAN, and G. D. GU, *Phys. Rev. B* **59**, 576 (1999).

[35] S. M. KHALIL, *J. Phys. Chem. Solids* **64**, 855 (2003).

[36] C. JANOWITZ, U. SEIDEL, R. S. UNGER, L. DUDY, A. KRAPF, R. MANZKE, and H. HOCHST, *J. Supercond. Incorp. Novel. Mag.* **17**, 49 (2004).

[37] A. MAEDA, M. HASE, I. TSUKADA, K. NODA, S. TAKEBAYASHI, and K. UCHINOKURA, *Phys. Rev. B* **41**, 6418 (1990).

[38] I. NOWIK, I. FELNER, and E. R. BAUMINGER, *Phys. Rev. B* **45**, 4912 (1992).

[39] M. A. VAN VEENENDAAL, R. SCHLATMANN, G. A. SAWATZKY, and W. A. GROEN, *Phys. Rev. B* **47**, 446 (1993).

[40] N. HUDAKOVA, K. KNIZEK, and J. HEJTMANEK, *Physica C* **406**, 58 (2004).

[41] D. PRABHAKARAN and C. SUBRAHMANIAN, *Mater. Sci. Engg. B* **52**, 169 (1998).

[42] B. HONG and T. O. MASON, *J. Am. Ceram. Soc.* **76**, 635 (1993).

[43] M. MUROI and R. STREET, *Physica C* **246**, 357 (1995).

[44] V. P. S. AWANA, S. K. AGARWAL, R. RAY, S. GUPTA, and A. V. NARLIKAR, *Physica C* **191**, 43 (1992).

[45] R. P. GUPTA and M. GUPTA, *Phys. Rev. B* **49**, 13154 (1994).

Chapter 4

Superconducting properties of rare earth doped (Bi,Pb)-2212

Learn something about everything and everything about something.
— Thomas Henry Huxley, 1825–1895

4.1 Introduction

In Bi-2212 cuprate superconductors, the CuO_2 plane is believed to be responsible for the superconductivity. The impurities substituted at the Cu site are generally found to suppress the critical temperature (T_c) [1, 2] and the doping outside the CuO_2 plane changes the charge carrier concentration of the system. The superconducting properties of Bi-2212 superconductors are strongly dependent on the hole carrier concentration on the CuO_2 planes. The pure Bi-2212 system is slightly over-doped [3] and hence a careful tuning of the carrier concentration is required to optimize the superconducting properties of the system. Doping of aliovalent impurities or oxygen non-stoichiometry can change the carrier concentration considerably in Bi-based superconduc-

tors [4–7]. Doping of impurity atoms also produces atomic level crystal defects, lattice strains and other structural inhomogeneities in the superconducting matrix. These chemical inhomogeneities and disorders due to the doping strongly affect the critical temperature of these high T_c superconductors and hence the critical current density (J_c) of the system.

In the previous chapter (chapter 3), the influence of Pb-doping on the structural and superconducting properties of Bi-2212 superconductor was investigated. The results show that Pb-substitution at the Bi-site significantly enhances the self-field J_c while slightly deteriorate the T_c of the Bi-2212 superconductor which is attributed to the improved microstructure and current distribution of the system. Based on the previous work, Pb content of x = 0.5 is chosen for the present study. A few reports are available on the substitution of rare earth (RE) in Bi-2212 at Ca-sites. Most of the these previous RE-doping studies on Bi-2212 were done without Pb-doping at Bi-site [8–11] which concluded that even though RE substitution improves the structural stability of Bi-2212, the superconducting and the flux pinning properties show a degrading trend with increase in dopant concentration [12–14]. Our studies on co-doping of Pb and Y in Bi-2212 as presented in the previous chapter 3, have shown significant improvements in its superconducting and flux pinning properties [15–17]. As a continuation of the above studies, this chapter presents the preparation and characterization of Bi-2212 substituted with RE (Lanthanides) and Pb at Sr and Bi sites, respectively. The rare earth dopants are chosen with different ionic size ranging from La to Lu in the periodic table which include magnetic and nonmagnetic rare-earth.

4.2 Experimental details

RE substituted (Bi,Pb)-2212 samples with the nominal stoichiometry of $(Bi_{1.6}Pb_{0.5})(Sr_{2-x}RE_x)Ca_{1.1}Cu_{2.1}O_{8+\delta}$ were prepared by solid-state synthesis

using high purity oxides or carbonates, namely Bi_2O_3, PbO, $SrCO_3$, $CaCO_3$, CuO and RE_2O_3 (Aldrich, > 99.9 %). The RE chosen are La, Eu, Dy, Tb, Ho and Lu. The samples with different RE stoichiometry will be hereafter denoted as RE*x* where, *x* is the stoichiometry. Our trials on Y-addition show that the best superconducting properties for these samples lie between the stoichiometric range of ($0 \leq x \leq 0.5$). The accurately weighed ingredients were ground homogeneously using Agate balls and bowl in a planetary ball-mill (Fritsch Pulversette 6) for 2 hours in acetone medium. The homogeneous mixtures were kept in a muffle furnace with a uniform hot-zone area of 15 cm x 15 cm with temperature stability and accuracy better than ±0.5 °C. A programmable temperature controller (Eurotherm 2404) and a standard S-type thermocouple (NPL, UK) were used for the accurate monitoring and control of temperature. The samples underwent three stages of calcination in air at 800 °C for 15 h + 815 °C for 40 h + 830°C for 40 h with a heating rate of 3 °C/min. Between each stage of calcination, the samples were ground in acetone medium to improve the homogeneity. The calcined powders were then pelletized (12 mm diameter and about 1 mm thickness) under a pressure of 500 MPa. The pellets were heat-treated for 120 h in two stages with a heat treatment schedule of 845 °C for 60 h + 848 °C for 60 h and a heating rate of 1 °C/min with an intermediate pressing under the same pressure.

The structural and phase analyses of the samples were done using XRD (Philips X'pert Pro) equipped with an X'celerator and a monochromator at the diffracted beam side (Step size: 0.0167°, Time per step: 45 seconds). Phase identification was performed using X'pert Highscore software in support with the ICDD-PDF2 database. The microstructure of freshly fractured surface of the samples were done using scanning electron microscope (SEM, JEOL JSM 5600LV) with an accelerating voltage of 15 kV in secondary ion emission mode. The elemental analysis of the samples was done using energy dispersive X-ray spectroscope (EDS) attached to SEM. The bulk density of the sintered pellets was estimated by measuring their mass and geometrical dimensions.

Cylindrical pellets were shaped into rectangular form with the dimensions 12 x 4 x 1 mm^3 on which the potential leads, separated by a distance of 5 mm, were placed at the central part of the specimen. The transition temperature (T_c) of the samples was determined by the four-probe dc resistance method by cooling the sample in a liquid N_2 cryostat with the provision for vacuum. In order to minimize the contact resistance, four silver strips were fixed on to one surface of the pellet during pressing. Leads of high quality copper were soldered to silver strips. The outer two leads were connected to a programmable dc current source (Keithely model: 220) and a constant current of 10 mA was used for the resistance measurement. The voltage drop between the inner two leads was measured using a programmable nano voltmeter (Keithely model: 181 & 2182). The transport J_c of the samples under self-field were measured in a LN_2 bath cryostat, with a provision for vacuum at 64 K, using four-probe method. A programmable temperature controller (Lakeshore 340) was used for the accurate monitoring of the temperature with a stability and accuracy of $\pm$ 0.01 K. The direction of current was parallel to the direction of pressed surface and the magnetic field was perpendicular to the pressed surface of the pellet. Critical current (I_c) values of the samples were determined using standard criterion of 1 μV/cm, derived from the resistance between voltage terminals. The J_c values of the (Bi,Pb)-2212 were calculated from I_c and the total cross-sectional area of the samples.

4.3 Results and discussion

4.3.1 X-ray diffraction analysis

The XRD patterns of the samples after final stage heat-treatment show that the RE-free and the RE substituted samples contain (Bi,Pb)-2212 phase only [Figures 4.1(a)–4.1(f)]. The (*hkl*) values of each peaks are marked in the fig-

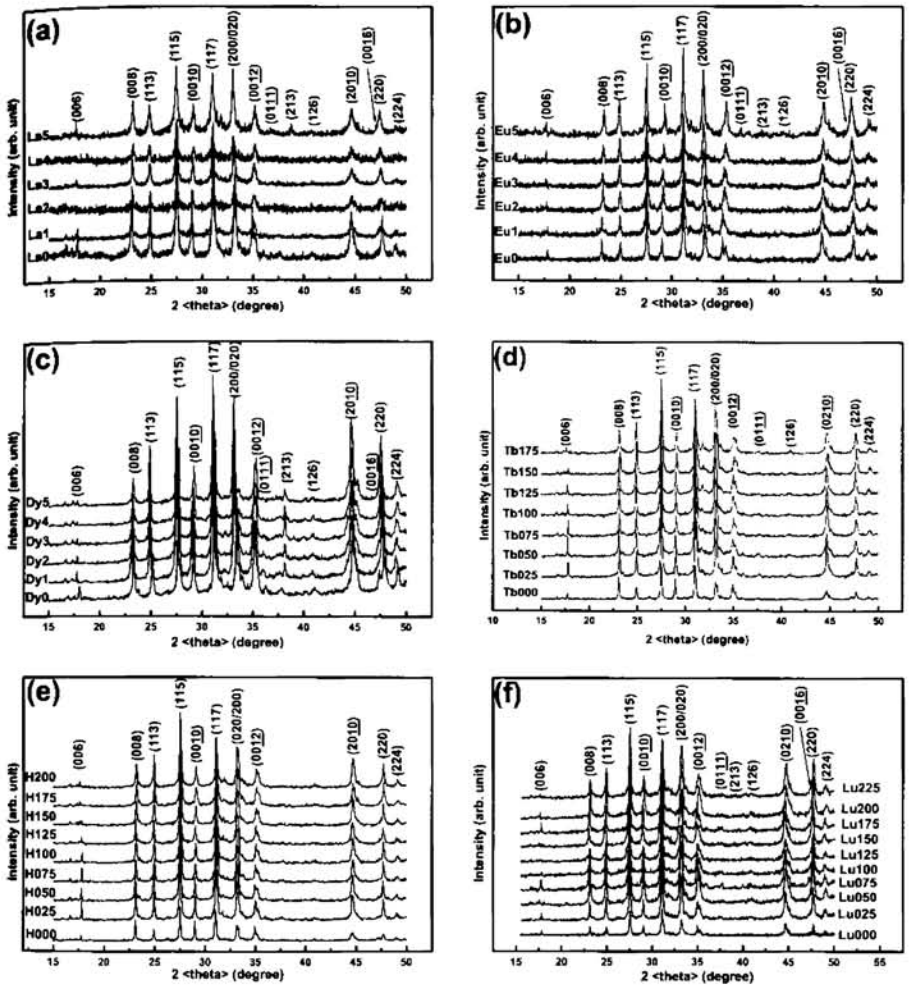

Figure 4.1: XRD patterns of the RE substituted (Bi,Pb)-2212 samples after last stage heat treatment at 848 °C. (RE = La, Eu, Dy, Tb, Ho and Lu.)

ure. In order to avoid the effect of slight variations in the processing conditions, a RE-free sample is prepared with every batch of RE substitution for a better comparison. The XRD patterns are analysed using the X'pert High-score software. It is found that no secondary phase containing RE or any other cation is detected even up to the highest value of investigated x, at this stage

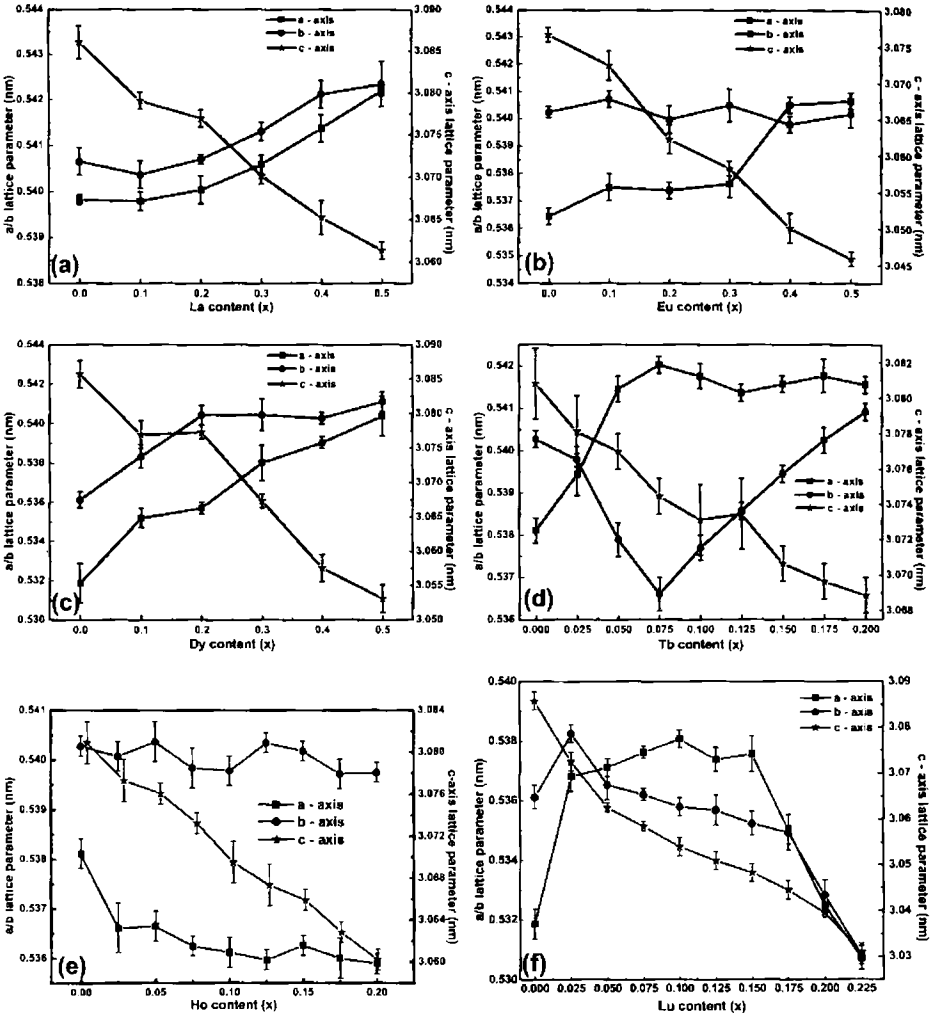

Figure 4.2: Variation in the lattice parameters of the RE substituted (Bi,Pb)-2212 samples. (RE = La, Eu, Dy, Tb, Ho and Lu.)

within the detection limit of the instrument. The absence of secondary phases suggests that all the reactant phases are converted into the (Bi,Pb)-2212 and the substituted RE is incorporated into the crystal structure of (Bi,Pb)-2212 superconductor.

Lattice parameter variations of RE-free and RE substituted samples calculated by considering an orthorhombic symmetry for (Bi,Pb)-2212 system using the formula, $\left(\frac{1}{d^2}\right) = \left(\frac{h^2}{a^2} + \frac{k^2}{b^2} + \frac{l^2}{c^2}\right)$ are shown in Figure 4.2(a)–4.2(f), where d is the inter-planar spacing and (hkl) are the Miller indices. A marked variation is observed in the crystal structure of RE substituted samples compared to RE-free sample. It is found that for the RE-free sample, b-axis value is greater than a-axis (b > a). With increase in RE-content except for Ho, the orthorhombic symmetry of the system changes to a pseudo-tetragonal symmetry at higher x, where the a and b lattice parameters almost coincide. Ho substituted samples maintain its orthorhombic symmetry up to its highest level of doping. It is generally noted that the a/b-axis parameters of La, Eu, Dy substituted samples show an increasing trend, while Lu substituted sample shows a decreasing trend. Tb substituted samples show a decreasing tendency in b-axis parameter up to Tb075 and then increases to form a pseudo tetragonal structure. No appreciable change in a/b axis parameters is observed for Ho substituted samples. The variations in the a/b lattice parameters are associated with the increase in Cu–O bond length in CuO_2 planes, which controls the dimensions in the basal planes of (Bi,Pb)-2212 system [11].

A general tendency of systematic contraction in the c-axis length is observed with increase in RE-content, indicating the incorporation of RE atoms into the system. This is because in Bi-based cuprate superconductors, when a trivalent cation RE^{+3} (ionic radii between 0.0890 and 0.1052 nm) replaces a divalent cation Sr^{+2} (0.132 nm), additional oxygen in the Bi-O layers of the structure is incorporated in order to establish the charge neutrality. As a result, the repulsion between Bi-O planes gets reduced due to the reduction in the net positive charge in the Bi-O planes. This results in the contraction of Bi-O layers and causes the reduction of the c-axis length. The anisotropy of the system decreases with these changes in the lattice parameters [18]. The variation in lattice parameters is also reflected in the change in cell volume of RE substi-

tuted samples (Table 4.1 and 4.2). For example, the cell volume of La, Eu and Dy increases slightly with RE content. Tb substituted samples also show an increase in cell volume after an initial decrease up to $x = 0.075$. Ho and Lu substituted (Bi,Pb)-2212 samples show a large reduction in cell volume which is due to the large reduction in the c-axis length of these superconductors. The important result noticed is that the c-axis contraction is dependent on the ionic radii of the RE dopant. The decrease in the c-axis length is gradual for the RE with larger ionic radii while the shrinkage is drastic when a RE with smaller ionic radii is substituted. For example, when La is substituted, the value of c-axis parameter decreased from 3.087 nm to 3.061 nm for a change in x from 0.0 to 0.5, while for Lu substituted sample, the c-parameter decreases from 3.085 nm to 3.031 nm between $x = 0.0$ to 0.225.

Using the XRD patterns of both pellet and powdered samples, the Lotgering index (F) is calculated (Table 4.1–4.2) using the equation $F = \frac{(P_a - P_r)}{(1 - P_r)}$, where P is defined as $P = \frac{\Sigma I(00l))}{\Sigma I_{total}}$, the suffix 'a'and 'r' denote diffraction patterns of

Rare earth	Sample (x)	Cell volume (nm^3)	Density (gcm^{-3})	F	T_c (K)	J_c (Acm $^{-2}$)	ρ_{298K} (± 0.01) ($\mu\Omega$m)	ΔT_c (± 0.01) (K)
RE-free	0.000	0.880	5.55	0.92	80.4	109	3.16	5.40
	0.1	0.898	5.44	0.84	89.3	455	15.74	7.85
	0.2	0.899	5.52	0.82	90.6	687	20.41	9.83
La	0.3	0.899	5.60	0.70	91.3	73	28.90	10.46
	0.4	0.900	5.85	0.59	94.7	24	34.86	16.57
	0.5	0.900	5.93	0.51	86.1	10	39.34	19.38
	0.1	0.893	5.43	0.73	92.8	1196	2.82	9.55
	0.2	0.888	5.44	0.69	95.7	1062	2.75	10.5
Eu	0.3	0.889	5.48	0.62	89.1	48	8.94	11.3
	0.4	0.890	5.59	0.57	85.9	9	12.88	11.8
	0.5	0.890	5.63	0.54	77.0	NM*	15.67	12.3

*Not measurable

Table 4.1: Different parameters observed for RE-free and La and Eu substituted (Bi,Pb)-2212 samples

Rare earth	Sample (x)	Cell volume (nm^3)	Density (gcm^{-3})	F	T_c (K)	J_c (Acm^{-2})	ρ_{298K} (± 0.01) ($\mu\Omega m$)	ΔT_c (± 0.01) (K)
RE-free	0.000	0.880	5.55	0.92	80.4	109	3.16	5.40
	0.1	0.887	5.55	0.75	89.6	587	2.81	7.75
	0.2	0.890	5.52	0.73	90.2	1392	2.76	8.46
Dy	0.3	0.892	5.47	0.68	91.5	850	6.32	8.87
	0.4	0.890	5.41	0.64	92.3	324	11.04	16.37
	0.5	0.893	5.36	0.56	91.1	85	15.11	18.87
	0.025	0.896	5.50	0.85	84.7	364	2.25	6.05
	0.050	0.896	5.48	0.78	86.5	970	2.95	6.93
	0.075	0.894	5.43	0.74	88.5	1810	2.98	7.77
Tb	0.100	0.895	5.34	0.69	90.6	1384	3.38	8.33
	0.125	0.896	5.29	0.63	92.0	1055	3.87	8.68
	0.150	0.897	5.25	0.60	95.1	760	4.38	9.02
	0.175	0.898	5.20	0.59	96.4	682	5.80	9.55
	0.200	0.899	5.18	0.57	97.3	275	6.75	10.48
	0.025	0.892	5.47	0.90	84.6	302	2.92	7.21
	0.050	0.892	5.43	0.87	87.7	875	3.09	7.90
	0.075	0.890	5.40	0.85	88.5	1203	3.15	8.43
Ho	0.100	0.888	5.40	0.85	91.6	946	3.20	8.98
	0.125	0.888	5.37	0.83	91.8	883	3.26	9.74
	0.150	0.888	5.35	0.79	93.5	407	3.30	10.45
	0.175	0.886	5.35	0.79	95.4	95	3.36	11.67
	0.200	0.885	5.31	0.77	97.7	51	3.40	10.87
	0.025	0.888	5.56	0.88	88.1	342	4.88	8.84
	0.050	0.883	5.55	0.85	89.5	909	5.45	9.55
	0.075	0.882	5.52	0.82	93.5	1015	5.54	12.60
Lu	0.100	0.880	5.46	0.80	94.2	1380	6.30	13.70
	0.125	0.878	5.40	0.80	94.6	990	6.40	13.75
	0.150	0.877	5.38	0.75	95.6	785	8.52	12.30
	0.175	0.871	5.35	0.70	97.4	530	9.64	10.90
	0.200	0.862	5.23	0.63	99.1	62	10.24	9.83
	0.225	0.854	5.10	0.55	89.0	15	17.60	6.45

Table 4.2: Different parameters observed for RE-free, Dy, Tb, Ho and Lu substituted (Bi,Pb)-2212 samples

the pellet sample with the crystallites aligned along *(00l)* and powdered sample with random orientation of crystallites, respectively [19]. Lotgering index represents the degree of texturing in the grains. Bi-2212 system is inherently oriented in the (00*l*) direction due to its characteristic layered growth along the a-b plane, which is further enhanced by the repeated pressing process and hence, the reflections from the oriented (00*l*) planes have high intensities. It is observed that as the RE-content increases, the F-value decreases monotonically for all the RE substituted samples. The maximum value of F is obtained for RE-free sample (0.92).

4.3.2 Microstructural analysis

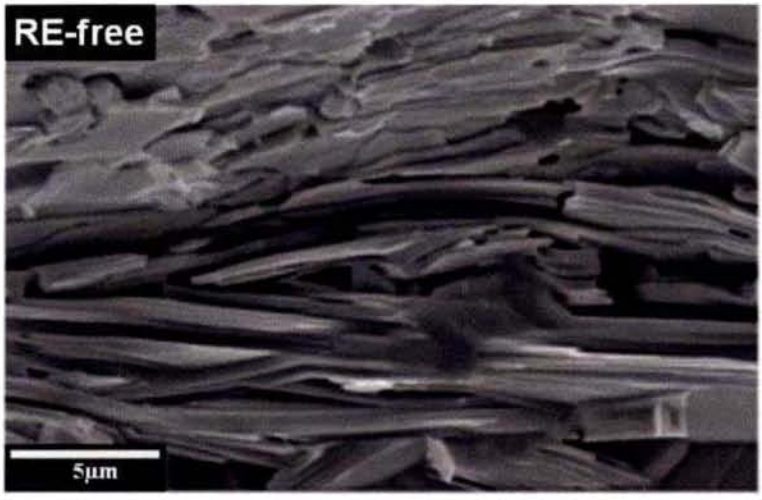

Figure 4.3: SEM micrograph of the fractured surface of the RE-free (Bi,Pb)-2212 sample.

The SEM micrographs of freshly fractured surfaces of RE-free and RE substituted (Bi,Pb)-2212 samples are shown in Figure 4.3 and Figures 4.4–4.8, respectively. The structural morphology of the samples varies with increase in x value. The $x = 0$ sample (RE-free, figure 4.3) shows clear and characteristic flaky grains revealing the layered growth mechanism, typical of (Bi,Pb)-2212.

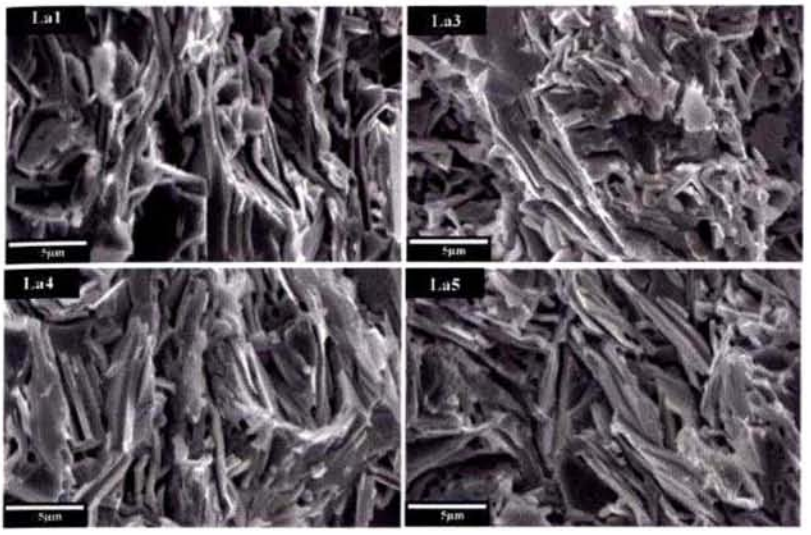

Figure 4.4: SEM micrographs of the fractured surface of La substituted (Bi,Pb)-2212 samples.

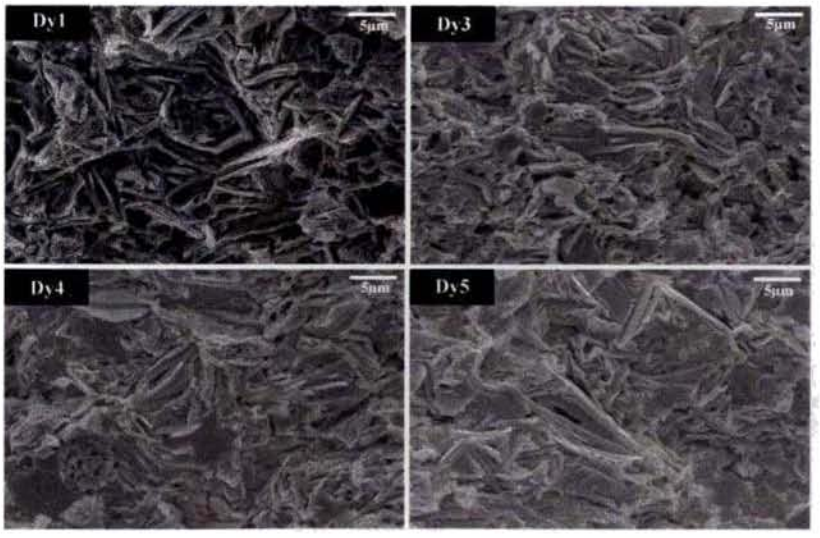

Figure 4.5: SEM micrographs of the fractured surface of Dy substituted (Bi,Pb)-2212 samples.

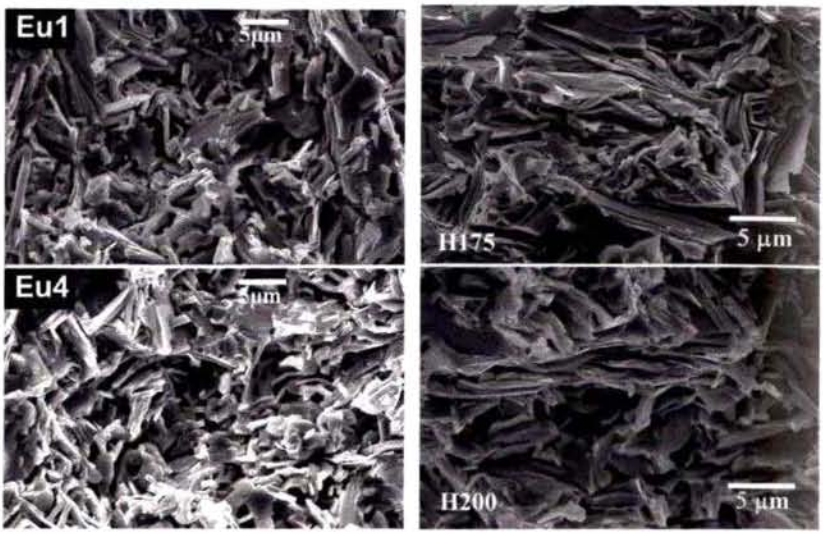

Figure 4.6: SEM micrographs of the fractured surface of Eu substituted (left panel) and Ho substituted (right panel) samples.

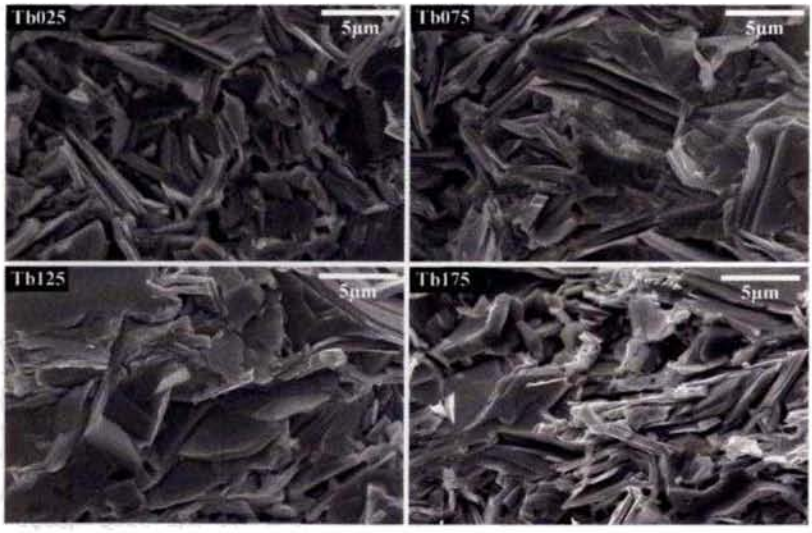

Figure 4.7: SEM micrographs of the fractured surface of Tb substituted (Bi.Pb)-2212 samples.

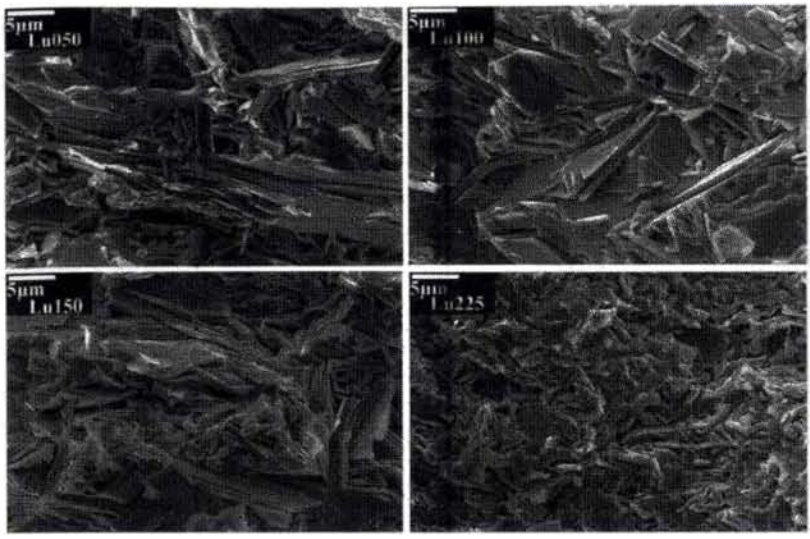

Figure 4.8: SEM micrographs of the fractured surface of Lu substituted (Bi,Pb)-2212 samples.

But, as x value increases, the porosity of the samples increases due to the disrupted grain growth. This leads to a reducing trend in the bulk density of the RE substituted samples (Table 4.1 and 4.2). Considering the texturing or grain alignment of samples, RE-free shows the best structure compared to all other samples. This is further evidenced from the Lotgering index (F) calculation of the samples. Secondary phases or its colonies are not detected in any of the samples, even up to the highest value of investigated x. Among the measured RE substituted samples, La, Dy and Tb substituted samples show better microstructure than Eu, Ho and Lu substituted samples which are sintered at similar conditions. The result is also reflected in the final bulk density values of La, Dy and Tb substituted also (Table 4.1 and 4.2). This deterioration in the microstructure plays an important role in limiting the self-field J_c of the system, since the weak links associated with the grain boundaries are known to limit the J_c values of superconductors. The possible reasons for the formation of these weak links are the misorientation of grain boundaries and the

compositional variations at the grain boundaries. In the case of RE substituted samples, the misorientation gradually increases with an increase in RE content (as shown in Figure 4.4–4.8).

4.3.3 Compositional analysis

Compositional analysis was performed by EDS attached with SEM on a number of large-flaky single-grains (spot analysis) and typical EDS patterns of

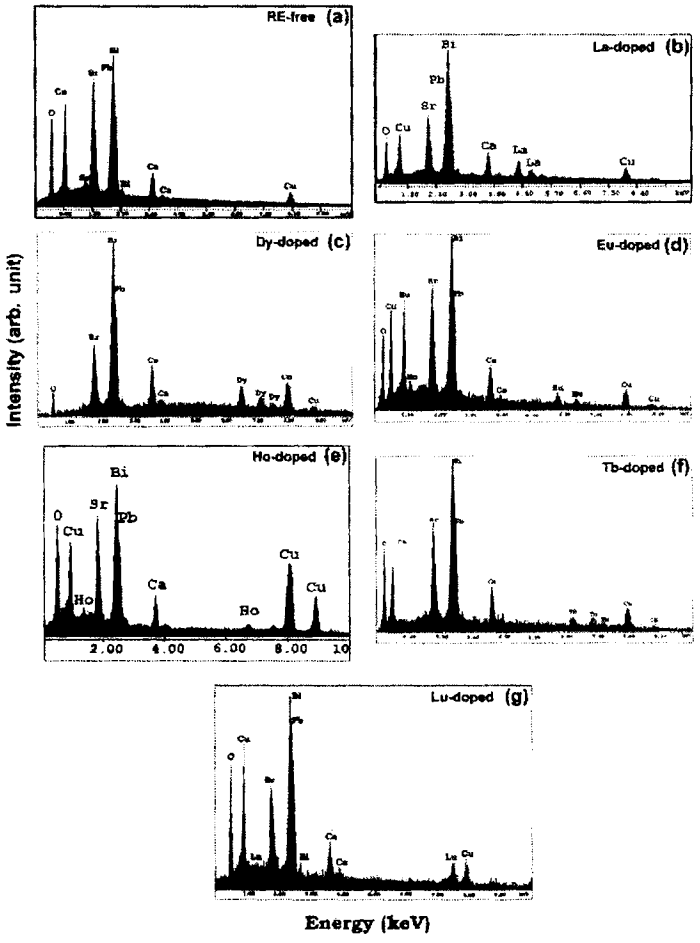

Figure 4.9: EDX spectrographs of the RE-free and RE substituted (Bi,Pb)-2212 samples.

RE-free and RE substituted (Bi,Pb)-2212 grains with the highest RE content in each category are shown in Figure 4.9. The figure shows the presence of RE in the doped sample with a corresponding decrease in Sr peaks in comparison with the RE-free sample. It also shows that the ratio of RE/Sr in the (Bi,Pb)-2212 grains is almost equal to that of the corresponding starting composition for each x, which indicates that the substituted RE is successfully incorporated in the crystal structure of (Bi,Pb)-2212. The quantitative data of the cations in all the doped samples estimated from EDX by keeping the intensity of Cu as standard, is given in Table 4.3. It can be seen that the stoichiometry of (Bi,Pb) reduces and remains almost invariant in all the samples. The initial stoichiometry of (Bi,Pb) is taken in excess in order to compensate this reduction, which is attributed to the volatile nature of Bi and Pb. The quantitative data in table 4.3 also shows that the stoichiometry of Sr and RE in the final samples vary according to the nominal stoichiometry envisaged, within a limit around $\sim$ 10 %. Hence, the data confirms the successful substitution of RE at the Sr-site in (Bi,Pb)-2212 system.

	Stoichiometry							
Samples	(Bi,Pb)		Sr		RE		Ca	
	Initial	Final	Initial	Final	Initial	Final	Initial	Final
RE-free	2.10	2.01	2.000	1.95	0.000	0.00	1.10	1.04
La5	2.10	1.99	1.500	1.42	0.500	0.44	1.10	1.05
Eu5	2.10	1.98	1.500	1.40	0.500	0.45	1.10	1.05
Dy5	2.10	2.00	1.500	1.41	0.500	0.44	1.10	1.03
Tb200	2.10	1.99	1.800	1.68	0.200	0.17	1.10	1.06
H200	2.10	1.99	1.800	1.69	0.200	0.16	1.10	1.06
Lu225	2.10	2.01	1.775	1.62	0.225	0.20	1.10	1.04

Table 4.3: Quantitative data obtained from the compositional analysis on EDX for RE-free and RE substituted (Bi,Pb)-2212 samples with highest RE content.

4.3.4 Resistivity – Temperature (ρ-T) measurements

Figures 4.10 and Figures 4.11–4.16 show the temperature dependence of resistivity (ρ–T) of RE-free and RE substituted samples, respectively. The critical temperature (T_c) of the samples is determined by estimating the temperature at which the resistivity starts dropping from a linearly varying metallic behaviour ($\frac{d\rho}{dt} > 0$), while cooling it. It is observed that all the samples show metallic behaviour above the T_c except for H200 and Lu225. It shows that the T_c increases with increase in RE concentration. The maximum T_c obtained for La, Eu and Dy substituted samples are 94.7 K (x = 0.4), 95.7 K (x = 0.2) and 92.3 K (x = 0.4), respectively, while the T_c obtained for Tb, Ho and Lu substituted samples are 97.3 K, 97.7 K and 99.1 K at x=0.200, respectively. It is clear from the figures 4.11–4.16 that among the RE substituted samples, the maximum T_c is shown by Lu substituted sample (99.1 K) which is $\sim$ 19 K higher than the RE-free. H200 sample shows a unique iso-resistivity behaviour ($\frac{d\rho}{dt} \sim 0$) right above T_c, while an onset of the superconductor to semiconductor transition ($\frac{d\rho}{dt} < 0$) is observed in Lu225. These peculiar behaviour observed at the highest RE concentration marks the onset of the metal-to-insulator transition (MIT).

The hole carrier concentration of the RE substituted samples showing a superconducting transition is calculated using the phenomenological formula, $\frac{T_c}{T_{c-max}} = 1 - 82.6(p_h - 0.16)^2$ where, p_h is the hole carrier concentration/Cu atom [20] and the dependence of T_c on hole concentration is given in figure 4.17. The results show that as the dopant level increases, the hole carrier concentration continues to decrease which makes the system optimally doped, where the T_c of the RE substituted samples becomes maximum. Beyond the optimum level, the system is transformed into an underdoped state with lesser amount of hole carrier concentration resulting in the visible observation of iso-resistivity and MIT as in the case of H200 and Lu225 samples. This can be understood by the following explanation. It is well known that RE-free

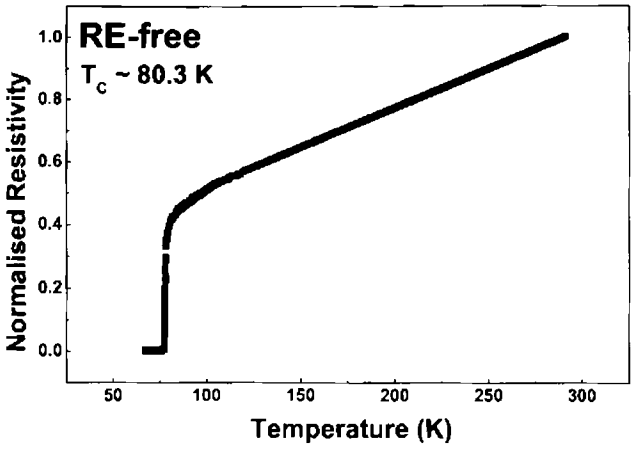

Figure 4.10: Temperature dependence of resistivity of RE-free (Bi,Pb)-2212 superconductor.

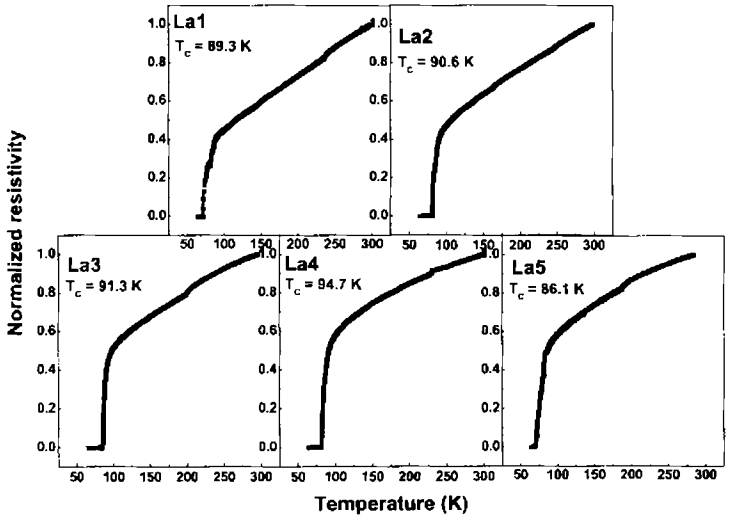

Figure 4.11: Temperature dependence of resistivity of La substituted (Bi,Pb)-2212 superconductor.

(Bi,Pb)-2212 system is inherently "overdoped" with holes. When RE^{+3}/RE^{+4} ions are substituted for Sr^{+2}, each substitution of RE provides additional electrons to fill the vacant holes in the crystal. Hence, the hole concentration in the

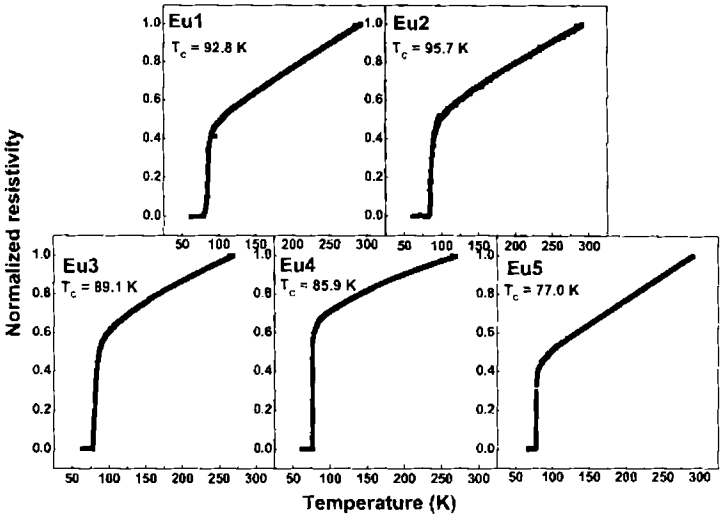

Figure 4.12: Temperature dependence of resistivity of Eu substituted (Bi,Pb)-2212 superconductor.

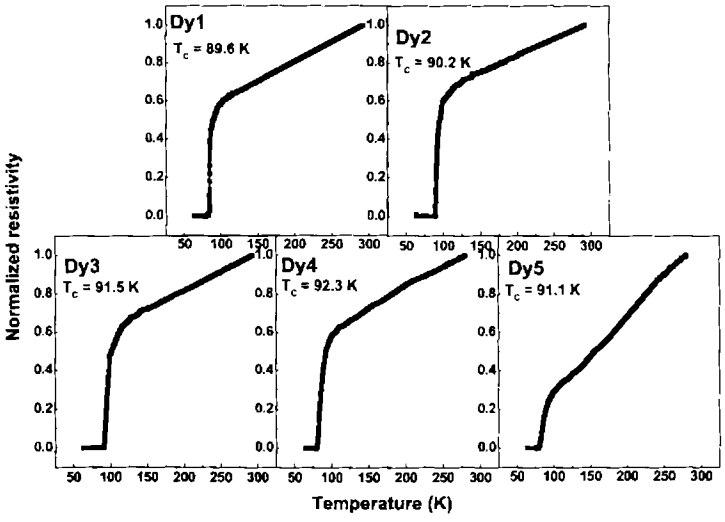

Figure 4.13: Temperature dependence of resistivity of Dy substituted (Bi,Pb)-2212 superconductor.

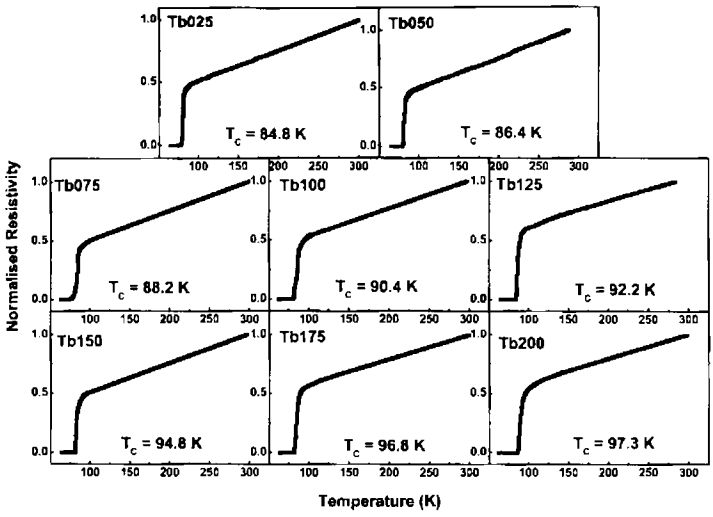

Figure 4.14: Temperature dependence of resistivity of Tb substituted (Bi,Pb)-2212 superconductor.

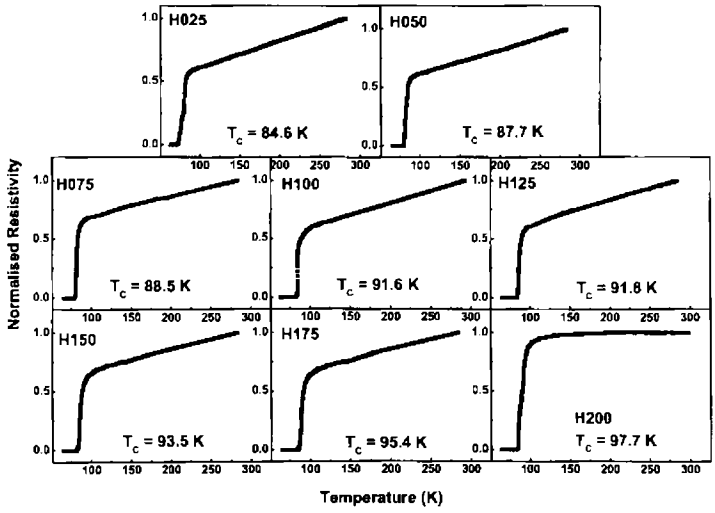

Figure 4.15: Temperature dependence of resistivity of Ho substituted (Bi,Pb)-2212 superconductor.

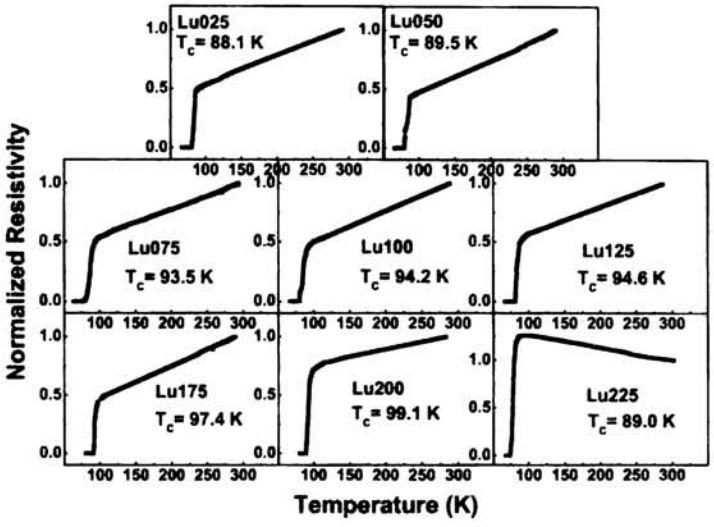

Figure 4.16: Temperature dependence of resistivity of Lu substituted (Bi,Pb)-2212 superconductor.

CuO_2 plane decreases. This controls the hole concentration in the CuO_2 planes and when the RE concentration reaches the optimum stoichiometry, the system becomes "optimally doped" leading to enhanced T_c, J_c and normal state conductivity. Beyond this "optimally doped state" the system becomes "underdoped" due to the large reduction of hole concentration which detonates the transformation of the conduction mechanism of (Bi,Pb)-2212 from metallic to semiconductor or insulator. The transition width, ΔT_c is also found to increase with increase in RE content (Table 4.1 and 4.2). This increase in the ΔT_c is due to the changes in chemical as well as electronic inhomogeneity in the (Bi,Pb)-2212 system caused by the variation in the charge carrier concentration due to RE substitution.

The normal state resistivities (ρ_{300}) of RE-free and RE substituted samples are given in table 4.1 and 4.2. The data indicates that the normal state resistivity of RE-free (Bi,Pb)-2212 is minimum as compared to RE substituted samples. ρ_{300} systematically increases with the increase in RE content, but it

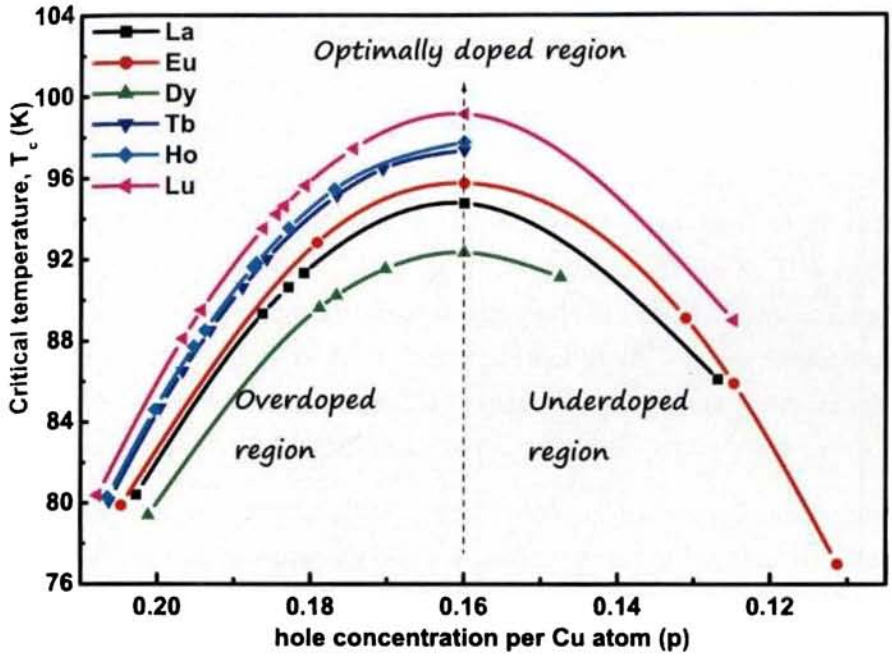

Figure 4.17: Dependence of T_c on the hole carrier concentration of the RE substituted (Bi,Pb)-2212 superconductors.

specifically depends on the substituted RE. La substituted (Bi,Pb)-2212 samples show relatively high values of ρ_{300} while Ho substituted samples show the least values. At higher RE contents the increase in the ρ_{300} is drastically high. Such an enormous increase in the ρ_{300} is due to the increased porosity of RE substituted (Bi,Pb)-2212 superconductor, which increases the resistive weak links between the grains.

4.3.5 Transport critical current density (J_c) measurements

The variation in the transport J_c determined at 64 K of RE-free and RE substituted (Bi,Pb)-2212 samples is shown in figure 4.18. The self-field J_c is

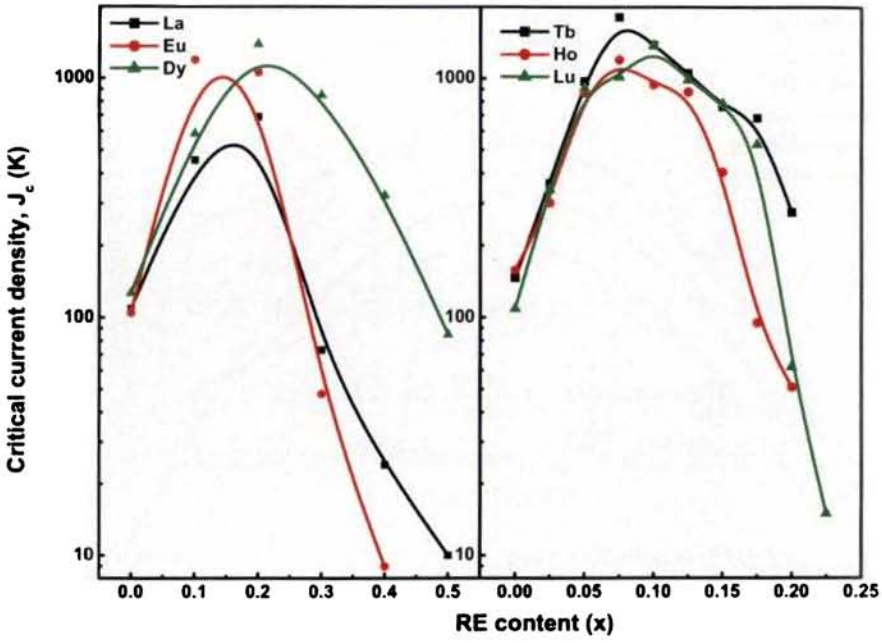

Figure 4.18: Variation in the transport J_c (at 64 K) of the RE-free and RE substituted (Bi,Pb)-2212 samples.

found to increase significantly with RE substitution and it reaches a maximum at around $x = 0.1 - 0.2$ for La, Eu and Dy and around $x = 0.050 - 0.125$ for Tb, Ho and Lu and then decreases at higher RE concentrations. Moreover, the value of J_c also depends on the substituted RE. The pure sample shows a J_c between the range of 109 – 160 A/cm^2, while the maximum J_c obtained by RE substitution is in the range of 687 – 1810 A/cm^2 at 64 K. This shows that the J_c is enhanced drastically at the optimum doping concentration which is around $x = 0.075$, 0.100 and 0.200 for Tb and Ho, Eu and Lu and La and Dy, respectively. The increase in transport J_c is $\sim 6 - 18$ times higher, when compared to the RE-free (Bi,Pb)-2212 sample. The enhancement in the transport J_c can be explained as follows. The replacement of Sr with RE results in the chemical and electronic re-arrangement of the charge reservoir layers (Sr-O/Bi-O/Sr-O)

adjacent to the CuO_2 layers through which the actual supercurrent is believed to flow. The crystal defects created due to the RE substitution is mainly confined in the Sr-layer. At self-fields, vortices confined in the CuO_2 layers are effectively pinned by the defects in the Sr-layer which leads to the formation of strongly coupled Josephsons vortices in the CuO_2 layer. Hence, RE substitution in (Bi,Pb)-2212 increases the Josephsons coupling strength between the CuO_2 layers across the blocking layers (Sr-O/Bi-O/Sr-O). This improves the self field J_c of the optimized RE substituted (Bi,Pb)-2212 superconductors. The improvement in T_c of RE substituted (Bi,Pb)-2212 is due to the decrease in the hole concentration in the Cu-O plane to its optimal level, which also contributes towards the transport J_c.

Further, RE substitution alone cannot produce the observed enhancement in J_c. The electrical conductivity of the blocking layers of Bi-2212 is systematically enhanced, and the anisotropy is substantially reduced by the doping of Pb atoms into the blocking layers (Bi-O) [21, 22]. This increases the Josephson coupling strength between the CuO_2 layers across the insulating Bi-O layers [23], which in turn increases the c-axis conductivity, and as a result, J_c increases. In addition, the flux-pinning centers introduced by the RE^{+3}/RE^{+4} ion in the (Bi, Pb)-2212 lattice enhance the self-field J_c. Thus, it is concluded that the enhancement in J_c of RE substituted samples is because of the chemical and electronic re-arrangement introduced due to the dual effect of RE and Pb co-doping in Bi-2212. At higher x values, the J_c of the RE substituted samples decreases. This is because, at higher RE concentrations, grain boundary weak-links and porosity would contribute to the significant degradation of the bulk density. Thus, it is concluded that T_c does not depend strongly on the microstructure while J_c does depend on it.

The drastic decrease of J_c value at higher RE concentrations is attributed to a large decrease in charge carrier concentration, increased porosity and weak links due to the heavy doping of RE in (Bi,Pb)-2212 system. Furthermore, at higher RE contents, excess oxygen content is incorporated into oxygen-

deficient Bi-O layers, which makes it more insulating. This increases the c-axis resistivity, hence, weakening the Josephson coupling strength between the CuO_2 layers across the Bi-O layers, resulting in the reduction of the self-field J_c at higher x. The reduction of the hole concentration beyond the optimum level at higher RE concentration also triggers the MIT in (Bi,Pb)-2212 system.

4.4 Conclusions

This chapter presents the experimental results on the structural and superconducting properties of RE substituted (Bi,Pb)-2212 $[(Bi_{1.6}Pb_{0.5})(Sr_{2-x}RE_x)Ca_{1.1}Cu_{2.1}O_{8+\delta}]$ superconductors studied for different RE concentrations ($0 \leq x \leq 0.5$) and the results are compared with RE-free (Bi,Pb)-2212 superconductor. It is observed that a significant structural and electronic changes takes place in the system due to RE substitution. As a result, the critical temperature (T_c) and critical current density (J_c) increase remarkably at optimum RE concentrations. The variations in these properties are gradual for REs : La, Eu and Dy for which the optimum superconducting properties were observed at x = 0.3–0.4, while for REs : Tb, Ho and Lu, these properties drastically change with the increasing RE content and the optimum superconducting properties were observed at x = 0.175–0.200. The maximum value of T_c is observed at different x values depending on the substituted RE. The increase in T_c as well as J_c is explained by the dual effect of the decrease in the hole concentration in CuO_2 planes from the overdoped to an optimally doped state and the improvement of coupling between the CuO_2 layers across the charge reservoir layer achieved by RE-doping. Beyond the optimum levels, the T_c gets reduced and an underdoped condition is attained due to further reduction in the charge carrier concentration, which triggers a metal to insulator transition in (Bi,Pb)-2212 system. J_c also decreases rapidly at higher x because of the weakening of the Josephson coupling strength and the increased porosity and weak-links.

References

[1] J. M. TARASCON, P. BARBOUX, P. F. MICELI, L. H. GREENE, G. W. HULL, M. EIBSHUTZ, and S. A. SUNSHINE, *Phys. Rev. B* **37**, 7458 (1998).

[2] B. V. HEDT, W. LIIECK, K. WESTERHOLT, and H. BACK, *Phys. Rev. B* **49**, 9898 (1994).

[3] R. P. GUPTA and M. GUPTA, *Phys. Rev. B* **49**, 13154 (1994).

[4] V. P. S. AWANA, S. K. AGARWAL, A. V. NARLIKAR, and M. P. DAS, *Phys. Rev. B* **48**, 1211 (1993).

[5] A. THAMIZHAVEL, D. PRABHAKARAN, R. JAYAVEL, and C. SUBRAMANIAN, *Physica C* **275**, 279 (1997).

[6] A. Y. ILYUSHECHKIN, T. YAMASHITA, L. BOSKOVIC, and I. D. R. MACKINNON, *Supercond. Sci. Technol.* **17**, 1201 (2004).

[7] X. CHEN, J. LIANG, J. MIN, J. LI, and G. RAO, *Phys. Rev. B* **50**, 3431 (1994).

[8] K. K. UPRETY, J. HOVART, X. L. WANG, M. IONESCU, H. K. LIU, and S. X. DOU, *Supercond. Sci. Technol.* **14**, 479 (2001).

[9] Q. CAO, K. Q. RUAU, S. Y. LI, X. H. CHEN, G. G. QIAN, and L. Z. CAO, *Physica C* **334**, 237 (2000).

[10] E. BACA, V. HOLGUIN, W. LOPERA, and P. PRIETO, *Physica C* **341-348**, 655 (2000).

[11] R. J. SANDERSON and K. C. HEWITT, *Physica C* **425**, 52 (2005).

[12] S. SINGH, *Physica C* **294**, 249 (1998).

[13] H. JIN and J. KOTZLER, *Physica C* **325**, 153 (1999).

[14] C. A. M. DOS-SANTOS, G. S. PINTO, B. FERREIRA, and A. J. S. MACHADO, *Physica C* **354**, 388 (2001).

[15] P. M. SARUN, A. BIJU, P. GURUSWAMY, and U. SYAMAPRASAD, *J. Am. Ceram. Soc.* **90**, 3138 (2007).

[16] A. BIJU, P. M. SARUN, R. P. ALOYSIUS, and U. SYAMAPRASAD, *J. Alloys and Comp.* **454**, 46 (2008).

[17] P. M. SARUN, R. SHABNA, S. VINU, A. BIJU, and U. SYAMAPRASAD, *Physica B* **404**, 1602 (2009).

[18] C. N. VAN HUONG, C. HINNEN, and J. M. SIFFRE, *J. Mater. Sci.* **32**, 1725 (1997).

[19] W. GAO and J. VANDER-SANDE, *Supercond. Sci. Technol.* **5**, 318 (1992).

[20] L. KRUSIN-ELBAUM, G. BLATTER, and T. SHIBAUCHI, *Phys. Rev. B* **69**, 220506 (2004).

[21] T. MOTOHASHI, Y. NAKAYAMA, T. FUJITA, K. KITAZAWA, J. SHIMOYAMA, and K. KISHIO, *Phys. Rev. B* **59**, 14080 (1999).

[22] B. ZHAO, W. H. SONG, J. J. DU, and Y. P. SUN, *Physica C* **386**, 60 (2003).

[23] R. KLEINER and P. MULLER, *Phys. Rev. B* **49**, 1327 (1994).

Chapter 5

Microstructural refinement and its effect on the flux pinning properties of RE substituted (Bi,Pb)-2212 superconductors

In theory there is no difference between theory and practice. In practice there is.

— Lawrence Peter "Yogi" Berra, 1925 – (85 years, Alive).

5.1 Introduction

Large-scale applications of high temperature superconductors (HTSs) such as their use in superconducting cables are impeded by the fact that polycrystalline materials (the only practical option) support significantly lower current densities than single crystals. The transport critical current density (J_c) across a grain boundary drops exponentially with the misorientation angle [1,2]. The

average misorientation angle in HTS can be reduced by improving the texture of grains [3, 4]. Among Bi-based cuprate superconductors described as $Bi_2Sr_2Ca_{n-1}Cu_nO_y$, Bi-2212 (n=2) has received a lot of attention and extensive research efforts have been directed towards the synthesis and study of this system ever since its discovery by Maeda et al. [5] due to its potential for making tapes and wires with high J_cs. The material not only has high transition temperature (T_c), but also has extremely high critical magnetic field (H_{c2}) [6]. It is less susceptible to degradation due to oxygen loss and less sensitive to attack by water and carbon dioxide compared to any other HTS. Its melting point is lower, being in the range 870–900 ^oC. However, in the processed material, the J_c is low because of the factors such as weak linking at interfaces and the absence of strong pinning. The microstructure of Bi-2212 superconductor consists of platelet-like (flaky) grains with the ab-plane along the flat surface of the platelets. If the grains are aligned by stacking the platelets like a structure of bricks [7], a high J_c can be achieved in the ab-plane. However their poor performance under magnetic fields, which arises from the weak pinning of flux lines, still prevents its extensive high-field applications at relatively high temperatures. The weak flux pinning of Bi-2212 superconductor is due to its large anisotropy and short coherence length [8].

The flux pinning ability and hence the transport properties of Bi-2212 superconductor at high temperatures and high magnetic fields can be enhanced by reducing the anisotropy of the material [9] and by introducing artificial defects having a size matching the coherence length. First method strengthens the inter-layer coupling between CuO_2 layers which increases the flux pinning potential and in the later case, the artificial defects act as extra pinning centers. It was reported that Pb doping at Bi-site of Bi-2212 crystals significantly improves the c-axis conductivity by reducing the electromagnetic anisotropy [10], which enhances the intrinsic pinning and thereby improves the J_c [11, 12]. The introduction of artificial defects is carried out by the substitution of rare earth (RE) ions in the place of Ca/Sr, which stabilizes the crystal

structure of the (Bi,Pb)-2212 system and also acts as pinning centres. However, RE-doping usually deteriorates the flaky grain morphology and texture of (Bi,Pb)-2212 with increase in RE concentration [13–15]. The interesting feature to be noted in this case is that in spite of the deterioration of microstructure, the RE substituted samples exhibit much better J_c values and have better pinning capabilities as compared to the RE-free sample. This shows that there is a great scope for further improvement of J_c if the flaky grain morphology and texture of RE substituted (Bi,Pb)-2212 superconductor could be retained.

In the present chapter, an attempt is made to restore the grain morphology and texture of RE substituted (Bi,Pb)-2212 superconductors as in RE-free samples by precisely tuning the sintering temperature within a narrow range (846–860 °C). It has been possible to control the grain growth and tailor the microstructure of RE substituted (Bi,Pb)-2212 superconductors as desired and thereby produce superconductors with highly enhanced self-field J_c or with high in-field J_c.

5.2 Experimental details

The examined specimens with parent composition of $Bi_{1.6}Pb_{0.5}Sr_2Ca_{1.1}Cu_{2.1}O_{8+\delta}$ (RE-free) and RE substituted (Bi,Pb)-2212 ($Bi_{1.6}Pb_{0.5}Sr_{2-x}RE_xCa_{1.1}Cu_{2.1}O_{8+\delta}$, [where x = 0.075, 0.1, 0.1 and 0.2 for RE : Tb, Ho, Eu and La respectively]) were prepared by solid state route using high purity chemicals (Aldrich, > 99.9 %) such as oxides and carbonates of the ingredients (Bi_2O_3, PbO, $SrCO_3$, $CaCO_3$, CuO and RE_2O_3). The RE stoichiometry is chosen based on the optimum RE concentration where the best transport J_c was obtained (Chapter 4). The ingredients weighed accurately were thoroughly mixed and ground. The homogeneous ingredients thus obtained were subjected to a three stage calcination process in air at 800 °C /15 h + 820 °C /40 h + 840 °C/60 h. Intermediate grinding in acetone medium was done between

each stage of calcination to improve the homogeneity of the samples. After calcination, the samples were pelletized by applying a pressure of 500 MPa in a cylindrical die of 12 mm diameter. The average thickness of the pellets were around 1 mm. The pellets of RE-free sample was heat treated at 848 °C which is the optimized heat treatment temperature for RE-free sample, for 120 h (60 h + 60 h), with one intermediate pressing. The heat treatment was carried out in a large volume muffle furnace controlled by a Eurotherm 2040 temperature controller having a stability and accuracy better than ± 0.5 °C at 850 °C. The pellets of RE substituted samples were grouped into eight sets. Each set was heat treated at temperatures between 846 to 860 °C in steps of 2 °C for 120 h (60 h + 60 h), with one intermediate pressing under the same pressure. The samples heat treated between 846 and 860 °C are hereafter denoted as RExTemp, where RE is the rare earth used, x is the RE stoichiometry and Temp is the last two digits of the sintering temperature. For example, La260 denotes the La substituted sample with the stoichiometry x = 0.2 and heat treated at 860 °C. Similarly, La048 represnets the La-free sample heat treated at 848 °C.

The structural analysis of the samples were carried out using XRD (*Philips X'pert Pro*) equipped with *X'celerator* and a monochromator at the diffracted beam side. Phase identification was performed using X'pert Highscore software in support with the ICDD-PDF2 database. The microstructural and elemental analyses of the samples were done using SEM (*JEOL JSM 5600 LV*) and EDS, respectively. For electrical measurements, cylindrical pellets were cut into rectangular bars of dimension 10 x 4 x 1 mm^3. Current and potential leads of high-grade copper wires were soldered to the four metallised terminals of the samples. The transition temperature (T_c) of the samples was determined by the DC four-probe method using a LN_2 bath cryostat. A temperature controller (*Lakeshore L340*) was used for the accurate control and monitoring of temperature of the samples.

The transport critical currents of the samples in self- and applied fields were measured at 64 K using the four-probe method with the standard criterion of 1 μV/cm. The transport J_c–B characteristics was studied with the fields ranging from 0.0-1.4 T in a home-made experimental setup consisting of a bi-polar electromagnet and a sample holder between the poles. The setup was inserted in a LN_2 bath cryostat which can be cooled up to 64 K by applying vacuum. The direction of the current was parallel to the direction of the pressed surface and the direction of the magnetic field was perpendicular to the pressed surface of the pellet. All these measurements were automated using GPIB interfaced with a PC.

5.3 Results and Discussion

5.3.1 Crystalline and microstructural properties

The XRD patterns of RE-free and RE substituted (Bi,Pb)-2212 samples after the last stage heat treatment (Figures 5.1(a)-5.1(d)) show that all the samples contain only (Bi,Pb)-2212 phase and no peaks of any secondary phase are observed at this stage within the detection limit of the instrument. This indicates that all the reactant phases are converted into (Bi,Pb)-2212 and the substituted RE ions enter into the crystal lattice of (Bi,Pb)-2212. In order to bring out the variations in peak height and peak shift of the ***(00l)*** plane, the ***(008)*** peak of all samples are separately shown with better resolution in Figures 5.2(a)-5.2(d). It shows that when the heat treatment temperature of RE substituted samples is increased, the peak height corresponding to the ***(00l)*** planes also increases. This shows that the texturing of the grains improves with increase in heat treatment temperature.

Figures 5.2(a)-5.2(d) also show that the XRD peaks of the ***(008)*** plane shift towards higher 2θ angle and the value of this peak shift [$\delta(2\theta)$ = 0.185°, 0.156°, 0.36° and 0.190° for La, Eu, Tb and Ho, respectively.] is almost constant as compared to the reference sample (RE-free). The observed peak shift in the ***(00l)*** planes indicates that the c-axis length of the RE substituted samples decreases as compared to the reference sample. This decreased c-axis length shows that the substituted RE atom enters into the crystal structure. The lattice parameters of the RE-free and RE substituted samples were calculated by considering an orthorhombic symmetry for (Bi,Pb)-2212 system which shows that the lattice parameter values are independent of the heat treatment temperature. The c-axis lattice parameter of all the RE substituted samples vary with the

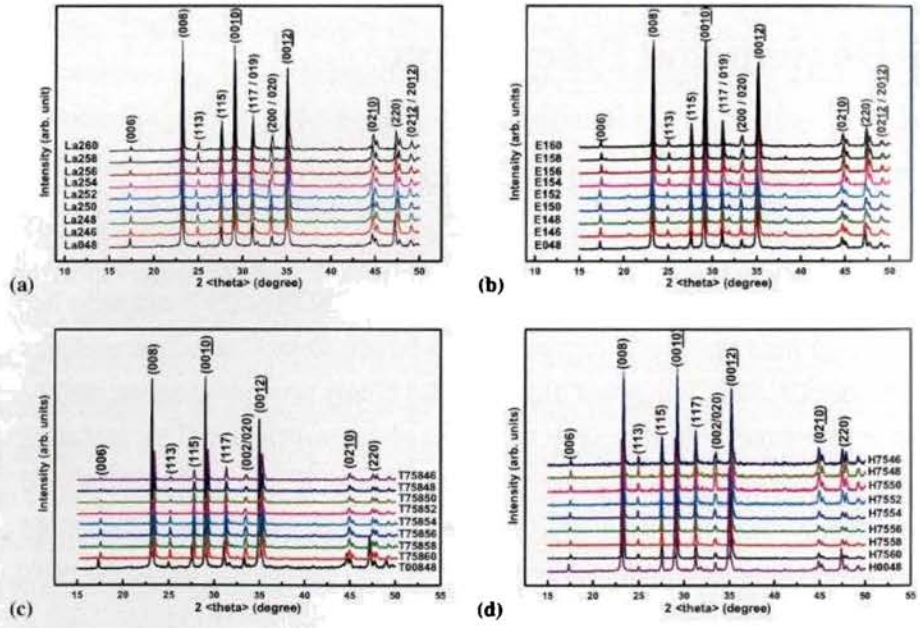

Figure 5.1: XRD patterns of RE-free and RE substituted (Bi,Pb)-2212 superconductor after last stage heat treatment at temperatures between 846 °C and 860 °C (RE = La, Eu, Tb, and Ho). The peak shift of ***(00l)*** planes of RE substituted (Bi,Pb)-2212 superconductor is clearly seen for (hkl) at (008), (00$\underline{1}$0) and (00$\underline{1}$2) at 2θ of 23.1°, 29.2° and 35.1°, respectively

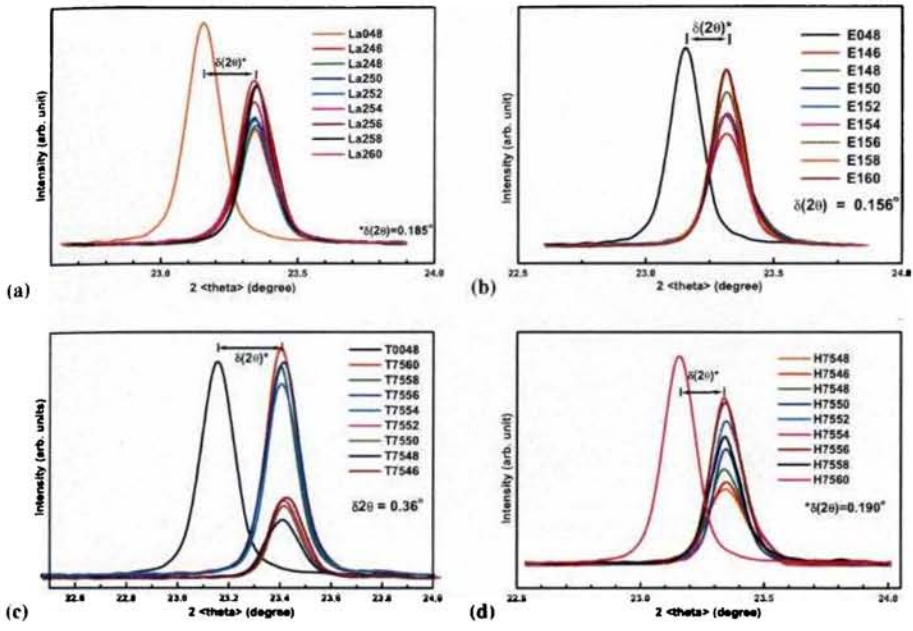

Figure 5.2: Variations in peak height and peak shift of the (***008***) peak of RE-free and RE substituted (Bi,Pb)-2212 superconductor (RE = La, Eu, Tb, and Ho) heat treated at different temperatures. The shift towards higher 2θ angles show the contraction of c-axis in the crystal structure of RE substituted (Bi,Pb)-2212 superconductors and the contraction is independent of the sintering temperature.

type of substituted RE and the values obtained are 30.725, 30.695, 30.405 and 30.732 Å within the accuracy of 0.005 Å for La, Eu, Tb and Ho, respectively. However, the c-axis length does not vary with the increase in the sintering temperature. Similar behaviour has been observed in the case of a and b axes, i.e. no structural change takes place with the variation in sintering temperature. A contraction in c-axis length is observed in all RE substituted samples as compared with the reference sample (c = 30.885 ± 0.005 Å), indicating the incorporation of RE atoms into the (Bi,Pb)-2212 system. The reason for the shrinkage in c-axis length is described in chapter 4 and [10, 16].

The Lotgering index (F) [17], a measure of the texture of the samples, is calculated from the XRD patterns of textured pellets and finely ground pow-

Table 5.1: Density, Lotgering index (F), self-field J_c, F_{Pmax}, field of occurrence of F_{Pmax} of RE-free and RE substituted (Bi,Pb)-2212 superconductors heat treated at different temperatures.

Sample	Density (g/cm^3)	Lotgering Index (F)	Self-field J_c (Acm^{-2})	Value of F_{Pmax} (x 10^3 Nm^{-3})	Field of F_{Pmax} (T)
RE-free	5.40	0.85	154	21	0.12
La246	5.25	0.69	458	463	0.52
La248	5.27	0.71	725	288	0.44
La250	5.35	0.75	876	258	0.44
La252	5.35	0.75	1009	234	0.40
La254	5.37	0.80	1120	183	0.32
La256	5.43	0.87	1241	114	0.28
La258	5.45	0.88	1301	94	0.28
La260	5.52	0.90	994	203	0.32
E146	5.10	0.51	625	680	1.24
E148	5.25	0.67	1233	646	0.76
E150	5.25	0.67	1381	644	0.80
E152	5.25	0.68	1500	925	1.20
E154	5.26	0.68	1608	1015	1.04
E156	5.38	0.75	1684	1120	1.08
E158	5.45	0.89	1736	1550	1.08
E160	5.46	0.89	1772	1530	1.08
T7546	5.15	0.56	1655	2220	0.84
T7548	5.20	0.62	1824	2590	0.84
T7550	5.33	0.65	1925	2520	0.76
T7552	5.42	0.72	2270	1450	0.78
T7554	5.48	0.76	2335	1120	0.62
T7556	5.56	0.87	2480	420	0.56
T7558	5.58	0.90	2540	410	0.62
T7560	5.58	0.90	2512	260	0.36
H7546	5.08	0.50	1118	1940	1.00
H7548	5.19	0.58	1288	1760	0.80
H7550	5.28	0.67	1415	1670	0.80
H7552	5.32	0.70	1739	1610	0.72
H7554	5.38	0.74	1986	1420	0.68
H7556	5.46	0.83	2460	1120	0.60
H7558	5.48	0.86	2263	1310	0.68
H7560	5.50	0.88	1903	1580	0.72

ders of all the samples and is given in Table 5.1. The results show that F is strongly dependent on the heat treatment temperature. As the heat treatment

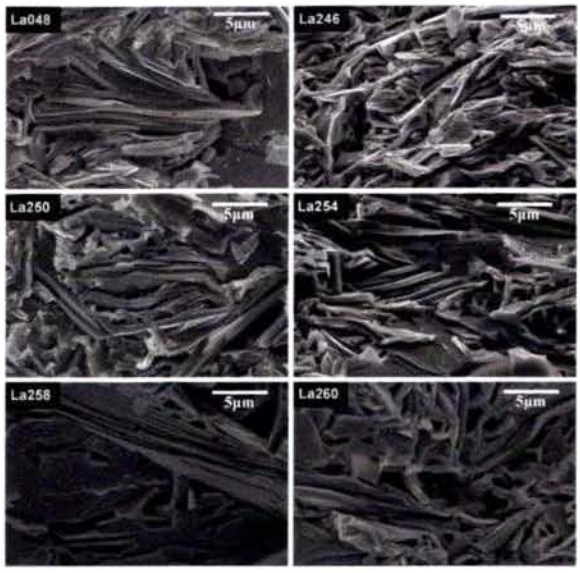

Figure 5.3: SEM micrographs of the fractured surface of the La-free and La substituted (Bi, Pb)-2212 samples heat treated at different temperatures.

temperature increases, the F value of the doped samples increases (from 0.69 to 0.90, 0.51 to 0.89, 0.56 to 0.90 and 0.50 to 0.88 for La, Eu, Tb and Ho respectively) up to a temperature of 860 °C. It is noted that the reference sample shows an F value of 0.85. A similar variation in the bulk density of RE substituted (Bi,Pb)-2212 samples is observed where, the density increases with the increase in the sintering temperature (Table 5.1). Thus, a very good texturing is expected to be induced in the microstructure of RE substituted samples by the selective sintering of the samples at optimized temperatures.

Figure 5.3–5.6 shows the scanning electron microscopy images of the fractured surfaces of RE-free sample heat treated at 848 °C and RE substituted samples heat treated at 846, 848, 850, 852, 854, 856, 858 and 860 °C. The grain morphology of the RE-free samples (La048, E048, T0048 and H0048) shows clear and flaky grains with layered growth typical of (Bi,Pb)-2212, whereas for RE substituted samples (La246 to La260, E146 to E160, T7546 to

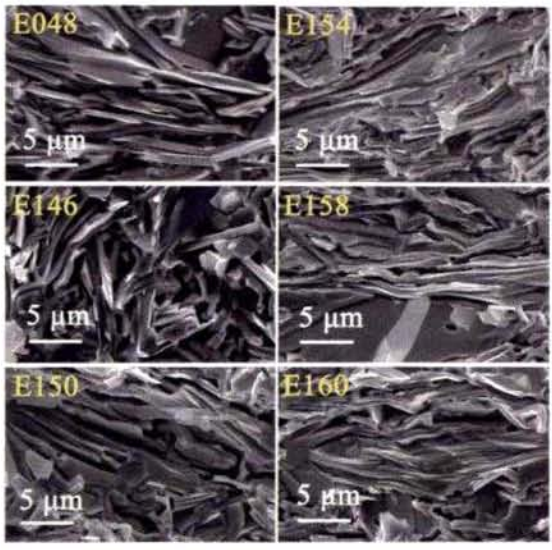

Figure 5.4: SEM micrographs of the fractured surface of the Eu-free and Eu substituted (Bi, Pb)-2212 samples heat treated at different temperatures.

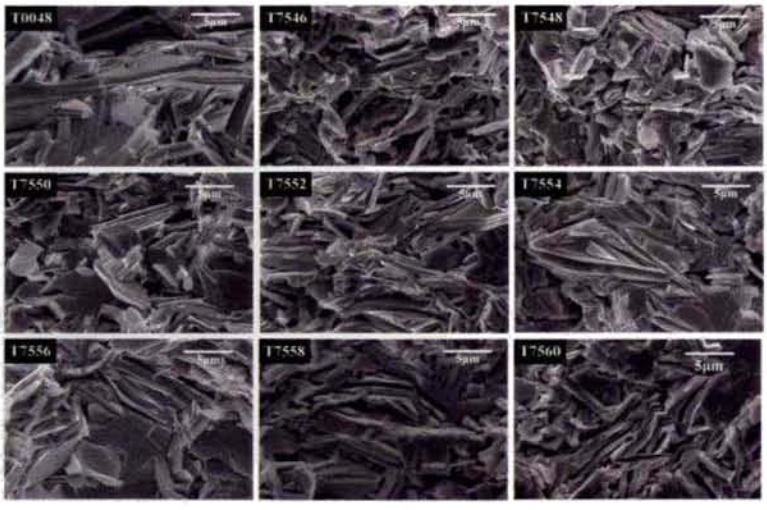

Figure 5.5: SEM micrographs of the fractured surface of the Tb-free and Tb substituted (Bi, Pb)-2212 samples heat treated at different temperatures.

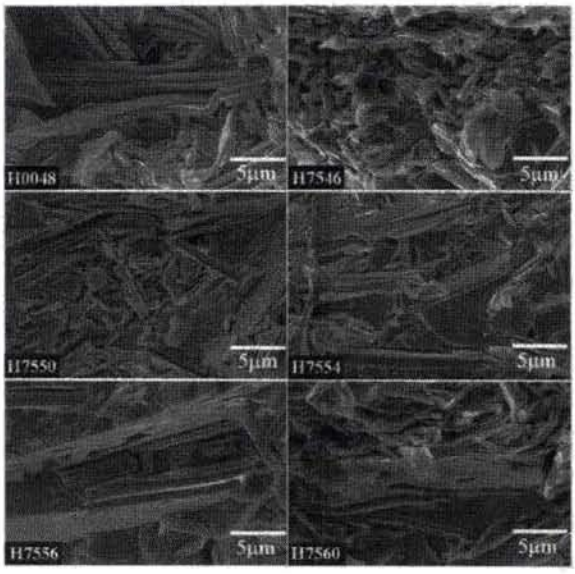

Figure 5.6: SEM micrographs of the fractured surface of the Ho-free and Ho substituted (Bi, Pb)-2212 samples heat treated at different temperatures.

T7560, H7548 to H7560), a systematic change in microstructure with respect to the heat treatment temperature is observed. For example, at lower sintering temperatures, the characteristic flaky morphology of pure (Bi,Pb)-2212 grains is no more found when RE is substituted in the system. The microstructure gets disrupted and the grains transform into smaller platelets with reduced texture. For RE substituted samples heat treated at higher sintering temperatures, the flaky morphology and texture reappear with gradual improvement and these variations can be related to the observed bulk density of the RE substituted samples (Table 5.1). The results show that the optimum heat treatment temperature for obtaining the best microstructure for the RE doped superconductor samples are 856 – 858 °C. This improved microstructure plays an important role in increasing the critical current density of the system.

The energy dispersive X-ray spectroscopic (EDS) analysis of RE substituted (Bi,Pb)-2212 grains (spot analysis) reveals the presence of RE in (Bi,Pb)-

2212 grains. The quantitative estimation of the cations from EDS patterns of these samples (keeping Cu as reference) shows that the approximate cationic composition are $Bi_{1.49}Pb_{0.45}Sr_{1.85}La_{0.185}Ca_{1.05}Cu_{2.1}$, $Bi_{1.51}Pb_{0.52}Sr_{1.83}Eu_{0.087}Ca_{1.04}Cu_{2.1}$, $Bi_{1.46}Pb_{0.53}Sr_{1.95}Tb_{0.065}Ca_{1.08}Cu_{2.1}$ and $Bi_{1.53}Pb_{0.46}Sr_{1.93}Ho_{0.061}Ca_{1.05}Cu_{2.1}$ for La, Eu, Tb and Ho substituted (Bi,Pb)-2212 superconductors. This clearly supports that the RE atoms are successfully substituted into the crystal structure of (Bi,Pb)-2212 system.

5.3.2 Transport superconducting properties

Measurement of T_c by resistance method shows that the RE substituted samples have much higher T_c values compared to the reference sample (RE-free sample). It is also found that the RE substituted samples show same T_c (90.8 K, 95.5 K, 88.5 K and 88.1 K for La, Eu, Tb and Ho, respectively) irrespective of the sintering temperature. The T_c measured for the RE-free sample is only 80.2 K. The self-field J_c of different samples are given in Table 5.1. The transport J_c value increases with increase in heat treatment temperature (Table 5.1) and finally the samples heat treated at higher temperatures show the maximum J_c (1301 Acm^{-2}, 1772 Acm^{-2}, 2540 Acm^{-2} and 2460 Acm^{-2} for La, Eu, Tb and Ho, respectively). This enhancement in J_c is obviously due to the improvement in microstructure of the RE substituted samples. The reference sample processed at its optimum temperature shows a J_c value of only 154 Acm^{-2}.

The field dependence of normalized J_c [$J_c(B)/J_c(0)$] is shown in figure 5.7(a)–5.7(d). The J_c–B characteristics of the RE substituted samples are found to be much better than that of the reference sample. That is, the deterioration of J_c due to the magnetic field is significantly reduced as a result of RE substitution. This shows that the doping of RE at the Sr-site enhances the flux pinning properties of (Bi,Pb)-2212. In the case of RE substituted samples, the sample heat treated at lower sintering temperatures 846–850 °C gives the best J_c–B

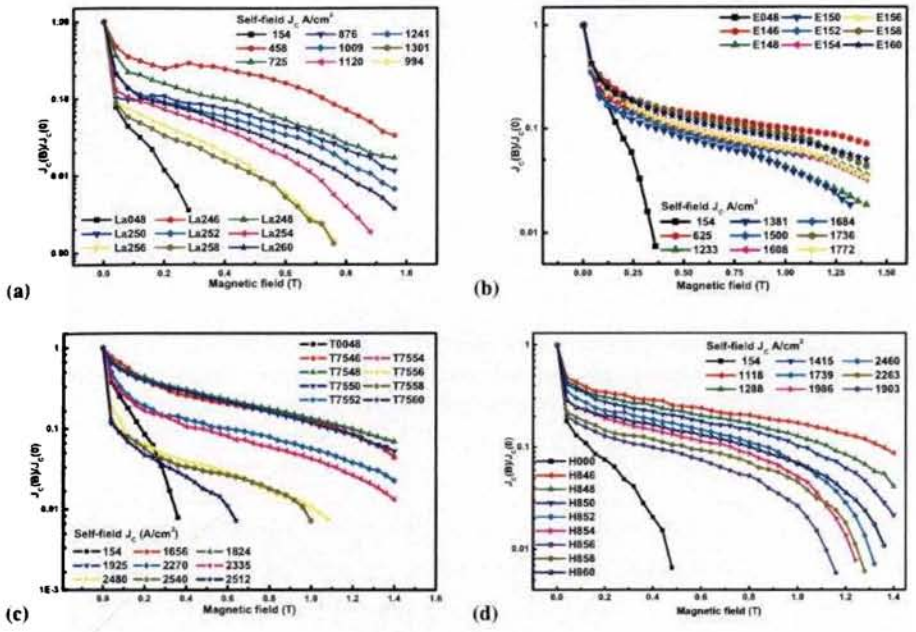

Figure 5.7: Variation of normalized J_c as a function of applied magnetic field of RE-free and RE substituted (Bi,Pb)-2212 samples heat treated at different temperatures.

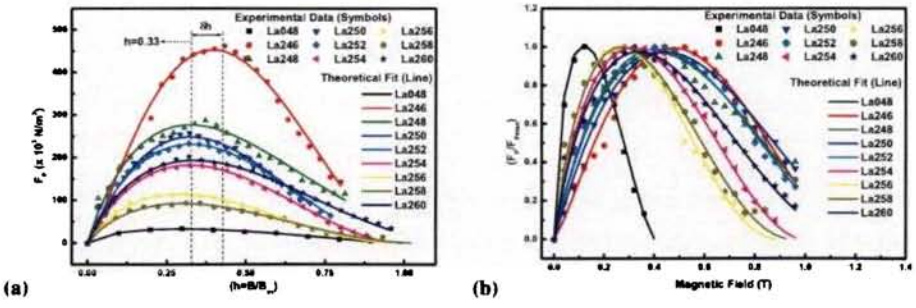

Figure 5.8: Variation of (a). pinning force density (F_P) as a function of h (B/B_{irr}) and (b). normalized pinning force density as a function of magnetic field of La-free and La substituted (Bi,Pb)-2212 superconductor heat treated at different temperatures.

characteristics but its self-field J_c value is lower than the maximum obtained self-field J_c, but it is about 5, 9, 12 and 9 times higher for La, Eu, Tb and Ho

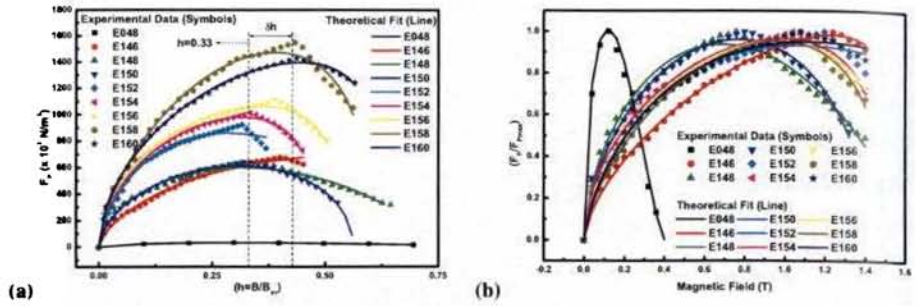

Figure 5.9: Variation of (a). pinning force density (F_P) as a function of h (B/B_{irr}) and (b). normalized pinning force density as a function of magnetic field of Eu-free and Eu substituted (Bi,Pb)-2212 superconductor heat treated at different temperatures.

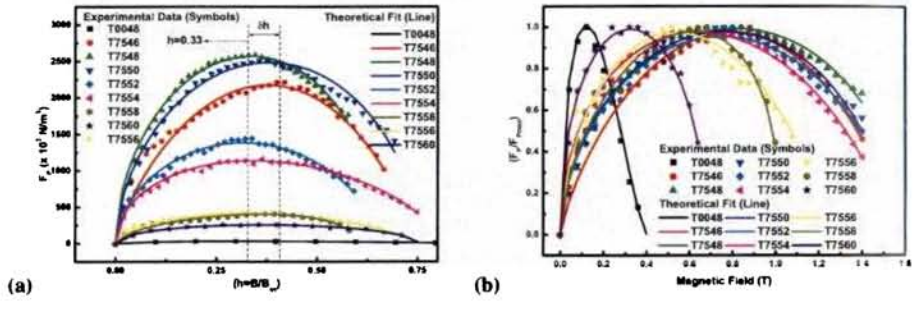

Figure 5.10: Variation of (a). pinning force density (F_P) as a function of h (B/B_{irr}) and (b). normalized pinning force density as a function of magnetic field of Tb-free and Tb substituted (Bi,Pb)-2212 superconductor heat treated at different temperatures.

substituted samples respectively than the reference sample. As the heat treatment temperature increases, the J_c–B performance of RE substituted samples decreases and the sample heat treated at higher sintering temperatures 858–860 °C shows the least J_c–B performance among the RE substituted samples, but it shows a higher self-field J_c about 9, 12, 17 and 16 times for La, Eu, Tb and Ho substituted samples respectively than the reference sample (Table 5.1). The result can be understood from the variation in the microstructure of the samples given in figures 5.3–5.6. The microstructure of samples heat treated

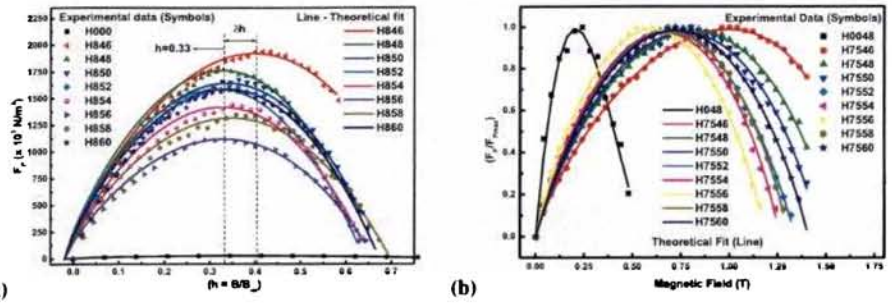

Figure 5.11: Variation of (a). pinning force density (F_P) as a function of h (B/B_{irr}) and (b). normalized pinning force density as a function of magnetic field of Ho-free and Ho substituted (Bi,Pb)-2212 superconductor heat treated at different temperatures.

at lower sintering temperatures shows that the grains are smaller, rounded and less textured and hence the pinning due to the grain boundary is more effective leading to the better J_c–B performance. However, more grain boundary weak-links in these samples reduce the self-field J_c. In RE substituted samples heat treated at higher sintering temperatures, the flaky grains are more textured due to the optimum heat treatment temperature which leads to lesser pinning and higher self-field J_c. Further, the decrease of J_c with magnetic field is slower for the RE substituted samples heat treated at temperatures between 846 and 852 °C than that of RE-free sample. This shows the enhanced flux pinning properties of RE substituted samples.

To investigate the flux pinning properties of superconductors, the determination of pinning force density ($F_P = J_c \times B$) [18] is a very fruitful tool which is widely accepted in transport current measurements. The dependence of volume pinning force density F_P, on the reduced magnetic field ($h = B/B_{irr}$) and variation of normalized pinning force density (F_P/F_{Pmax}) as a function of magnetic field of the RE-free and RE substituted samples are shown in figures 5.8(a)–5.11(b), respectively. It is seen that the maximum value of F_P is shifted to much higher field values for RE substituted samples heat treated between 846 and 852 °C. The value of F_{Pmax} and the peak position of its oc-

Table 5.2: Fitting parameters (A, p, q and B_{irr}), and reduced field (h = B/B_{irr}) at F_{Pmax} of RE-free and RE substituted (Bi,Pb)-2212 superconductors heat treated at different temperatures.

Sample	A	p	q	B_{irr} (T)	Reduced field at F_{Pmax}
RE-free	3.50	0.624	1.480	0.40	0.30
La246	9.31	1.292	2.055	1.20	0.43
La248	9.41	0.957	1.992	1.18	0.37
La250	7.54	1.054	2.192	1.37	0.32
La252	6.13	0.940	1.949	1.25	0.32
La254	5.62	0.868	1.925	1.00	0.32
La256	6.56	0.904	2.203	0.90	0.31
La258	5.97	0.846	2.158	0.90	0.36
La260	6.28	0.868	2.300	0.82	0.39
E146	6.59	1.009	2.018	3.10	0.40
E148	5.76	0.874	2.091	2.17	0.35
E150	4.69	0.868	1.521	2.35	0.34
E152	5.90	0.839	2.321	3.79	0.32
E154	4.84	0.773	1.951	3.11	0.34
E156	4.33	0.764	1.739	2.77	0.43
E158	4.10	0.807	1.502	2.49	0.43
E160	5.12	0.680	2.639	2.48	0.44
T7546	4.12	0.947	1.130	2.10	0.40
T7548	4.00	0.711	1.522	2.43	0.36
T7550	3.73	0.707	1.357	2.02	0.37
T7552	3.45	0.707	1.244	2.36	0.33
T7554	3.34	0.676	1.158	1.87	0.33
T7556	3.23	0.666	1.133	1.64	0.34
T7558	2.55	0.661	0.676	1.72	0.36
T7560	2.30	0.548	0.640	0.90	0.40
H7546	2.38	0.820	0.503	2.50	0.40
H7548	3.10	0.890	0.774	2.42	0.33
H7550	3.18	0.903	0.810	2.46	0.33
H7552	3.79	0.978	0.964	2.11	0.34
H7554	3.26	0.912	0.831	2.00	0.34
H7556	3.39	0.895	0.882	1.81	0.33
H7558	3.34	0.933	0.842	2.06	0.33
H7560	3.44	0.921	0.882	2.00	0.36

currence for RE-free and RE substituted samples are given (Table 5.1). It can be observed that the F_{Pmax} values of RE-substituted samples sintered at relatively lower temperatures are higher than the RE-free samples and the peak

positions of F_P/F_{Pmax} for these samples appear at higher magnetic fields up to 1.24 T as against 0.12 T for RE-free sample at 64 K. This indicates that the irreversibility lines (I.L.) of the RE substituted samples sintered at relatively lower temperatures shift towards much higher applied magnetic fields. This confirms that the flux pinning strength of (Bi,Pb)-2212 significantly increases not only with RE substitution but also by the the fine tuning of the sintering temperature.

The flux pinning behaviour of a (Bi,Pb)-2212 superconductor is further analysed using Dew-Hughes model using the equation given by $\left(\frac{F_P}{F_{Pmax}}\right) = A \left(\frac{B}{B_{irr}}\right)^p \left(1 - \frac{B}{B_{irr}}\right)^q$ [19], where A, p and q are numerical fitting parameters. Due to the short coherence length of (Bi,Pb)-2212, two sorts of pinning are usually dominant, namely, δl pinning and δT_c pinning. For δl pinning, the value of p = 1, q = 2 and reduced field at F_{Pmax}, $h_{max} = 0.33$ whereas for δT_c pinning, the value of p = 1, q = 1 and $h_{max} = 0.50$. It is found that all sets of data are found to fit well with the Dew-Hughes equation [solid parabolic lines in figures 5.8(a)–5.11(b)]. The fitting parameters, A, p, q and B_{irr} are tabulated (Table 5.2). For RE-free sample, the values of p and q are found to be 0.624 and 1.480, respectively. But for RE substituted samples, heat treated between 846 and 860 °C, the values of p and q are found to be closer to 1 and 2 respectively, which decreases with the increase in heat treatment temperature. For samples heat treated at 852 – 858°C, the maximum value of F_{Pmax} appeared at h = 0.33–0.34 which is in very close agreement with the theoretically predicted value of h for point defects (h = 0.33) [19]. Hence, the main pinning mechanism of these samples is the point pinning due to point defects which cause spatial variation in the charge carrier mean free path (l) near the lattice defects arising out of the substitution of RE atoms at the Sr site. However, for samples heat treated between 846 – 848 °C and 858 – 860 °C, the peak position of F_{Pmax} appears to shift up to h = 0.40–0.45. That is, in RE substituted (Bi,Pb)-2212 samples heat treated between 846 – 848 °C and 858 – 860 °C, different pinning mechanisms are simultaneously active. Comparing

the shift in the peak position of reduced field, h with the theoretical model, it is concluded that in addition to point pinning, grain boundary pinning is also effective in these samples. These results show that the irreversibility lines of the RE substituted samples get shifted towards higher magnetic fields and temperatures and the flux pinning strength of RE substituted samples sensitively depend on the heat treatment temperature. Based on the above pinning analysis, it is found that the sample heat treated at 846 °C shows the maximum flux pinning strength among all the RE substituted samples and F_P attains a maximum value of 463, 1550, 2590 and 1940 ($\times 10^3$) Nm^{-3} for La, Eu, Tb and Ho substituted samples (Figures 5.8(a)–5.11(b)). The data also shows that the pinning mechanism depends not only on the sintering temperature but also on the ionic radii of the substituted RE. The main pinning mechanism in (Bi,Pb)-2212 superconductor substituted La and Eu are caused by δl pinning, while the Tb and Ho show δT_c pinning. Thus selection of RE and the proper sintering temperature is necessary to develop a hybrid (Bi,Pb)-2212 superconductors suited for both self- and in-field applications.

5.4 Conclusions

It is possible to tailor the microstructure and hence the critical current density and flux pinning properties of RE substituted (Bi,Pb)-2212 superconductors by appropriate choice of the RE and the sintering temperature. The results indicate the properties are highly temperature sensitive. Since all the RE substituted samples of a particular type have the same amount of RE, the additional electrons supplied to the system due to RE substitution is almost the same. Consequently, the hole concentration in that type of RE substituted (Bi,Pb)-2212 superconductors are identical and hence T_c is invariant for these samples. Now, the J_c value of RE substituted samples depends only on the microstructural and flux pinning aspects. The reason for the enormous increase

of self-field J_c value of the samples heat treated at relatively higher sintering temperatures is evident from the formation of the refined microstructure with respect to the grain texturing as seen in SEM images while disruption of the refined microstructure with decreased texture reduces the self-field J_c of the samples heat treated at lower sintering temperatures. Also, the pinning analysis demonstrates that the substitution of RE in (Bi,Pb)-2212 superconductor significantly enhances its flux pinning strength at a relatively high temperature of 64 K, which also contributes to the final J_c of the RE substituted (Bi,Pb)-2212 superconductors.

The observed results from the investigation of the microstructural and flux pinning properties of RE substituted (Bi,Pb)-2212 superconductors prepared at different temperatures ranging from 846 to 860 °C point towards the importance of fine tuning of heat treatment temperature in the preparation of RE substituted (Bi,Pb)-2212 superconductors. The results show that it is possible to tailor their properties catering to different applications by proper selection of the sintering temperature. For instance, the RE substituted samples prepared at comparatively low temperatures (846 – 850 °C) are useful for magnetic field applications due to their better flux pinning properties. Whereas, the samples prepared at higher temperatures (854 – 860 °C) are useful for self-field applications due to their enhanced self-field current carrying capacity. The results also open up an avenue to prepare RE substituted (Bi,Pb)-2212 superconductors incorporating hybrid self- and applied field properties by selecting a suitable sintering temperature.

References

[1] H. HILGENKAMP and J. MANNHART, *Rev. Mod. Phys.* **74**, 485 (2002).

[2] R. F. KILE, J. P. BUBAN, M. VARELA, A. FRANCESCHETTI, C. JOOSS, Y. ZHU, N. D. BROWNING, S. T. PANTELIDES, and S. J. PENNYCOOK, *Nature* **435**, 475 (2005).

[3] B. A. MARINKOVIC, S. K. XIA, E. T. SERRA, and F. RIZZO, *Mateirals Chemistry and Physics* **91**, 301 (2005).

[4] H. FUJII, Y. HISHINUMA, H. KITAGUCHI, H. KUMAKURA, and K. TOGANO, *Physica C* **331**, 79 (2000).

[5] H. MAEDA, Y. TANAKA, M. FUKUTOMI, and T. ASANO, *Jpn. J. Appl. Phys.* **27**, L209 (1988).

[6] Y. KOIKE, T. NAKANOMYO, and T. FUKASE, *Jpn. J. Appl. Phys.* **27**, L841 (1988).

[7] L. BULAEVSKII, J. CLEM, L. GLAZMAN, and A. MALOZEMOFF, *Phys. Rev B* **45**, 2545 (1993).

[8] M. P. MALEY, *J. Appl. Phys.* **70**, 6189 (1991).

[9] S. NOMURA, H. YOSHINO, and K. ANDO, *Supercond. Sci. Technol.* **6**, 858 (1993).

[10] B. ZHAO, W. H. SONG, J. J. DU, and Y. P. SUN, *Physica C* **386**, 60 (2003).

[11] K. K. UPRETY, J. HORVAT, X. L. WANG, M. IONESCU, H. K. LIU, and S. X. DOU, *Supercond. Sci. Technol.* **14**, 479 (2001).

[12] I. CHONG, Z. HIROI, M. IZUMI, J. SHIMOYAMA, Y. NAKAYAMA, K. KISHIO, T. TERASHIMA, Y. BANDO, and Y. TAKANO, *Science* **276**, 770 (1997).

[13] A. BIJU, P. M. SARUN, R. P. ALOYSIUS, and U. SYAMAPRASAD, *Mater. Res. Bull.* **42**, 2057 (2007).

[14] A. BIJU, P. M. SARUN, R. P. ALOYSIUS, and U. SYAMAPRASAD, *Supercond. Sci. Technol.* **19**, 1023 (2006).

[15] P. M. SARUN, R. SHABNA, S. VINU, A. BIJU, and U. SYAMAPRASAD, *Physica B* **404**, 1602 (2009).

[16] J. EKIN, T. LARSON, A. HERMANN, Z. SHENG, K. TOGANO, and H. KUMAKURA, *Physica C* **160**, 489 (1989).

[17] W. GAO and J. B. VANDER-SANDE, *Supercond. Sci. Technol.* **5**, 318 (1992).

[18] M. R. KOBLISCHKA and M. MURAKAMI *Supercond. Sci. Technol.* **13**, 738 (2000).

[19] D. DEW-HUGHES, *Phil. Mag.* **30**, 293 (1974).

Chapter 6

Studies on the pinning energy of RE substituted (Bi,Pb)-2212 superconductors

Take time to deliberate, but when the time for action has arrived, stop thinking and go in.

— Napoleon Bonaparte, 1769–1821.

6.1 Introduction

A very important parameter of a type-II superconductor is the critical current density (J_c) at which the Abrikosov vortices depin and start to move under the influence of the Lorentz force. The vortex drift induces an electric field (E) which causes a voltage drop along the superconductor. Consequently, at current densities $J > J_c$ energy is dissipated and the resistivity $\rho = E/J$ becomes finite. In high T_c superconductors (HTSs) thermally activated depinning of flux lines causes energy losses even at $J < J_c$. HTSs are, therefore, better char-

acterized by their nonlinear current-voltage law E = E(J), which defines J_c as the current density at which E(J) deviates noticeably from zero and starts to rise steeply, according to a power law $E = E_c(J_c/J)^n$ with $n \gg 1$ which reflects the abruptness of the transition and determines the suitability of the superconductor for technological applications and E_c is the standard criterion of $1\mu V/cm$ [1–4]. The finite E at $J < J_c$ leads to the decay of persistent currents and to a decrease of magnetic moment which causes flux creep. The sharpness of the E-J characteristics is governed by the microstructural homogeneity, flux-creep [5] and/or the vortex glass-liquid transition [6] of the superconductor.

A high n-value is associated with good homogeneity. The dependence of the n-value on the magnetic field is related to the quality of a superconductor. The resistive transition index is observed to fall with the increase in magnetic field. The steeper the negative slope, the more dominant is the role of the microstructure. Together with the critical current density (J_c), the n-value is important in applications such as persistent-mode NMR magnets [7] for extrapolating to the low operating electric fields, and cable-in-conduit-conductor fusion magnets for calculating operating margins and interpreting data for prototype systems [8–10]. The origin of the n-value in high-temperature superconducting wires is generally attributed to distributions in the critical current [11–16] arising from distributions in the elementary flux-pinning forces (intrinsic effects) [11, 12] and from nonuniformities in the cross-sectional area of the superconducting filaments (extrinsic effects) [14–16]. Thus the n-value is being commonly used as a quantitative figure of merit or 'quality index' [4]. Hence, the E-J characteristics are closely related to the intrinsic properties. This complex mechanism of dissipation in HTSs is a matter of interest because of their technological significance and a detailed analysis of E-J characteristics is essential for a better understanding of the relationship between the microstructure and current carrying properties of polycrystalline superconductors rather than single crystals for practical applications. In this chapter, a detailed analysis of the E-J characteristics and the associated n-indices of RE-free and

RE substituted (Bi,Pb)-2212 superconductor at different magnetic fields are discussed and an assessment of the suitability of the material for application in persistent mode magnets is performed.

6.2 Experimental details

Samples with the nominal stoichiometry of $Bi_{1.6}Pb_{0.5}Sr_{2-x}RE_xCa_{1.1}Cu_{2.1}O_{8+\delta}$ ($0 \leq x \leq 0.5$ and RE = Gd, Tb, Dy and Ho) were prepared by solid-state synthesis using high purity oxides and carbonates, namely Bi_2O_3, PbO, $SrCO_3$, $CaCO_3$, CuO and Tb_4O_7 (Aldrich, > 99.9 %). The ingredients were accurately weighed using an electronic balance and thoroughly homogenized using a planetary ball-mill with agate bowl and balls in acetone medium for 2 hours. The homogeneous mixtures, thus obtained were calcined in three stages in air at 800°C for 15 h + 815°C for 40 h + 830°C for 40 h. Intermediate grinding in acetone medium was done between each stage of calcination to improve the homogeneity of samples. The samples were then pelletized under a pressure of 500 MPa. The pellets were heat-treated for 120 h with a schedule of 845°C for 60 h + 848°C for 60 h employing an intermediate pressing under the same pressure. In order to confirm the phase formation and superconductivity, the structural and superconducting characterisations were performed as mentioned in the previous chapters. The samples are hereafter denoted as RE*x*, where RE is the rare earth used and *x* represents the last digits of the RE stoichiometry. For example, Tb150 and H150 denote the Tb and Ho substituted samples with the stoichiometry, $x = 0.150$. Similarly, G0, Dy0, Tb000 and H000 represent RE-free samples.

Current and potential leads of high-grade copper wires were soldered to the samples with silver coating. Cylindrical pellets were shaped into rectangular form with the dimensions $12 \times 4 \times 1$ mm^3 on which the potential leads, separated by a distance of 5 mm were placed at the central part of the specimen.

The transport J_c in the self-field and E-J characteristics of the samples under zero and fixed fields namely, 0.32 T and 0.64 T, were measured at 64 K by four-probe method in a liquid N_2 bath cryostat with provision for vacuum. The direction of current was parallel to the direction of the pressed surface and magnetic field was applied perpendicular to the pressed surface of the pellet. A computer controlled dc-pulse method with four-probe arrangement was used to determine E-J characteristics using a constant current source (Aplab 9711P) and subsequently to determine the transport I_c of the samples. The pulse method effectively minimize the Joule heating from current leads and contacts by providing sufficient cooling time between each pulse. Thus it also avoids the influence of the ramp-rate on E-J characteristics. Transport critical current (I_c) values were determined using the four-probe method with a standard criterion of $1\mu V/cm$, derived from the resistance between voltage terminals. The J_c values of the pure and RE substituted (Bi,Pb)-2212 samples were calculated from I_c and the total cross-sectional area of the samples.

6.3 Transport E-J characteristics

From the structural analysis of the samples, it is clear that substituted RE atoms have successfully entered in the crystal structure of (Bi,Pb)-2212 system. The substitution of a trivalent/tetravalent RE atom in the crystal structure of (Bi,Pb)-2212 controls the hole concentration of the CuO_2 layers as a whole. This controlling mechanism of holes in the CuO_2 planes is discussed in chapter 4, i.e., when trivalent/tetravalent RE atoms are substituted into the (Bi,Pb)-2212 system, each RE atom supply additional electrons to the system which fills the holes present in the crystal. Hence, the hole concentration in the CuO_2 plane decreases and the system reaches an optimal doped state with an increased T_c. The variation of T_c with RE concentration is given in table 4.1 in chapter 4. The results show that the RE substituted (Bi,Pb)-2212 samples have

much higher T_c values at optimum concentrations compared to the RE-free sample.

The RE-free and RE substituted (Bi,Pb)-2212 samples are further analysed from the E-J characteristics using one-dimensional flux-creep model, wherein the flux-creep is caused by a thermally activated motion of flux-lines in superconductors. This motion is characterized by a velocity, strongly dependent on the local current density. Maxwell's equation of the form,

$$\left(\frac{\partial B}{\partial t}\right) = -\left(\frac{\partial E}{\partial x}\right) \tag{6.1}$$

is used to understand the flux motion in the presence of applied magnetic field where, E is the local electric field which can be related to the flux density and the velocity of the thermally-activated flux motion υ by the relation, $E = \upsilon B$. The velocity of the vortex motion in a thermally activated process is given by

$$\upsilon = \upsilon_c e^{-[U(J)/k_B T]} \tag{6.2}$$

where U(J) is the pinning barrier potential and υ_c is the velocity when U(J) = 0, U_c is the pinning energy. In the case that the pinning energy has a logarithmic dependence on the current,

$$U(J) = U_c \, ln \left(\frac{J_c}{J}\right) \tag{6.3}$$

and it follows that the electric field equals [17]

$$E = E_c \left(\frac{J_c}{J}\right)^n \tag{6.4}$$

Figures 6.1-6.4 show the E-J characteristics (log E – log J curves) of the RE-free and RE (Gd, Dy, Tb and Ho) substituted (Bi,Pb)-2212 samples measured at 0.0, 0.32 and 0.64 T at 64 K. The important inference is that the self-field

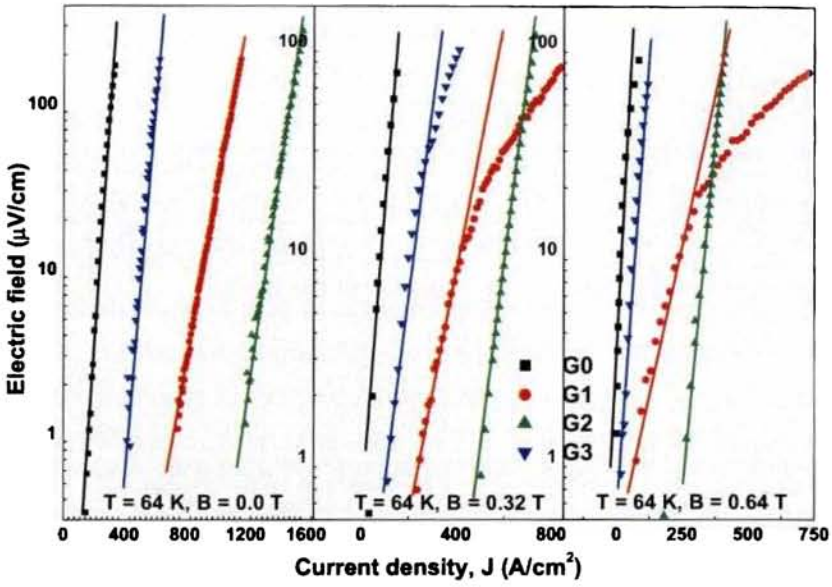

Figure 6.1: E-J characteristics of Gd substituted (Bi,Pb)-2212 superconductors at 0.32 and 0.64 T compared with Gd-free sample.

J_c of all the RE substituted samples are higher than the pure sample. The self-field J_c attains a peak value after a systematic increase as the RE content increases. The observed peak value of self-field J_c is higher than the RE-free sample. Almost a linear behaviour is seen in the E-J characteristics measured at 0.0, 0.32 and 0.64 T which is due to the thermally activated flux-flow. All the E-J characteristics fit well with the equation log E = n ln J + C, where C is a constant and the slopes of these curves give the n-index, which has been tabulated in table 6.1. It is found that, both in self-and in-fields, the maximum value of n-index is obtained at the same x value for each RE where their best properties were obtained (Gd, Dy, Tb and Ho substituted samples show best properties at x = 0.2, 0.2, 0.075 and 0.075, respectively) and hence a maximum current flow with minimum dissipation of energy. At self-fields all the samples show relatively high n-index while at in-fields, it decreases (Table 6.1), since the n-index is a field dependent parameter. The Gd and

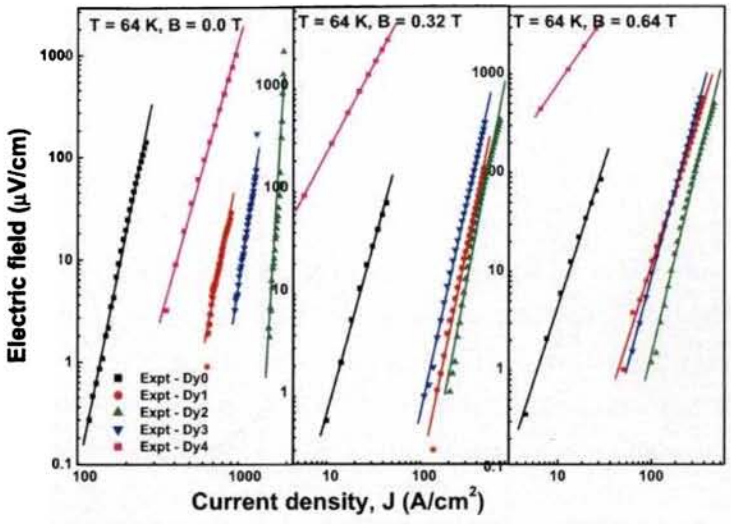

Figure 6.2: E-J characteristics of Dy substituted (Bi,Pb)-2212 superconductors at 0.32 and 0.64 T compared with Dy-free sample.

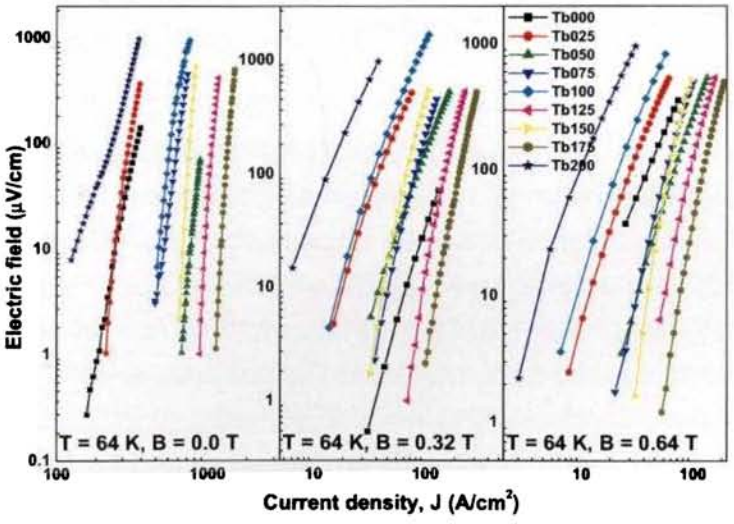

Figure 6.3: E-J characteristics of Tb substituted (Bi,Pb)-2212 superconductors at 0.32 and 0.64 T compared with Tb-free sample.

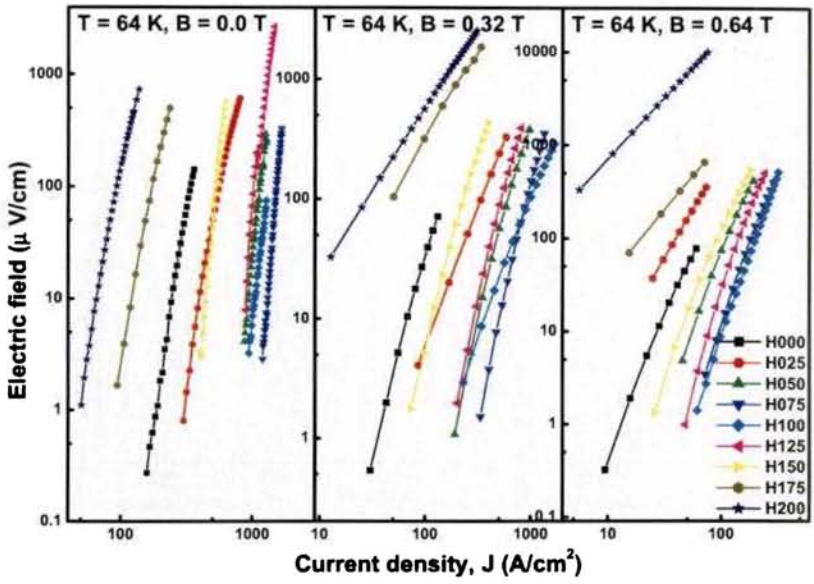

Figure 6.4: E-J characteristics of Ho substituted (Bi,Pb)-2212 superconductors at 0.32 and 0.64 T compared with Ho-free sample.

Tb/Ho substituted samples have better n-index (n>15) at 0.0 T and 0.32 T for x values 0.2 and ($0.050 \leq x \leq 0.125$), respectively. However, in contrast to Gd and Dy substituted samples, Tb and Ho substituted samples have an n-index greater than 15 even at an applied field of 0.64 T at 64 K for x values ($0.075 \leq x \leq 0.125$) and ($0.050 \leq x \leq 0.125$) respectively. The Dy substituted samples show the best self-field performance, but has a comparatively poor in-field performance. The observations reveal that at self-field and applied-fields (0.32 T and 0.64 T), the flux-lines are in glass-state (weak creep) for samples with n>15 and those in all the remaining samples with n<15 are in liquid-state (strong creep) [18].

The decay of persistent current in a superconducting magnet is found to be closely related to the n-index of the superconductor. In the case of an NMR magnet, the decay of the magnetic field and hence, the decay of the persistent

current should be smaller than 10^{-2} ppm/h. For an n-index ~20, the magnitude of the persistent current is calculated to be only 36% of J_c and a high value of persistent current density of 55% J_c is obtained for an n-index of ~34 for the Bi-2212 insert magnet of the high-field NMR magnet system [17]. Thus, the RE substituted (Bi,Pb)-2212 samples with an n>20 at applied fields, under transport current flow, can be used for magnetic applications such as insert-magnets. A correlation between n-value (or U_c) and J_c for different samples is observed by comparing the U_c-curves (Figures 6.5(a)–6.5(d)) with the J_c values (Table 6.1), i.e., high J_c values are generally found for samples with large n-values (n>15), while small J_c values (x<0.05) are typically observed for samples with low n-values (n<15). Thus, the general trend in the observed dissipation is that the flux-creeping effects in RE substituted (Bi,Pb)-2212 samples are weaker for the samples with larger n-indices and vice-versa. In the present work, the observed high n-indices in RE substituted (Bi,Pb)-2212 samples are at a temperature as high as 64 K and hence, there is a great scope for further drastic increase in n-indices at 4.2 K.

Figures 6.5(a)–6.5(d) show the variation of U_c as estimated from the n-index with respect to x. It reveals that REs, [Tb and Ho] and [Gd and Dy], when substituted with x=0.075 and x=0.200, respectively, show the best flux pinning capability as evident from a peaking of U_c, both for self-field and in-fields namely, 0.32 T and 0.64 T. The relative performance of RE substituted samples in self- and in-fields is evaluated by comparing its U_c values with those of the RE-free sample and the U_c values are given in table 6.1. The RE-free sample shows U_c values of 29.0 ± 0.1 meV in the self-field (~ 4, 10, 7 and 6 times lesser than best sample of Gd, Dy, Tb and Ho, respectively.) and 18.4 ± 0.1 meV and 6.6 ± 0.1 meV at 0.32 and 0.64 T (which is also lesser than best sample Gd, Dy, Tb and Ho substituted samples), respectively. It is also observed that all the RE substituted samples have better U_c compared to the RE-free sample. Hence, it is concluded that the RE substituted samples have much better flux pinning properties than the RE-free sample.

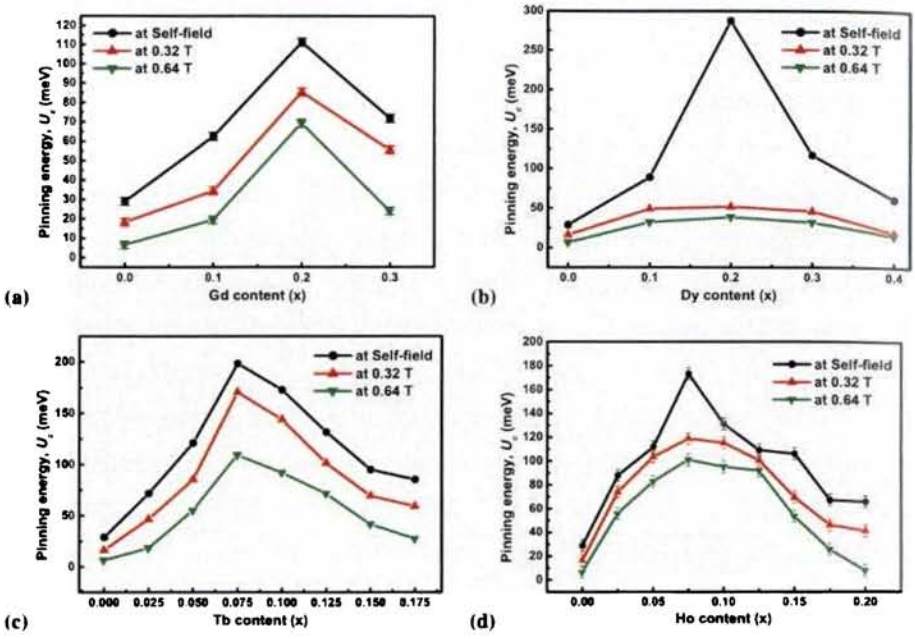

Figure 6.5: Dependence of characteristic pinning energy (U_c) on RE concentration at self- and in-fields (0.32 T and 0.64 T).

The estimated values of activation barrier of vortex motion U(J) in self- and in-fields are determined and are shown in figures 6.6–6.9 which show a logarithmic dependence on the current density over a wide range. The results show that deterioration of U(J) due to the magnetic field is significantly reduced as a result of RE substitutions. This shows that doping of RE atoms at the Sr-site enhances the flux pinning properties of (Bi,Pb)-2212 superconductor. The activation potential required for the motion of fluxons is higher for RE substituted samples with higher J_c and U_c (or n-values), while the least is observed for the RE-free under the transport supercurrent flow. From the figure 6.6–6.9 results, it is clear that the REs, [Tb and Ho] and [Gd and Dy], when substituted with x=0.075 and x=0.200, respectively, sample has the best flux pinning strength. On extrapolating the curve to a point U(J)=0, the J_c (at 64 K) at self- and applied fields can be found out. From the relation, $U(J) = U_c \ln\left(\frac{J_c}{J}\right)$, it is

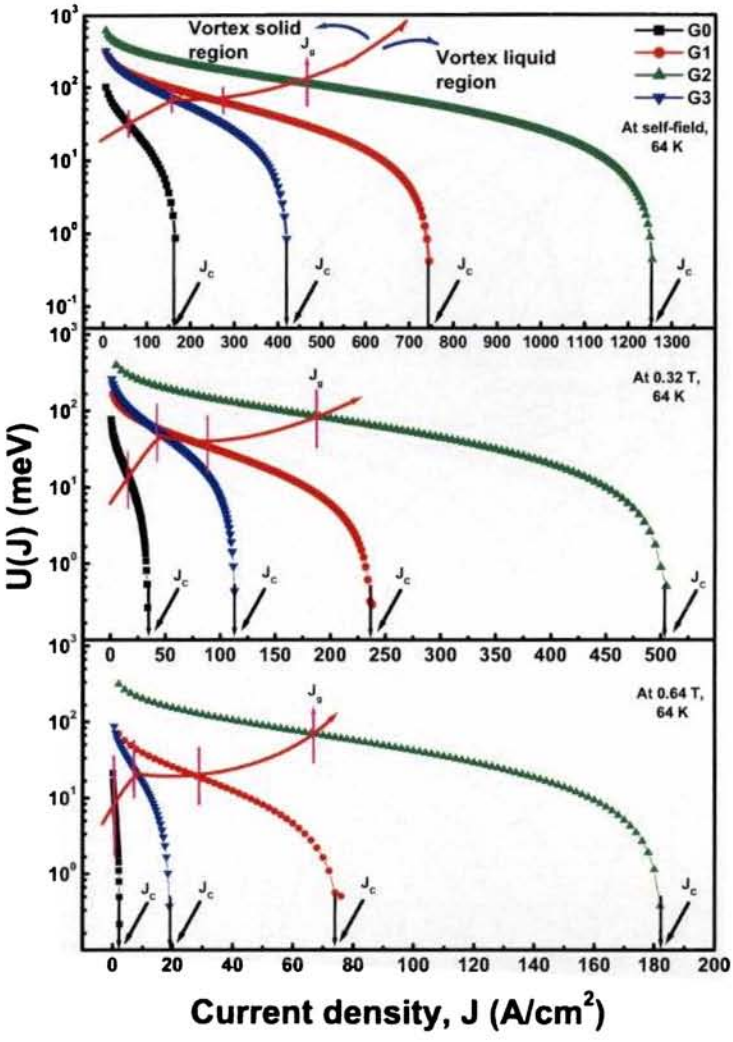

Figure 6.6: Variation of flux-creep activation barrier U(J) of Gd-free and Gd substituted (Bi,Pb)-2212 superconductors in self and applied fields.

seen that when current density (J) becomes (1/e) times J_c (denoted as J_g) then $U_c = U(J_g)$, where J_g is the current density for the transition from vortex-glass to vortex-liquid state. The value of J_g determines the onset of the solid vortex-

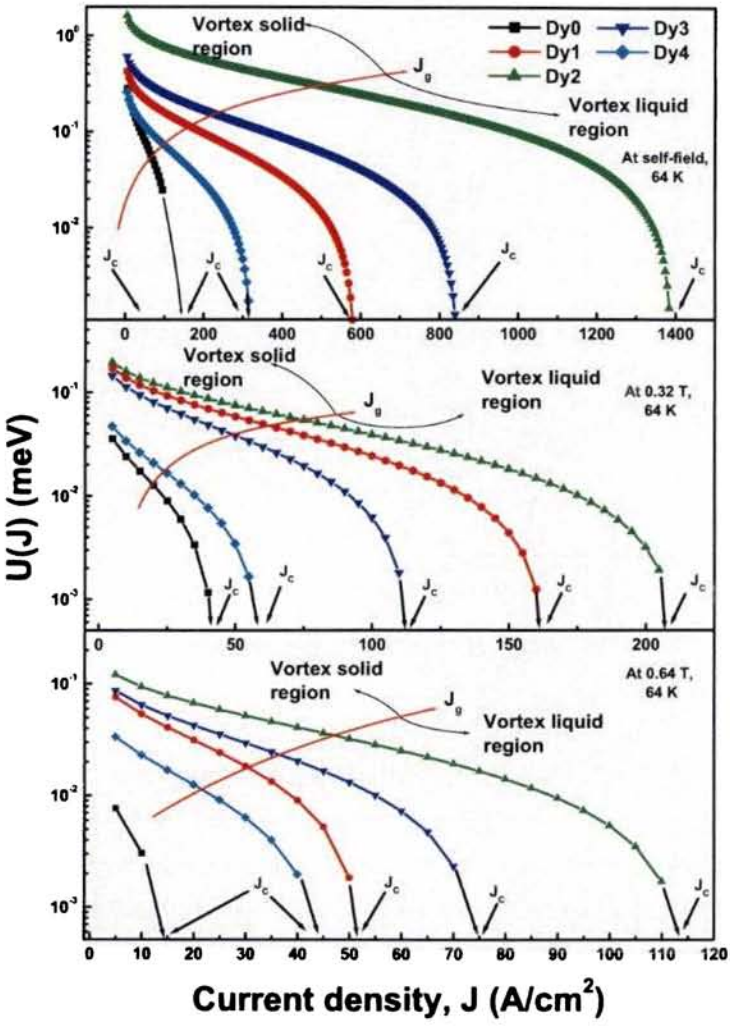

Figure 6.7: Variation of flux-creep activation barrier U(J) of Dy-free and Dy substituted (Bi.Pb)-2212 superconductors in self and applied fields.

glass to liquid transition, i.e., the vortices are in the solid-glass state for $J<J_g$ and it starts to melt to vortex-liquid state for $J>J_g$. This clearly reveals that RE substituted (Bi.Pb)-2212 superconductors exist in a solid-glass state at a much

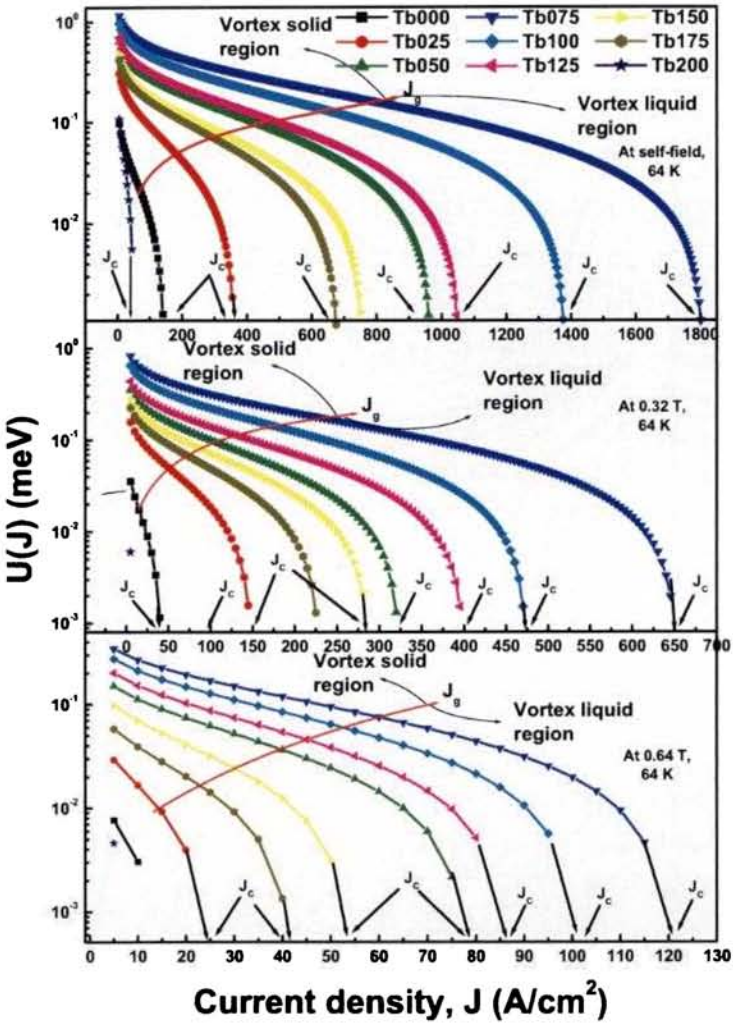

Figure 6.8: Variation of flux-creep activation barrier U(J) of Tb-free and Tb substituted (Bi,Pb)-2212 superconductors in self and applied fields.

higher current density in self- and applied-fields as compared with RE-free samples. This is another evidence for the strong pinning effect of vortices in the RE substituted (Bi,Pb)-2212 samples.

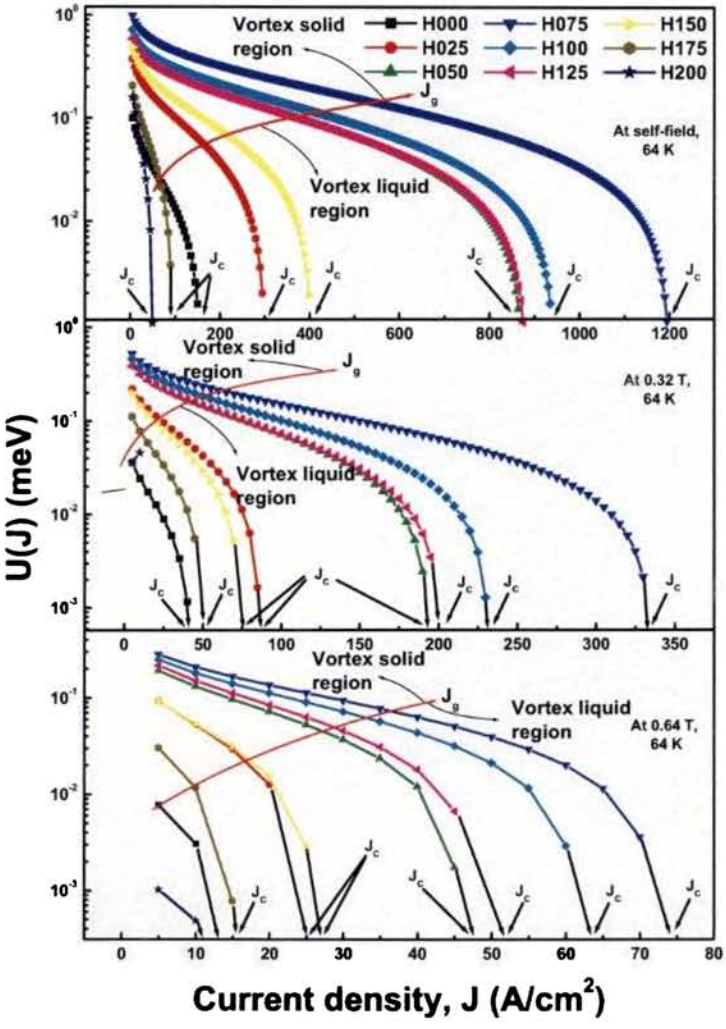

Figure 6.9: Variation of flux-creep activation barrier U(J) of Ho-free and Ho substituted (Bi,Pb)-2212 superconductors in self and applied fields.

The origin of the n-value is generally attributed to the distribution in the elementary flux-pinning centers (intrinsic effects) and from the non-uniformities in the cross-sectional area of the superconductor (extrinsic effects). Here, for

Table 6.1: Self-field J_c and self-and in-field n-indices and U_c observed for RE-free and RE (Gd, Dy, Tb and Ho) substituted (Bi,Pb)-2212 superconductors.

RE	RE content	J_c (at self-field)	n-index at			U_c (meV) at		
	(x)	(A/cm^2)	0.0 T	0.32 T	0.64 T	0.0 T	0.32 T	0.64 T
RE-free	0.0	170	5.20	3.30	1.20	29.0	18.4	6.6
Gd	0.1	750	11.30	6.25	3.50	62.4	34.5	19.5
	0.2	1260	20.15	15.50	12.55	111.3	85.5	69.3
	0.3	425	13.00	10.05	4.35	71.8	55.5	24.0
Dy	0.1	587	16.12	8.92	5.85	89.0	49.3	32.3
	0.2	1393	52.07	9.42	7.00	287.6	52.0	38.7
	0.3	849	21.18	8.38	5.82	117.0	46.3	32.1
	0.4	324	11.12	3.44	2.76	61.4	19.0	15.2
Tb	0.025	364	13.00	8.47	3.35	71.8	46.8	18.4
	0.050	970	21.90	15.50	10.00	121.1	85.6	55.2
	0.075	1810	35.90	30.95	19.80	198.4	170.9	109.5
	0.100	1384	31.30	26.10	16.70	172.8	144.1	92.3
	0.125	1055	23.85	18.40	13.00	131.7	101.6	71.7
	0.150	761	17.20	12.60	7.60	95.0	69.5	41.9
	0.175	683	15.45	10.80	5.00	85.2	59.5	27.7
Ho	0.025	301	16.60	14.00	10.56	87.9	74.0	55.8
	0.050	875	21.14	19.60	15.68	111.8	103.7	83.0
	0.075	1202	32.72	22.50	19.15	173.1	118.9	101.2
	0.100	946	24.75	21.80	18.00	131.0	115.4	95.3
	0.125	883	20.60	19.02	17.40	109.0	100.7	92.0
	0.150	407	20.04	13.17	10.14	106.0	69.7	53.7
	0.175	95	12.66	8.76	4.90	67.0	46.3	25.9
	0.200	51	12.44	7.86	1.55	65.8	41.6	8.2

samples with n>15, the intrinsic effects dominate and hence high n-values are observed [11, 12] leading to higher self-and in-field J_cs. This reveals that these samples have good flux-pinning capabilities and homogeneity and are the potential candidates for magnetic applications. At higher RE concentrations, the n-index decreases due to the domination of extrinsic effects such as the non-uniformities in the microstructure of (Bi,Pb)-2212 (weak-links). Thus, the re-

duction of n-index and hence, J_c is primarily due to collective effect of the total resistance of the network of weak-links, distributed throughout the sample.

Doping of Pb at Bi-site of Bi-2212 decreases the electromagnetic anisotropy (γ) and enhances c-axis conductivity (σ_c) which slightly improves the Josephson coupling strength between the CuO_2 layers across the charge reservoir layer (Bi-O) which results in slight improvement in J_c. At sufficiently low temperatures ($T < T_c$) and magnetic fields ($H < H_{irr}$), the flux lines form 3D vortices in (Bi,Pb)-2212 superconductor. As the temperature and field increases, these 3D flux line vortices undergo a change-over to 2D pancake vortices which are mainly confined in CuO_2 layers. Thus, the control over the hole concentration in CuO_2 layer is very essential and this is achieved by RE substitution at the Sr-site of (Bi,Pb)-2212. The controlling mechanism of holes in the CuO_2 planes is described in chapter 4. The origin of the enhanced n-values (or U_c) is generally attributed to the intrinsic effects, namely, the distribution in the elementary flux pinning forces ($f_p = \vec{j_c} \times \vec{B}$). The main reason for the enhanced flux pinning and the high in-field performance of RE substituted (Bi,Pb)-2212 superconductor is attributed to the crystal defects created by Pb and RE atoms in the Bi and Sr-layers, respectively. Hence, at higher temperatures in presence of external field, the 2D vortices confined in the CuO_2 layer are strongly coupled due to Pb doping in Bi-layer, and is effectively pinned by the defects in the Sr-layer due to RE substitution. Excess oxygen content is incorporated into the oxygen deficient Bi-O layers which makes it more insulating due to the RE substitution at higher concentrations. Thus, the Josephson coupling strength between the CuO_2 layers across the insulating layers becomes weaker at higher RE concentrations, which deteriorates the self- and in-field performance of RE substituted (Bi,Pb)-2212 at higher x.

6.4 Conclusions

In the present chapter, the magnetic field dependence of the n-indices is investigated, characterizing the E-J characteristics of RE-free and RE substituted (Bi,Pb)-2212 superconductor. The E-J characteristics are successfully explained by the flux-creep theory. It is found that the samples with n>15 and $J<J_g$ show a glass-state for flux-lines, indicating their improved flux-pinning ability due to the creation of point defects by the substituted RE atoms. The behaviour is clearly seen from U_c as well. A correlation between n-indices and the J_c of RE substituted (Bi,Pb)-2212 superconductor is also observed. A deeper insight into the superconducting behaviour of RE substituted (Bi,Pb)-2212 superconductors has been obtained by comparing the self-and in-field n-indices. The highly enhanced n-value beyond 15 at applied fields under transport current flow shows that the modified material is a promising candidate for magnetic applications such as insert-magnets of high-field NMR.

References

[1] E. H. BRANDT, *Phys. Rev. B* **52**, 15442 (1995).

[2] D. M. J. TAYLOR, S. A. KEYS, and D. P. HAMPSHIRE, *Physica C* **372**, 1291 (2002).

[3] P. BRUZZONE, *Physica C* **401**, 7 (2004).

[4] A. K. GHOSH, *Physica C* **401**, 15 (2004).

[5] S. N. COPPERSMITH, M. INUI, and P. B. LITTLEWOOD, *Phys. Rev. Lett.* **64**, 2585 (1990).

[6] D. S. FISHER, M. P. A. FISHER, and D. A. HUSE, *Phys. Rev. B* **43**, 130 (1991).

[7] T. MIYAZAKI, *IEEE Trans. Appl. Supercond.* **9**, 2505 (1999).

[8] N. MITCHELL, *Physica C* **401**, 28 (2004).

[9] M. MARTOVETSKY, *Physica C* **401**, 22 (2004).

[10] N. MITCHELL, *Fusion Eng. Des.* **66-68**, 971 (2003).

[11] D. P. HAMPSHIRE and H. JONES, *Cryogenics* **27**, 608 (1987).

[12] R. WÖRDENWEBER, *Rep. Prog. Phys.* **62**, 187 (1998).

[13] H. S. EDELMAN and D. C. LARBALESTIER, *J. Appl. Phys.* **74**, 3312 (1993).

[14] W. H. WARNES, *J. Appl. Phys.* **63**, 1651 (1988).

[15] W. H. WARNES and D. C. LARBALESTIER, *Appl. Phys. Lett.* **48**, 1403 (1986).

[16] J. W. EKIN, *Cryogenics* **27**, 603 (1987).

[17] D. V. SHANTSEV, A. V. BOBYL, Y. M. GALPERIN, and T. H. HOHANSEN, *Physica C* **341-348**, 1145 (2000).

[18] H. KUMAKURA, A. MATSUMOTO, Y. S. SUNG, and H. KITAGUCHI, *Physica C* **384**, 283 (2003).

Chapter 7

Conclusions and future directions

7.1 Conclusions

The objectives of the present work, As stated in section 1.9 of chapter 1 were to develop RE doped Bi-2212 superconductor with novel properties by proper selection of the RE, doping level and optimization of the process parameters and to investigate the effects of RE doping on the structural and superconducting properties of Bi-2212 superconductor.

The role of RE doping on superconducting and flux pinning properties of Pb substituted Bi-2212 superconductor has been studied since, it is an efficient tool to understand the underlying mechanism of high T_c superconductors. Previous RE doping studies in Pb-free Bi-2212 show that there is not much improvement in T_c or in the flux pinning properties and there is no work which reports the effect on J_c.

RE substituted Bi-2212 superconductors are prepared through solid state process by proper selection of RE (from La to Lu), and its doping level. The samples were prepared in bulk polycrystalline form. To evaluate the perfor-

mance of the samples, various measurements like phase analysis, lattice parameter studies and texture studies by XRD, microstructural examination by SEM equipped with EDS, density measurement, critical current density (J_c), critical temperature (T_c), J_c–B and E–J characteristics were performed.

The main conclusions of the present work are :

1. Standardized the doping level of Pb at the Bi-site of Bi-2212 superconductor in the range of $x = 0.4 - 0.5$. Optimized Pb-substituted sample enhances the self-field J_c about 3 times and slightly depresses the T_c of the Bi-2212 superconductor compared to the Pb-free sample. The enhancement of J_c is found to be due to the improved microstructure and the increase in the c-axis conductivity of the system.

2. Initial studies on the effects of Y addition in Pb doped Bi-2212 show that the electronic structure of the system changes by reducing hole concentration. The T_c and J_c are significantly enhanced for optimum Y concentration. Pb co-doping results in the increased c-axis conductivity due to the strong Josephson coupling between CuO_2 layers at lower Y contents. At higher doping levels secondary phases containing Ca and Sr are observed . The changes in the electrical and superconducting properties are due to the interference of structural as well as electronic properties induced by Pb and Y co-doping.

3. The structural and superconducting properties of RE substituted (Bi,Pb)-2212 superconductor studied for different RE concentrations between the range ($0 \leq x \leq 0.5$) and the results are compared with RE-free (Bi,Pb)-2212 superconductor. Significant structural changes occur with the increase in RE content which supports the substitution of RE in the (Bi,Pb)-2212 structure. Microstructure of RE substituted (Bi,Pb)-2212 superconductor deteriorates with increase in RE content. Even then, the critical temperature (T_c) and critical current density (J_c) are significantly enhanced at an optimum RE concentration. The maximum values of T_c as

well as J_c are observed at different x values and the improvements are about 12 K – 19 K, in T_c and 6 – 18 times in J_c depending on the substituted RE. The increase in T_c as well as J_c is explained by the dual effect of the decrease in the hole concentration in CuO_2 planes to an optimum level and the improvement of coupling between the CuO_2 layers which is achieved by RE-doping. Beyond the optimum levels, T_c and J_c reduce due to decreased charge carrier concentration which triggers a Metal to insulator transition (MIT) in (Bi,Pb)-2212 system.

4. The effect of sintering temperature of RE substituted (Bi,Pb)-2212 superconductors is investigated systematically. The microstructural variations are highly temperature-sensitive. T_c is invariant with the sintering temperature for the same RE content. The J_c value of RE substituted samples depends mainly on the RE content and the microstructural and flux pinning aspects. The enormous increase of self-field J_c of the samples heat treated at higher sintering temperatures is due to the formation of the refined microstructure. While the formation of disrupted grains with decreased texturing reduces the self-field J_c of the samples heat treated at lower sintering temperatures.

5. The investigation of the microstructural and flux pinning properties of RE substituted (Bi,Pb)-2212 superconductors prepared at different temperatures ranging from 846 to 860 °C point towards the importance of fine tuning of heat treatment temperature in the preparation of RE substituted (Bi,Pb)-2212 superconductors to tailor their properties catering to different applications. The method can be used to prepare RE substituted (Bi,Pb)-2212 superconductors incorporating hybrid self- and applied field properties by selecting a suitable sintering temperature.

6. The pinning analysis clearly demonstrates that the substitution of RE in (Bi,Pb)-2212 superconductor significantly enhances its flux pinning strength at a relatively high temperature of 64 K by the introduction

of point defects, which also contribute to the J_c of the RE substituted (Bi,Pb)-2212 superconductor.

7. The magnetic field dependence of the n-indices of RE substituted (Bi,Pb)-2212 superconductors are investigated characterizing the E-J characteristics of RE-free and RE substituted (Bi,Pb)-2212 superconductor. RE substituted (Bi,Pb)-2212 superconductors show better flux pinning properties at self- and applied fields. The samples with n>15 and $J<J_g$, a glass-state for flux-lines, which in turn shows their improved flux-pinning ability. The behaviour is clearly seen from U_c as well. Also, a correlation between n-indices and the J_c of RE substituted (Bi,Pb)-2212 superconductor is observed. A deeper insight into the superconducting behaviour of RE substituted (Bi,Pb)-2212 superconductors has been achieved by comparing the self-and in-field n-indices. The highly enhanced n-value up to 15 at applied fields under transport current flow suggests that these materials are promising candidates for magnetic applications.

7.2 Future directions

The present research work reports the development of novel RE substituted (Bi,Pb)-2212 superconductors with improved self- and in field superconducting properties. However, there are many issues to be addressed before taking these products for practical applications. A detailed investigation needs to be carried to study the magnetic field derived anomalies such as thermo-magnetic fluctuations, para-conductivity, flux creep, etc in the RE substituted (Bi,Pb)-2212 superconductors. At higher RE concentrations, the occurrence of the phenomenon known as metal to insulator transition (MIT) in the normal state was observed due to the large decrease in the hole carrier concentration and subsequent transformation of (Bi,Pb)-2212 system into an extreme under-doped state. A systematic and a careful study of this unusual normal

state property of (Bi,Pb)-2212 system is required to understand its impact on high temperature superconductivity and to enlighten the mechanisms, since it reveals the reason behind the origin of insulating states as well as the basic character of the metallic state induced by the cation substitution (RE). Future efforts may be directed towards the preparation of wires and tapes using the newly developed formulations so that their highly improved superconducting properties can be exploited for conductor applications in self- and in-fields at relatively high temperature of 64 K, the freezing point of liquid Nitrogen.

Appendix A

A.1 List of symbols

Å	:	Angstrom
α(T)	:	Temperature coefficient of resistance
α, β, γ	:	Angles of a unit cell
$\Delta(0)$	:	Superconducting energy gap
ΔT_c	:	Transition width
κ	:	Ginzburg Landau parameter
λ	:	Wavelength
λ_F	:	Fermi wavelength
λ_L	:	Penetration depth
Ω	:	Unit of resistance
ϕ_0	:	Magnetic flux quanta
ψ(r)	:	Wave function
ρ	:	Resistivity
ρ_a, ρ_b	:	in-plane resistivity
ρ_c	:	out-of-plane resistivity
ρ_{th}	:	Theoritical bulk density
θ	:	Angle of diffraction
θ(r)	:	Phase factor
θ_c	:	Critical angle
ξ	:	Coherence length
A	:	Cross sectional area
a, b, c	:	lattice parameters

a_0	:	Interatomic distance
B	:	Magnetic field
c and $c^\dagger$	:	Creation and annihilation operator
F	:	Lotgering Index
F_x	:	Volume percentage of phase x
F_P	:	Flux pinning force
F_{Pmax}	:	Maximum flux pinning force
h, k, l	:	reciprocal lattices
I_{total}	:	Integrated peak intensity of mixture
I_x	:	Integrated peak intensity of phase x
k_B	:	Boltzmann's constant
L	:	Interdopant atomic distance
l	:	length
n_s^*	:	Density of superelectrons
t	:	Transfer parameter
v	:	velocity of TAFF
v_c	:	Critical velocity of TAFF
A, p, q	:	Dew Hughes fitting parameters
p_h	:	Hole carrier concentration/Cu atom
B_{irr}	:	Irreversibility field
C_i	:	Weight percentage of investigated element
C_s	:	Weight percentage of standard element
d	:	Interplanar spacing
E	:	Electric field
E_o	:	Critical electric field
H_c	:	Critical magnetic field
H_{c1}	:	Upper critical field
H_{c2}	:	Lower critical field
$I_{(00l)}$	:	Intensity of (00l) plane
I_i	:	Peak intensity of investigated element
I_s	:	Peak intensity of standard element
J	:	Current density
J_c	:	Critical current density
J_g	:	Current density for vortex glass to liquid transition

k+/k-	:	Wave vector
$I_{(hkl)}$	:	Integrated intensity of hkl planes
n	:	order of reflection
$N_s(E,\theta)$	:	Density of state function
nm	:	Nanometer
P_r	:	Intensity ratio of randamised powder
P_a	:	Intensity ratio of textured pellet
Pa	:	Pascal
r	:	Position vector
R	:	Resistance
T_c	:	Critical temperature
U_c	:	Pinning energy
U(J)	:	Pinning potential barrier
Vol. %	:	Volume percentage
Wb	:	Weber
wt. %	:	Weight percentage

A.2 List of abbreviations

ASCII	:	American standard code for information interchange
BCS	:	Bareen Cooper Schreiffer
BSCCO	:	Bismuth strontium calcium copper oxide
BSE	:	Back scattered electron image
CERN	:	European Council for Nuclear Research
DOS	:	Density of states
EDS	:	Energy dispersive X-ray spectrometer
GB	:	Grain boundary
GPIB	:	General purpose interface borad
HP	:	Horse power
HTS	:	High temperature superconductor
IBM	:	International Business Machine
ICDD	:	International consortium for diffraction data
LTS	:	Low temperature superconductor
MIT	:	Metal to insulator transition
NMR	:	Nuclear magnetic resonance

PC	:	Personal computer
PDF	:	Powder diffraction file
RE	:	Rare earth
RIR	:	Resudual intensity ratio
RRR	:	Resudual resistivity ratio
RVB	:	Resonance valance bond
SEI	:	Secondary electron image
SEM	:	Scanning electron microscope
TAFF	:	Thermally activated flux flow
USD	:	United states doller
XRD	:	X-ray diffractometer
YBCO	:	Yttrium barium copper oxide

List of Figures

List of Tables

Colophon

This dissertation was prepared in LaTeX 2_ε using the "sunthesis" class derived from hepthesis.

Title	**:– Studies on the development of novel rare-earth doped (Bi,Pb)-2212 superconductors with enhanced properties.**
Author	**:– Pallian Murikkoli Sarun.**
Prepared on	**:– Lenovo 3000 Notebook (G400).**
Operating system	**:– GNU Linux Workstation (Debian lenny 5.0.2 KDE).**
Packages	**:– Kile, TeXlive, Gcrystal, GIMP, Origin, PDFCreator.**
File size	**:– 9,848 kB.**
Completed on	**:– June 23, 2010.**